PERFORMANCE ANALYSIS OF AIR HEATED AND DUAL HEATED HUMIDIFICATION-DEHUMIDIFICATION CYCLES

BY

SAAD ABDUL JAWAD

A Thesis Presented to the
DEANSHIP OF GRADUATE STUDIES

KING FAHD UNIVERSITY OF PETROLEUM & MINERALS

DHAHRAN, SAUDI ARABIA

In Partial Fulfillment of the
Requirements for the Degree of

MASTER OF SCIENCE

In

MECHANICAL ENGINEERING

April, 2020

KING FAHD UNIVERSITY OF PETROLEUM & MINERALS

DHAHRAN, SAUDI ARABIA

DEANSHIP OF GRADUATE STUDIES

This thesis, written by Saad Abdul Jawad under the direction of his thesis advisor and approved by his thesis committee, has been presented to and accepted by the Dean of Graduate Studies, in partial fulfilment of the requirements for the degree of MASTER OF SCIENCE in MECHANICAL ENGINEERING.

Dr. Mohamed A. Antar
Advisor

Dr. Zuhair Mattoug Gasem
Department Chairman

Nov. 10, 2020

Dr. Syed M. Zubair
Member

Dr. Suliman Saleh Al-Homidan
Dean of Graduate Studies

Dr. Atia E. Khalifa
Member

07-12-2020
Date

Table of Contents

ACKNOWLEDGEMENTS

All praise to Allah for blessing me with health, patience, and knowledge to conclude my thesis work.

I convey my deep sense of respect and gratitude to Prof. Dr. Mohamed A. Antar for his valuable guidance, profound suggestions and kind supervision. I acknowledge him for providing necessary scientific directions in implementing ideas. I am thankful to Prof. Dr. Syed M. Zubair and Dr. Atia E. Khalifa for their constructive feedback which helped me develop a wider perspective to my work.

My sincere thanks must go to Mr. Peter from maintenance department for generously offering me his valuable time in resolving technical issues during experimentation. I compliment faculty and administrative staff at the mechanical engineering department for their professional support and prompt guidance.

I am also grateful to my parents for providing me with emotional strength, moral guidance and financial support. I deeply thank my siblings for their encouragement despite the long distance between us.

LIST OF TABLES

LIST OF FIGURES

NOMENCLATURE

Acronyms

GOR	gain output ratio
HCR	heat capacity ratio
RR	recovery ratio
MR	mass flowrate ratio
CAOW	closed air-open water
HDH	humidification-dehumidification
MAH	modified air heated
DH	dual heated
SEEC	specific electrical energy consumption

Symbols

$\dot{m}_w$	feedwater mass flowrate (kg/s)
$\dot{m}_{pw}$	freshwater mass flowrate (kg/s)
$\dot{m}_b$	brine mass flowrate (kg/s)
$\dot{m}_a$	air mass flowrate (kg/s)
T	temperature (C)
$\dot{Q}_{in}$	heat energy input (kW)
Q_r	heat rate ratio [$\dot{Q}_{in,water}/\dot{Q}_{in,air}$] (-)
ω	humidity ratio (kg_w/kg_a)
ϕ	relative humidity (-)
ε	effectiveness (-)
$\dot{S}_{gen}$	entropy generation rate (kJ/s.K)
$\dot{s}_{gen}$	specific entropy generation (kJ/kg.K)
h_{fg}	latent heat of vaporization (kJ/kg)
$	United States Dollar

Subscripts

w	water
a	air
pw	product water
b	brine
0	ambient state
h	humidifier
d	dehumidifier
ht	heater
1,2,3…	positions in layout
hum. / deh.	humidifier / dehumidifier

ABSTRACT

Full Name : Saad Abdul Jawad

Thesis Title : Performance Analysis of air heated and dual heated humidification-dehumidification cycles

Major : Mechanical Engineering

Date of Degree : April 2020

Humidification-dehumidification (HDH) desalination offers an effective decentralized solution to meet the potable water demands of small-scale communities. Amongst many configurations, the modified air heated (MAH) and dual heated (DH) HDH cycles have demonstrated promising results in several analytical studies. But these systems have rarely been evaluated in an experimental setting before. In the present study, both of these cycles are experimentally examined in a closed air-open water (CAOW) layout. Post-humidification air heating is performed in the MAH cycle. Whereas in the dual heated HDH system, water and air are heated before and after the humidification, respectively. An experimental rig is utilized to study the effect of changing mass flowrate ratio on the performance dynamics of theoretically acclaimed HDH configurations. The concept of heat rate ratio (Q_r) is explored practically by splitting up the heat energy between water and air streams in the DH-HDH cycle. Sequentially, two cases of Q_r being less than one and greater than one, are explored in detail. Results have shown that the DH system performs better than the MAH cycle. Maximum freshwater production rate in case of DH cycle is recorded to be 117.2 kg/day. However, MAH system has reported the freshwater productivity of 72.7 kg/day. Maximum deviation of experimental results from analytical model is ≈ 6 %.

ملخص الرسالة

الاسم الكامل : سعد عبد الجواد

عنوان الرسالة : تحليل أداء دورة الترطيب وإزالة الرطوبة المعدلة مع تسخين الهواء والتسخين المزدوج

التخصص : الهندسة الميكانيكية

تاريخ الدرجة العلمية : أبريل ٢٠٢٠

توفر تحلية المياه باستخدام الترطيب وإزالة الرطوبة (HDH) حلاً لامركزيًا فعالاً لتلبية متطلبات المياه الصالحة للشرب للمجتمعات الصغيرة. وهناك العديد من التصاميم المختلفة لمنظومات الترطيب وإزالة الرطوبة وقد أظهرت الدورات المعدلة لتسخين الهواء (MAH) ودورات التسخين المزدوج HDH (DH) نتائج واعدة في العديد من الدراسات التحليلية. لكن نادرًا ما تم تقييم هذه الأنظمة في بيئة تجريبية. في هذه الدراسة، وتم فحص كلتا هاتين المنظومتين بشكل تجريبي في دورة سريان مغلقة بالنسبة للهواء ومفتوحة بالنسبة لسريان الماء (CAOW). ويتم تسخين الهواء بعد الترطيب في دورة (MAH). بينما في نظام (HDH) المزدوج المسخن يتم تسخين الماء والهواء قبل وبعد الترطيب، على التوالي. ويتم استخدام منصة تجريبية لدراسة تأثير تغيير نسبة تدفق الكتلة على ديناميكيات الأداء لتكوينات (HDH) المشهود لها نظريًا. ويتم استكشاف مفهوم نسبة معدل الحرارة (Q_r) عمليًا عن طريق تقسيم الطاقة الحرارية بين تيارات الماء والهواء في دورة (DH-HDH). بالتتابع، كما تم استكشاف حالتين من (Q_r) أقل من واحد وأكبر من واحدة. وقد أظهرت النتائج أن نظام (DH) يعمل بشكل أفضل من دورة (MAH) كما تم تسجيل أقصى معدل لإنتاج المياه العذبة في حالة دورة (DH) ليكون ٢. ١١٧ كجم / يوم. وبالإضافة فقد أنتجت منظومة تسخين الهواء المعدل كمية من المياه العذبة تبلغ ٧. ٧٢ كجم / يوم. وقد بلغ أقصى انحراف للنتائج التجريبية من النموذج التحليلي ≈ ٪ ٦.

Intentionally left blank

CHAPTER : 1

INTRODUCTION

1.1 Desalination

Desalination is the method of separating or extracting excessive salts and minerals from the saline water to make it potable for human use. The required inputs for any seawater desalination process are feed water (i.e. seawater and brackish water) and an energy source. Subsequently, the resulting products include freshwater with considerably reduced amount of salts and brine with relatively higher salinity. Mainstream methods to desalinize water include large scale purification techniques that are centralized and energy intensive. Amid increasing global water scarcity, the desalinized water is widely used in municipal, agricultural and industrial sectors.

Conventional desalination processes can be classified in two major categories;

- Membrane Desalination
- Thermal Desalination

1.1.1 Membrane Desalination

Major types of membrane desalination processes are membrane distillation (MD), reverse osmosis (RO) and Electrodialysis (ED). MD is driven by a temperature gradient, which

generates difference in vapor pressure across a porous hydrophobic membrane that separates filtered vapor from saline water. Features of membrane distillation include low temperatures when compared to conventional (MSF, MED) processes, less fouling and compatibility with renewable energy sources (like solar) [1].

Reverse osmosis (RO) plants, on the other hand are pressure driven systems, utilizing grid electrical energy in most cases. Water is subjected to a pressure gradient across semi-permeable membrane, which then gets separated owning to different concentrations across the membrane. Amount of freshwater collected is highly dependent on the proportion by which pressure differential exceeds the osmotic pressure gradient. Pre-treatment of seawater is considered a necessity in RO plants to minimize fouling issues [2]. Due to its reasonable freshwater production rate and energy requirements, it has often been compared with multi-effect desalination (MED) process and is considered a valid competitor to conventional thermal desalination processes. RO setups can be integrated with renewable energy sources (like solar-PV, wind and wave energy) by converting different forms of energy to electricity first. RO process is generally dominant among seawater treatment plants and account for about 69% (65.5 million m^3/day) of global desalted water [3].

Lastly, electrodialysis (ED) employs an electrical field to segregate salt ions in the saline water that passes through stacked ion-exchange membranes. Salt ions migrate towards cation or anion exchange membranes based on their respective polarities. The possibility of utilizing PV based solar energy with ED units has been reported by authors and is being explored further [4].

1.1.2 Thermal Desalination

In the context of Middle East, thermal desalination has played a key role and is expected to do so over the next few decades. Excessive availability of solar energy and fuel resources in the region, are among many other reasons for this inclination. Commercial thermal desalination is classified into multi-stage flash (MSF) distillation, multi-effect evaporation (MEE or MED) and thermal or mechanical vapor compression systems (TVC/MVC). Freshwater from MSF accounts for nearly 23% of the global desalinated water and most of these units are employed by the Middle Eastern countries [5]. It consists of successive individual units with decreasing temperature and pressure, termed as stages. Latent heat of evaporation is recovered in each stage to preheat the seawater. Due to large-scale boiling, the scaling gets minimized on the heat-transfer tubes, relatively. Process utilizes moderate temperature steam usually exiting from turbines of a co-generation plant [6].

Multi-effect distillation (MED) has higher thermal performance than MSF, but at the cost of scaling on heat-transfer tubes. Vapor generated in each stage condenses out in the successive stage and in doing so it heats up the incoming brine feed. Like MSF, the pressure is lowered from effect-to-effect to improve the overall performance and aid evaporation process. Its performance ratio (PR) is proportional to the number of effects involved. But its sensitivity to leakage and practical limits on factors like temperature, keeps it away from being competitive with other mainstream technologies [7].

Vapor compression (VC) relies on pressure reduction and thermal energy provided by vapor compression to evaporate saline water. The compressor itself can be of either type; a mechanical compressor (MVC) or a steam ejector (TVC). TVC units are usually large in

sizes because the performance of such system improves by adjoining several stages. While for MVC the power consumed by the stage per unit freshwater remains unchanged, so adding stages does not make a difference it simply increases the carrying size or capacity of the unit. VC systems can be combined with MED/MSF plants in different configurations to form a hybrid setup, resulting in a better performance ratio of the system [8].

Use of conventional fuel resources is one of the biggest challenges facing the future of thermal desalination plants. To aid the streamline technology development in this domain, nuclear energy has often been seen as a feasible solution for co-generation. Extracting the required heat energy from nuclear reactors to drive the desalting processes can open new horizons in distillation science. Depending on the hybridization of nuclear reactor and desalination process, the cost of product water is estimated between 0.4-1.8 $\$/m^3$. Reliability in terms of fuel cost fluctuation and long-term environmental impacts are the motives behind the development in nuclear energy-based desalination. Moreover, the techno-economic analysis of the combined system has shown competitive figures when compared to the conventional desalination. Despite rapid development and recognition from the international atomic energy association (IAEA), countries without experience are holding back due to the concerns on safe operations and complex engineering [9].

1.2 The Global Water Situation

This section is subjected to discuss the analytical data available on the current global water situation. Water (H_2O) is an imperative ingredient for sustenance of life on the Earth. It holds functional significance to all the living creatures. Availability of water has a direct quantitative impact on the social, political and economic development of any particular

region in the World. Over the centuries, natural and aesthetic factors have forced the humans to populate areas that are closer to the freshwater bodies. A high-resolution study shows that only 10% of the global population lives beyond the 10 kms radius to a surface freshwater source. Furthermore, it is also revealed that over 50% of human population has inhabited areas that are within 3 kms to rivers or lakes [10]. Communities in Asia, Australia and Europe live in the closest proximities to water. However, areas with an arid climate, like North Africa and Middle East have the largest population distance to water bodies. Arguably, the physical distance to freshwater bodies is not as big of an issue as it was in the past. Modern pumping networks ensure the availability of water to large urban settlements with effective water supply management. Water purification and desalination along with several other water treatment techniques are in practice to fulfill the population needs in arid regions as well [11].

1.2.1 Water Scarcity: Reasons and Consequences

Among numerous influencing factors, population growth has imparted a statistically significant impact on the water demand and its usage patterns. Despite a decrease in growth rate from 2.1% (1965-70) to 1.1% (2015-2020), the human population continues to grow at a consistent pace. After adding 2 billion people since 1994, World's population now stands at 7.7 billion (2019). Moreover, the global population with prediction certainty of 95% is anticipated to size between 9.4 and 10.1 billion in 2050 [12]. Global variations in population growth, climate and socio-economic development are likely to become major water stressors in the near future.

Based on spatial connection between water resources and human activities, water stress predictions were made by the World resource institute (WRI) in 2015 to drive an effective water management at the global scale [13]. Using decadal prediction methodology [14], WRI has projected water scarcity over three 10-year periods, from 2020 to 2040. Accordingly, if water supply and demand variables and emissions were to remain unchanged till 2040 (business-as-usual), then eight out of first ten most water-stressed countries would be from the Middle East, as illustrated in the Figure 1.1. Moreover, the study has consecutively placed Saudi Arabia among the top ten countries that are likely to be at the forefront of global water scarcity in the coming decades. Global risk report 2019 compiled by the World economic forum (WEF) expects water crises to cast a severe societal impact. WEF projects that by 2030, the water scarcity will cause global water withdrawals to go beyond the World's renewable supplies by 2680 km^3, annually [15].

In an effort to prioritize sustainable future goals, WRI has conducted a risk assessment study estimating the monetary funding required to bridge the gap between the current and future water situation. An approximated cost of $113 billion is required annually from 2015-2030 to ensure sustainable access to the drinking water [16]. Correspondingly, Saudi Arabia needs to spend about $745 million annually (2015-2030), to counter potable water dilemma in the future. These figurative studies demand timely debate on emerging water-related issues. Some serious attention from a variety of decision-makers is required to financially collate the gap in global water management and to drive a tangible action.

Efficient water management is crucial to human prosperity and sustainable development of World economies. Under business-as-usual scenario, the regional gross domestic product (GDP) is expected to get severely affected due to water scarcity, by 2050. As

depicted in Figure 1.2, the GDP of Middle East and North African region is expected to take substantial impact from the developing water crisis [17]. Among several other factors, strain on freshwater availability will make eastern part of the World more vulnerable, in terms of food security.

With predicted regional warming, the Middle East is projected to face a difficult trade-off with food systems as well [18]. Most ground water reserves in the Middle Eastern countries are non-renewable and surface freshwater flows are minimal.

1.2.2 Safe Drinking Water

United Nations (UN)'s Sustainable Development Goal (SDG6) criteria for safely managed drinking water is that [19]:

- It is accessible on household (or plot) premises.
- Available when needed or for at least 12 hours/day.
- Free from bacterial and chemical contamination.

International Water Association (IWA) enlists two additional elements to this normative criteria. First being acceptability, which addresses the aesthetic and cultural outlook on drinking water, with subjective factors like odor and taste. Second is affordability, drinking water must be regulated and subsidized at a price that is suitable to all the people living in a community [20].

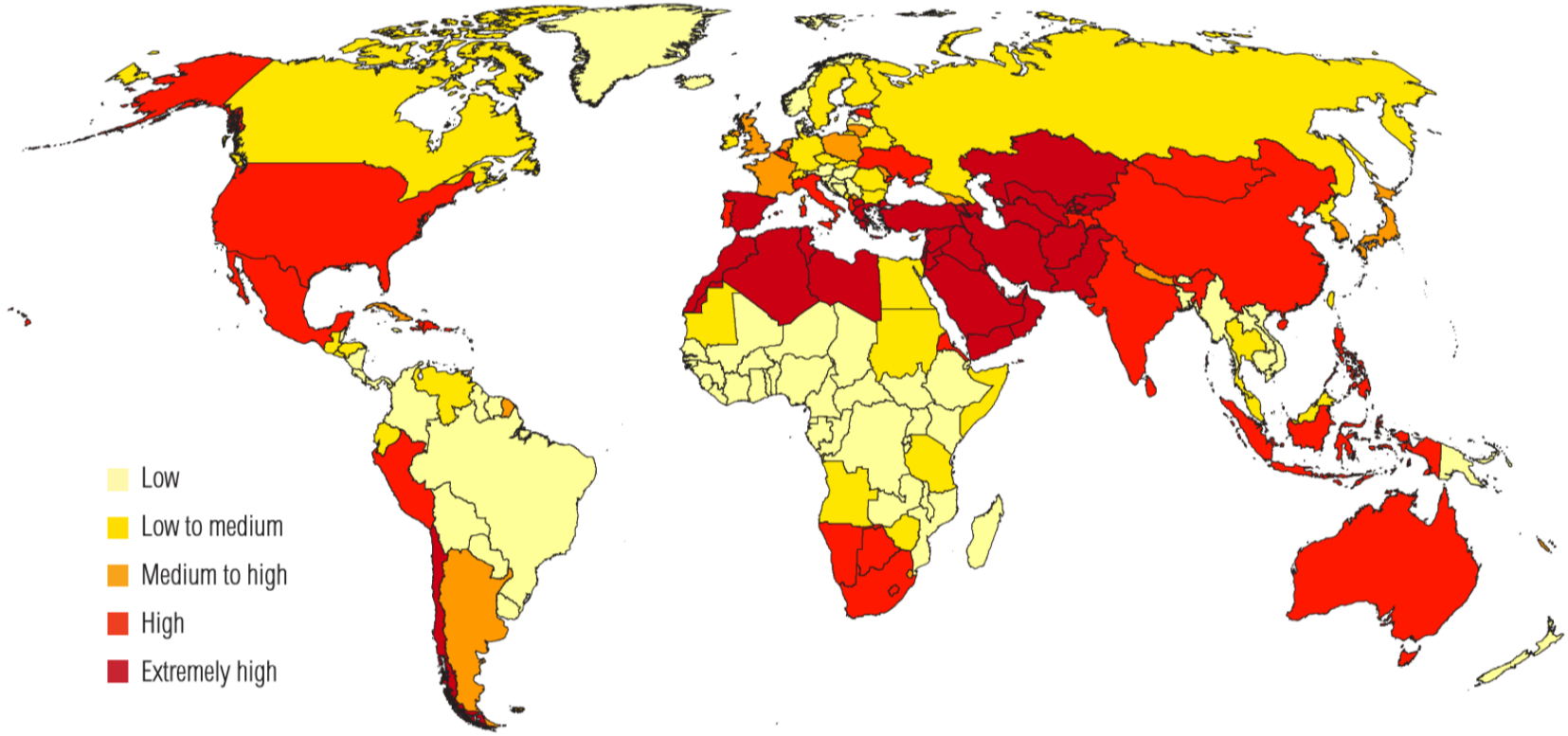

Figure 1.1 Country-level water stress in 2040 under business-as-usual policy regime [13]

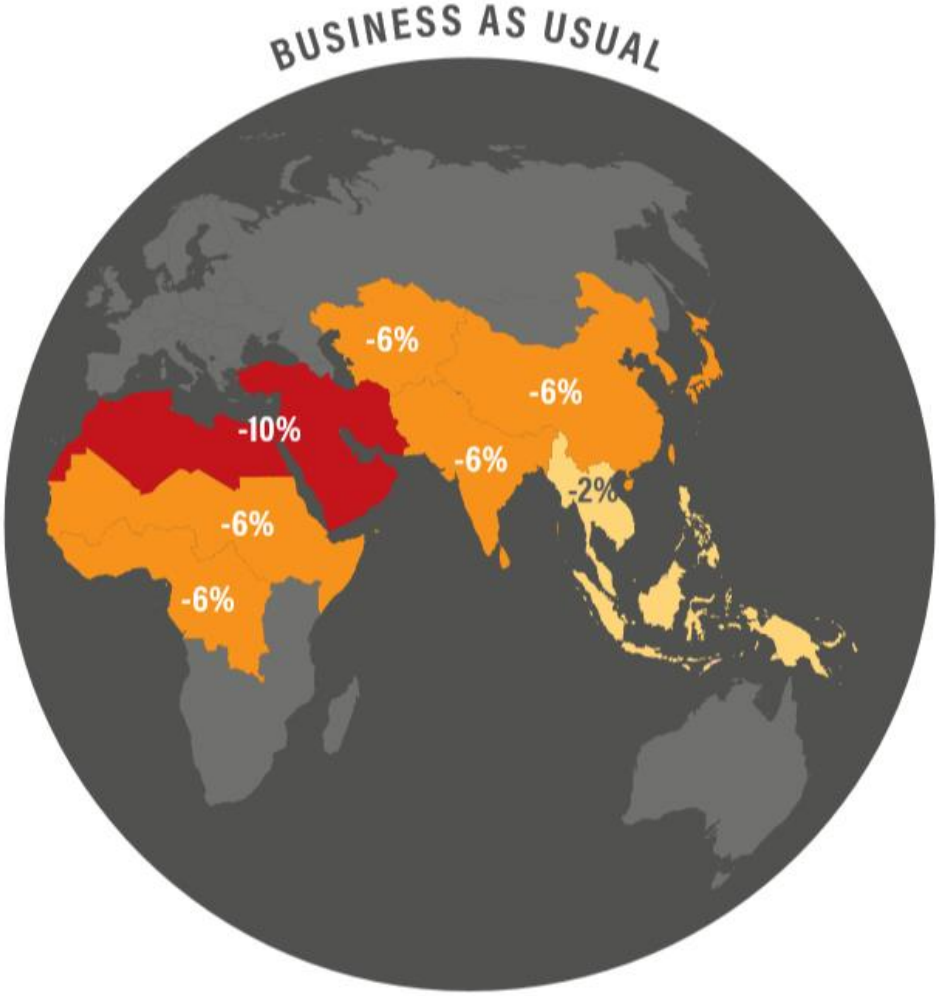

Figure 1.2 Projected variation in 2050 GDP due to water scarcity, under business-as-usual policy regime [17]

1.3 The Case of Saudi Arabia

Preceding sections have presented the relevant Worldwide stats on water and the global impact that water scarcity can impose in financial and societal terms. This section characterizes the water resources and their usage in the local context of Saudi Arabia.

According to the Food and Agriculture Organization (FAO), proven Saudi non-renewable groundwater reserves stand at 253.2 billion m^3 and possible reserves are approximated to be 705 billion m^3 [21]. With water withdrawals exceeding recharge, most of the fossil water reserves are suspected to have been exhausted over the past few years. In addition to that, the average renewable water resources per capita of Saudi Arabia stand well below the global averages [22]. This implies that the nation simply cannot rely on the natural water aquifers for its water needs. Water mismanagement by consumers and agricultural sector, has further depleted the kingdom's already scarce ground water reserves. Moreover, the regional temperature in some areas can reach up to 50 °C which produces hot and dry climate, adding to its water scarcity by seldom rainfalls (<144mm/year across the country). Despite all of this, nature's gift of excessive crude-oil has enabled Saudi Arabia to alleviate the situation by investing heavily in water-based technologies [23].

Water scarcity in the kingdom has found its resolve in desalination. Being able to afford a significant amount of capital, energy and distribution networks, Saudi Arabia has been quenching its water needs from the desalinated water. A sizeable volume of desalted water is produced for the municipal sector and is directed towards human consumption. As water desalination is responsible for supplying about 60% of the kingdom's water and around 70% of its drinking water demand [24]. With these stats, Saudi Arabia has the largest

production capacity of desalinized water [25]. According to the national Saline Water Conversion Corporation (SWCC), annual water production during 2018 was 1803.1 million m^3. Presently its recording the massive 5.6 Million m^3/day water outtake from its 33 nationwide plants [26]. Majority of these units are multi-stage flash (MSF) desalination plants, succeeded by the multi-effect distillation (MED) and Reverse Osmosis (RO) setups. Global distribution of desalination plants is shown in the figure 1.3 below, it is evident that the Arabian Peninsula in general and Saudi Arabia in particular holds a major share in water production capacity. Such huge operations (standing at 22 % of global production: SWCC) are made possible by continuous supply of conventional fuel and material resources. The kingdom operates 35 pumping stations, 286 water reservoirs and 7700km of distribution lines to its inland regions [27].

The Saudi Capital and a major metropolis, Riyadh meets over 50% of its water demands from desalinated seawater that is pumped from the Gulf coast to over an extended distance of 466 km. Such water-based services are expensive in terms of operating costs, especially when they are heavily subsidized, as local water tariffs contribute only 2.5% to revenues of the national water company (NWC) of Saudi Arabia. In Riyadh city, water demands are predicted to reach 1130 million m^3/year in 2020. Rising water services in the city would require $29 billion of financing by 2022, water treatment and distribution alone are expected to cost 45% of this total expenditure [28]. Meanwhile, it is obvious that such solutions are economically unsustainable and are able to meet the demands for as long as the enormous finances are available at hand. Water management in such megacities is largely dependent on the geological and geographical factors. In arid regions however, urbanization demands hefty investments in infrastructure which is an expensive affair.

Additionally, integrated water policies are expected to play a key role in the development of future-oriented sustainable economies [29].

Most recently, the negative environmental impacts of hypersaline concentrate have been raising concerns around the World. Brine is an essential by-product of desalination. When disposed in larger quantities, it is harmful to the aquatic life. Saudi Arabia alone shares 22.2 % of global brine production, an estimated 31.53 million m^3/day [20]. All of these figures demand an eco-friendly solution that is easy to deploy and can minimize the installation, operational and maintenance costs. Driven by these motives, the SWCC has involved itself in developing pilot plants, starting-off with several research collaborations to explore the better and economical solutions.

1.4 HDH Based Decentralized Seawater Desalination

The process development in humidification-dehumidification (HDH) water desalination is a vital link to the chain that seeks an energy efficient solution for clean water supplies. HDH desalination is a methodological imitation of the natural rain cycle. Over the past two decades, multiple research groups around the World have been trying to turn the HDH desalination, into an effective decentralized process by maximizing the product water output and minimizing the energy input [30]. Additionally, the flexible integration of an HDH unit with renewable energy resources has poured an integrative research into the subject matter. Solar and Geothermal energy resources have attracted considerable attention in this aspect [31].

1.5 Thesis Outline

- Chapter I highlights conventional desalination technologies, the present and future of water situation in the local and international perspective.
- Chapter II presents a detailed literature overview from numerous articles on humidification-dehumidification desalination, with different heating modes.
- Chapter III formulates mathematical representation and validation of modified air heated and dual heated humidification-dehumidification cycles.
- Chapter IV outlines the detail on instrumentation and test setup, experimental procedure and measurement uncertainties.
- Chapter V discusses experimental results and compares the extracted performance data with mathematical model.
- Chapter VI summarizes the study with conclusion, recommendations and the future scope.

1.6 Objectives

The objective of this study is to conduct a comparative evaluation of modified air heated and dual heated HDH systems by experimentation. Specific objectives are enlisted here;

- Mathematical modeling of modified air heated and dual heated humidification-dehumidification cycles.
- Experimental investigation of modified air heated humidification-dehumidification desalination cycle in a closed air-open water layout.

- Experimental analysis of air and water heated humidification-dehumidification desalination cycle in a closed air-open water loop.

1.7 Methodology

The study is formulated to assess the performance of humidification-dehumidification desalination cycles, in two different configurations. This section presents the methodology to achieve stated objectives, that are mainly associated to experimental analysis of the modified air heated and dual heated HDH desalination systems. The sequential order in which the study is executed is given as;

- A detailed literature review on maiden HDH desalination technologies is carried out to understand the basic working principles of humidification-dehumidification cycle and to explore the factors that are responsible for performance improvements.
- Modified air heated HDH cycle is inspected experimentally in CAOW layout at different mass flowrate ratios with fixed energy input and feedwater temperature.
- Air and water heated HDH cycle is experimentally investigated in CAOW layout by varying mass flowrate ratios at fixed feedwater temperature. Total energy input to cycle is distributed between the air and water streams to evaluate the impact of heat rate ratio on performance metrics of the system.
- Theoretical models of modified air heated and dual heated HDH configurations are formulated and then used to validate the outcomes of the experimental study.

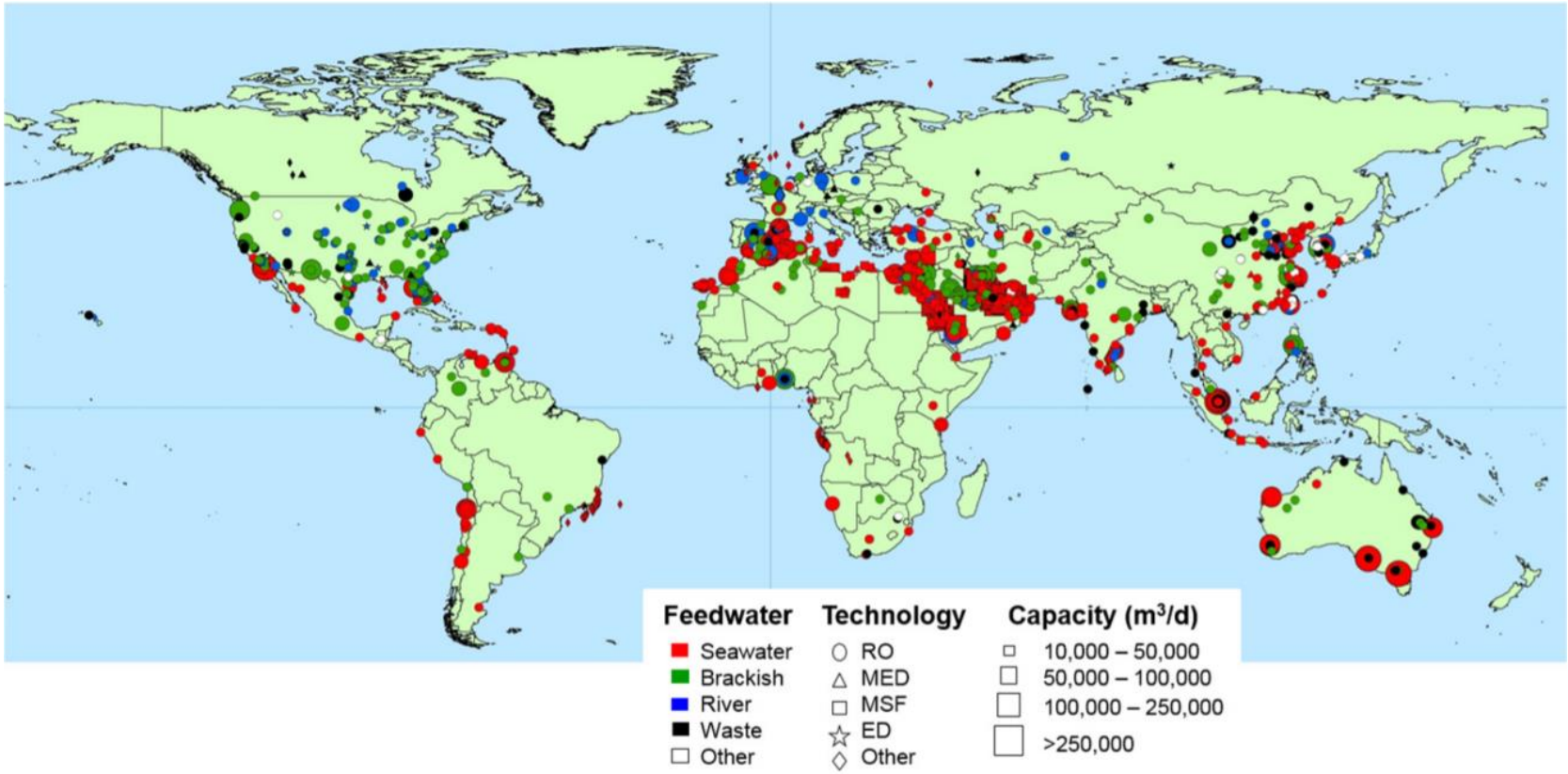

Figure 1.3 Distribution of large desalination plants by feedwater, technology type and capacity [3]

CHAPTER : 2

LITERATURE REVIEW

2.1 Humidification-Dehumidification Desalination

A typical HDH unit is composed of three primary subcomponents: a humidifier, an air or water heater and a dehumidifier. In the humidifier, a direct contact between air and incoming stream of saline water gives off humid air, which travels to the dehumidifier where water vapor is condensed, via indirect contact between air and incoming cold stream of saline water. This is a rather simple description of an HDH system. But when it comes to application, it can be put together in multiple configurations. Depending on whether the water or air stream is being heated, and if the streams leave the unit after a single pass or they are forced to circulate in a closed loop [32].

The subsystems in an HDH unit can be guided in different layouts to make unique operational cycles. Two conventional ways of classification are based on heating mode and cycle configuration. The former tells if air or water is being heated in the cycle and the later dictates flow of fluids through the cycle. For instance, when water circulates in a closed loop and ambient air is taken in through the humidifier and let out from dehumidifier, in an open space, it defines a closed water open air (CWOA) cycle. On contrary, when water goes in through dehumidifier and leaves from the humidifier as brine and air flows in a closed cycle, it delineates closed air open water (CAOW) cycle.

Furthermore, the HDH units can also be categorized on the basis of forced or natural circulation of air [30].

Working Principle: The functioning principle of a humidification-dehumidification desalination system is based on the point that air extracts some amount of vapor when it comes in contact with the seawater. In this mass exchange process, either air or saline water comes in as a pre-heated fluid. Since it is well-known that the air can carry greater quantities of vapor at higher temperatures. In the adjacent subcomponent (dehumidifier), part of this mixture gets in contact with the cooling coils and pure water is condensed out, while maintaining the air at humid condition. The cooling medium during condensation is the intake seawater, which gets preheated by recovering the heat energy. This heat recovery is of prime significance in controlling the operating costs of the unit. Beyond this energy retrieval, to compensate for the sensitive heat losses, an external heating source is still vital to operate the HDH cycle [33].

Technological review in this thesis is categorized on the basis of different modes in which fluid streams can be heated, in an HDH desalination system. Therefore, the succeeding sections would summarize some of the selected references on different HDH technologies.

2.1.1 Basic Water Heated HDH Cycle

Basic CAOW water heated HDH cycle starts its operation by pre-heating the saltwater in a dehumidifier and then heating it again in a water heater, which is then allowed to flow through a packing material in a humidifier where the heated brine comes in direct contact with the counter flowing stream of air. Carrier gas (Air+H_2O) then exits the humidifier and pass through a series of condensing surfaces in the dehumidifier, where it exchanges heat

with the incoming cold seawater. Humid air is simultaneously cooled and dehumidified owing to its temperature drop in the dehumidifier. The condensate is gathered at the exit of the dehumidifier as the product fresh water and air gets to recirculate through the humidifier and the cycle is repeated [32]. Figures 2.1 and 2.2 present the schematic diagram and psychrometric process of a water heated, humidification-dehumidification desalination system with a closed air-open water loop.

Eslamimanesh et al. [34] modeled the humidification and dehumidification process and concluded that heating the air at humidifier inlet and cooling water at dehumidifier inlet increased productivity. But increasing mass flow rate ratio in humidification column led to lower freshwater flowrate. Campos et al. [35] studied a CAOW-WH by mathematical modeling. They observed that the product water flowrate can be enhanced by increasing the heat absorption in the solar collector, increasing the humidifier height and decreasing seawater flowrate. The model also showed that the temperature of surrounding environment has little to no significant effect on the distillate flowrate.

Hermosillo et al. [36] investigated analytical performance of a water heated HDH cycle, operating in a CAOW loop and then verified the results experimentally. They showed that mass flow rates of air and water are the decisive factors in enhancing the amount of gained product water. Results also reported that an optimum mass flowrate ratio is needed to increase the productivity. Wang et al. [37] experimented with water heated photovoltaic (PV) driven HDH system where water heater, pump and blower were energized by solar power generated on the PV panels. They recorded an increase in water evaporation by increasing the temperature of brackish water. The study also recorded an increase in

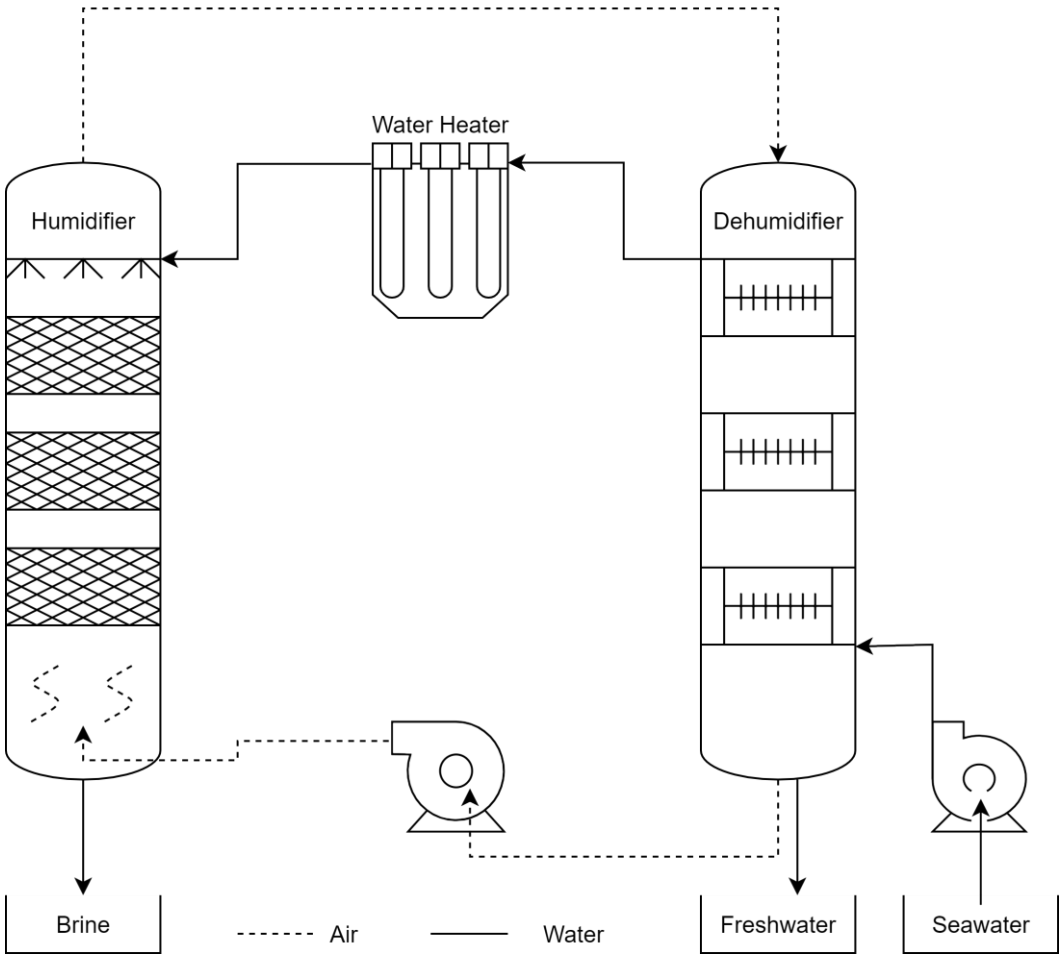

Figure 2.1 Schematic layout of the basic Water Heated HDH Cycle

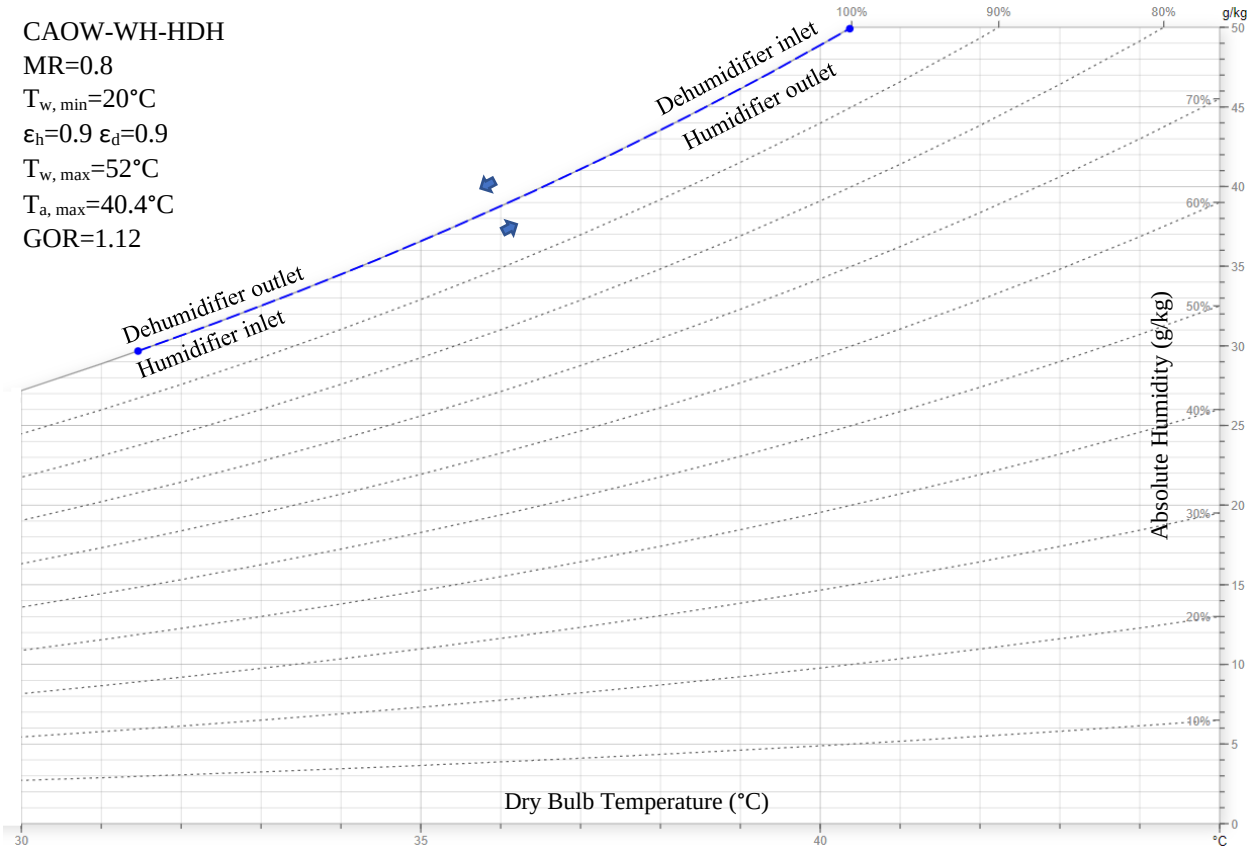

Figure 2.2 Representation of CAOW-WH-HDH cycle on psychrometric chart

condensation with decreasing cooling water temperature. Moreover, high freshwater produce was reported with the forced convection layout than the free convection mode. Hallaj et al. [38] studied a closed air cycle with an indoor and outdoor configurations by replacing the water heating unit with an electric heater and flat plate solar collector, for night and day operations, respectively. They witnessed an optimum value of mass flowrate ratio (MR) that maximizes the product water flowrate. Also, better performance was reported in the forced circulation case when maximum temperature of the cycle was low whereas the natural circulation was deemed suitable for higher top cycle temperatures. Their analysis showed that the outdoor units perform better when they are made of lighter materials. Otherwise, sizeable portion of energy received during early sunlight hours would be consumed as sensible heat to warm the component surfaces. Use of electric heating during the night operation was found to alleviate the issue of material selectivity by keeping the unit at relatively high temperatures, allowing it to operate for an extended period of 24 hours. Amer et al. [39] investigated the effect of different operating conditions and packing materials on the system productivity, experimentally. The configuration with wooden slates packing and forced circulation achieved maximum productivity of 5.8 liters/h. They also deduced that low water temperature at dehumidifier inlet leads to higher productivity, when forced circulation is used. Kang et al. [40] performed a parametric and experimental study on a closed air loop, two staged humidification and dehumidification water heated desalination cycle. They recycled latent heat of condensation by heating seawater in low and high temperature stages of the condenser. Additionally, residual brine at high temperature evaporation stage was reutilized by adding heat to it in the solar collectors therefore, recycling the heat of brine as well. Their system recorded the highest values of

72.6 kg/h and 2.44 for productivity and GOR, respectively. Zubair et al. [41] thermodynamically analyzed a closed air open water WH-HDH cycle by using an evacuated tube solar collector as water heater. Feasibility analysis for multiple locations in Saudi Arabia was performed. With specified design parameters, the system was capable of producing 16,430 liters of freshwater annually in Dhahran, SA. The cost of distilled water was observed to be ranging between 0.032 to 0.038 $/liter.

Over the last few decades, multiple hybridization strategies for HDH systems have also been analyzed and studied in detail to realize several conceptual designs. A detailed theoretical model of an HDH system integrated with a heat pump (HP) unit was presented by Lawal et al. [42]. They studied the performance metrics of a closed air open water cycle. Their model reported a maximum GOR of 7.63 at an effectiveness of 80% and mass flowrate ratio of 1.63, for the water heated cycle. This study was then further extended to include an experimental investigation with an open air-open water (OAOW) water heated HDH-HP cycle [43], where the proposed unit was able to produce freshwater and space conditioning, simultaneously. Their analysis showed that the system is capable of producing 287.8 liters/day of distillate and 3.07 kW of cooling load. Ghaebi et al. [44] proposed a trigeneration system with three working components consisting of solid-oxide fuel cell/gas turbine, heat recovery steam generator and a water heated HDH unit. They concluded that the trio can generate 1605 kW of electricity, 370.2 kW of heating load and 345.7 kg/h of distilled water for a small district. Zubair et al. [45] performed a comparative analysis on the water heated OAOW and CWOA systems with and without heat recovery, respectively. Their investigation illustrated that the CWOA water heated system with heat recovery from brine showed 100% better performance over the OAOW water heated cycle

without heat recovery. Results showed that the cost of product water from the system with brine recirculation was far less than the system that was not recovering heat from the brine. They also deduced that the influence of the dehumidifier effectiveness on system performance is greater as compared to the humidifier effectiveness. Narayan et al. [46] studied a novel HDH-RO hybridization driven by thermal vapor compression (TVC) using high temperature steam. They observed that high pressure of steam and an effective thermal vapor compression unit are the keys to the minimum energy consumption. The performance of this on-design system was shown to be competitive with the conventional MED and MSF plants for medium-scale production.

2.1.2 Basic Air Heated HDH Cycle

Basic air heated CAOW cycle heats the air to a maximum temperature, before it enters the humidifier, as shown in the figure 2.3. As the air passes through the humidifier, it gets saturated and its temperature drops. Further on, it gives away the vapor on interaction with the cooling surfaces and is heated again after leaving the dehumidifier [33]. However, there is a drawback associated to this kind of setup, as heating air before the humidifier causes the air to get cooled in the humidifier, eventually it results in reduction of the amount of heat that is recovered in the dehumidifier. Recent simulations have showed that the system performance for this kind of cycle is only marginally better than a solar still. One of the reasons behind is higher energy consumption when compared to the WH-HDH cycle. Partly, because water is being heated by the hot incoming air in humidifier and subsequently this energy cannot be recovered from the outgoing water stream, unless it is recirculated. To attenuate this situation, Chafik [47] devised a multistage cycle, where the

air was heated and humidified at first and then heated further in another stage to humidify it again. Increased humidity of air was expected to increase the production of fresh water. Chafik [48] achieved an increased exit humidity of air through four-stages of heating and humidification. But overall performance of the system improved fractionally, again the reason behind was the input energy that has to be supplied to the air for heating, at every stage. Not to mention the issue of air getting cooled in the humidification process, that remained intact during the operation.

Yamali and Solmus [49], theoretically investigated an open air closed water HDH desalination system. The air was heated before humidification using a double-pass flat plate solar air heater. Schematic of the system devised two separate loops for water circulation; a closed loop for humidifier where brine was recirculated with make-up seawater and another open loop for the dehumidifier where water flowed in a single pass to condense out vapor from the moist air. An increase in system productivity was witnessed by increasing the mass flowrates of inlet air and water stream to the humidifier. Moreover, increasing the inlet water temperature to humidifier and water mass in brine/make-up seawater storage tank lead to better system performance. Authors reported enhanced distillate production by increasing the water flowrate in condenser and lowering its temperature. Likewise, increasing the area of solar air heater gave higher product water flowrate. Mathematical modelling also illustrated that using double pass solar air heater increased freshwater productivity by 8% as compared to the case when single pass solar air heater was used. Mohamed and Minshawy [50] also proposed an air heated cycle with a common separation between the humidifier and dehumidifier, a parabolic trough solar collector was placed before the humidifier as air heater. System analysis showed that the

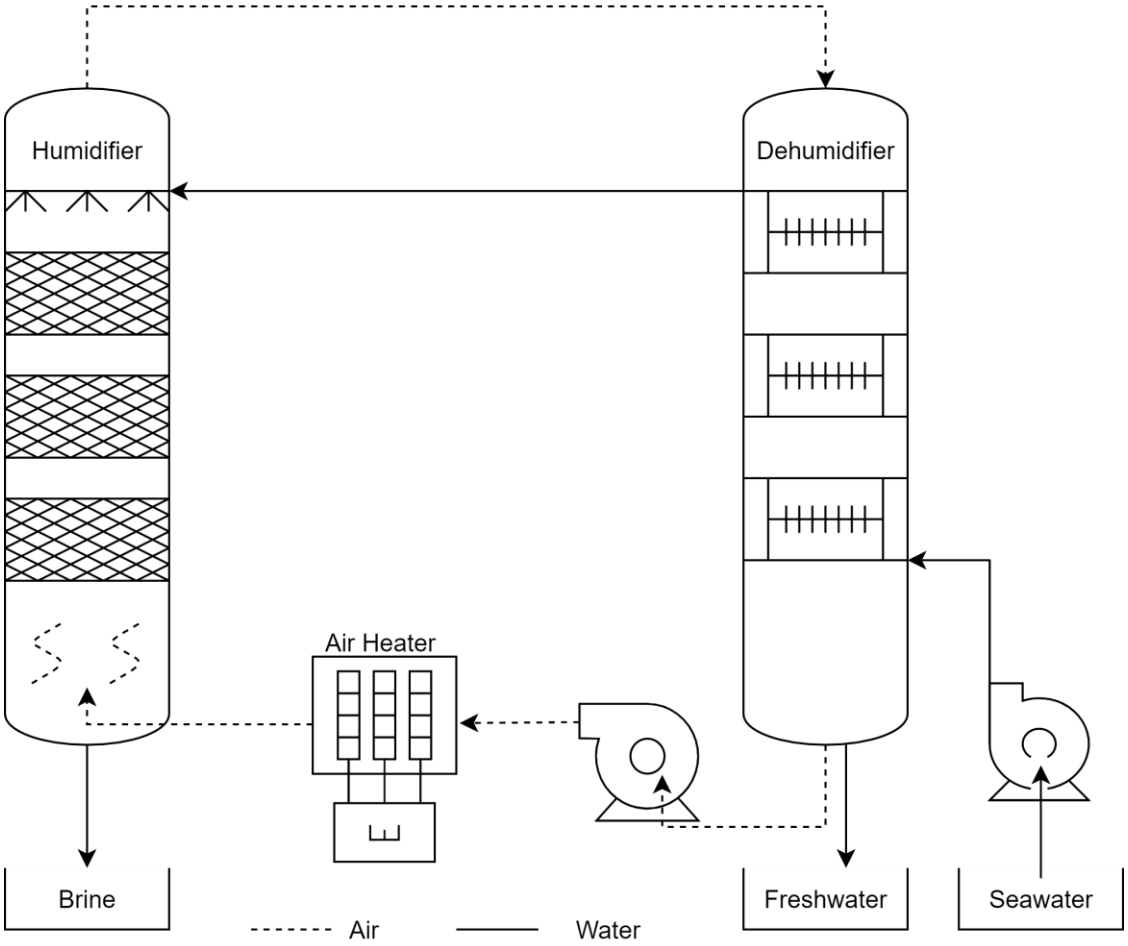

Figure 2.3 Schematic layout of the basic Air Heated HDH Cycle

duration of freshwater production could reach 42% of the daytime during summers in Helwan-Cairo, Egypt.

Antar and Sharqawy [51] performed an elaborated experimental study on a single stage and two stage air heated, closed air closed water (CACW) HDH desalination system. Solar collectors were used to heat the air before humidifier(s). The study reported pressure drop and heat losses in pipelines and consequently decreased the length of fittings to alleviate the problem. The authors have also reported a significant decline in the air temperature at humidifier's exit, due to the effect of sprayed water in humidifier that extracted the heat from incoming hot air. Their experimental setup recorded freshwater productivity of 3.5 liters/day with single stage and 6 liters/day with 2-stage air heated HDH system.

In another experimental evaluation, Houcine et al. [52] designed a pilot plant with single heating-humidifying-heating stage. Blower was used to circulate the air in a closed loop and solar collectors were employed to elevate the temperature of air before humidification. They used pad humidifier with three corrugated cellulose cassettes arranged in series and a finned-tube type dehumidifier where cooling medium for air was the incoming seawater. Three additional finned-tube heat exchangers were employed to preheat the seawater, being injected to the humidifier. The water was flowing in an open loop though dehumidifier and in a closed loop through heat exchangers. The freshwater however was collected from all four condensers. Experiments were performed for over an extended 6 months period. Temperature of air before dehumidification reached as high as 108°C with solar noon during the June (in Tunisia) which caused deformation of the corrugated polycarbonate material in solar collectors. Moreover, the condenser was able to heat the exiting seawater to 58.5°C when the ambient temperature was 36.5°C, air flowrate was 1500 kg/h and

seawater flowrate was 1000 liters/h. They concluded that the stream temperatures and productivity of water was strongly dependent on the solar irradiation. During the month of June, they collected an average 310 liters/day of distillate product water. Furthermore, the cost of freshwater was reported to be relatively higher due to expensive system components.

Ben Amara et al. [53], from the same research group conducted a preceding optimization study to analyze the experimental performance of the air heated cycle. They reported that increasing the mass flowrate ratio increased absolute humidity through the humidifier and then further increase in water flowrate, decreased it. This was attributed to the thermal capacity of air which was sufficient to heat water stream and exchange mass, at first. But then as air reached saturation the excessive seawater would have started to cool the moist air, decreasing its absorption capacity, temperature and eventually leading to decreased absolute humidity. The authors suggested an optimized water to air mass flowrate ratio of 45%. Number of heating-humidifying stages were advised to be 5 under system conditions. This estimate was based on the fact that with each heating humidifying stage the aperture between inlet and outlet absolute humidity through humidifier, shortens. Therefore, after a specific value of inlet absolute humidity to humidifier, the absorption capacity of moist air decreased, and further heating and humidification was rendered uneconomical.

Li et al. [54] experimented with an open air closed water, air heated HDH desalination system. They designed a novel evacuated tube solar air heater to suit the system requirements. Pad humidifier with cellulose packing material and finned-tube dehumidifier (each with separate water loop) were used as the main system components. Results indicated that the moist air stream at the exit of humidifier can reach up to 42°C with 97%

relative humidity, when the sprayed water temperature is elevated from 9°C to 27°C. They deduced that high air humidity and temperature at humidifier outlet can significantly improve the freshwater production without changing the air flowrate and cooling water temperatures.

2.1.3 Modified Air Heated HDH Cycle

In the present study, field of interest is the modified air heated (MAH) cycle, the conventional air heated cycle has been out of the picture due to its inefficient operation. But the practical significance of heating air has kept the research interest intact in the domain of air heated HDH units. In a CAOW modified AH cycle, saturated air-vapor stream from the humidifier enters an air heater, where it gets heated to the top cycle temperature and then condenses out the entrapped vapor in dehumidifier. The incoming preheated water stream from dehumidifier simultaneously heats and humidifies the air flow, in humidifier. Heat recovery is improved in this cycle as the energy added to the air stream is recovered in the condenser when it heats the incoming seawater to an elevated temperature. Additionally, water enters hotter than the air in humidifier which ensures an effective heat and mass transfer through the component. Layout of a closed air open water and modified air heated HDH system is illustrated in the figure 2.4 and the psychrometric process is shown in figure 2.5. This study will further analyze the performance dynamics of a modified air heated cycle.

Narayan et al. [55] performed a comparative study on the CAOW-MAH humidification-dehumidification desalination cycle. They reported the MAH cycle to be 300 times more

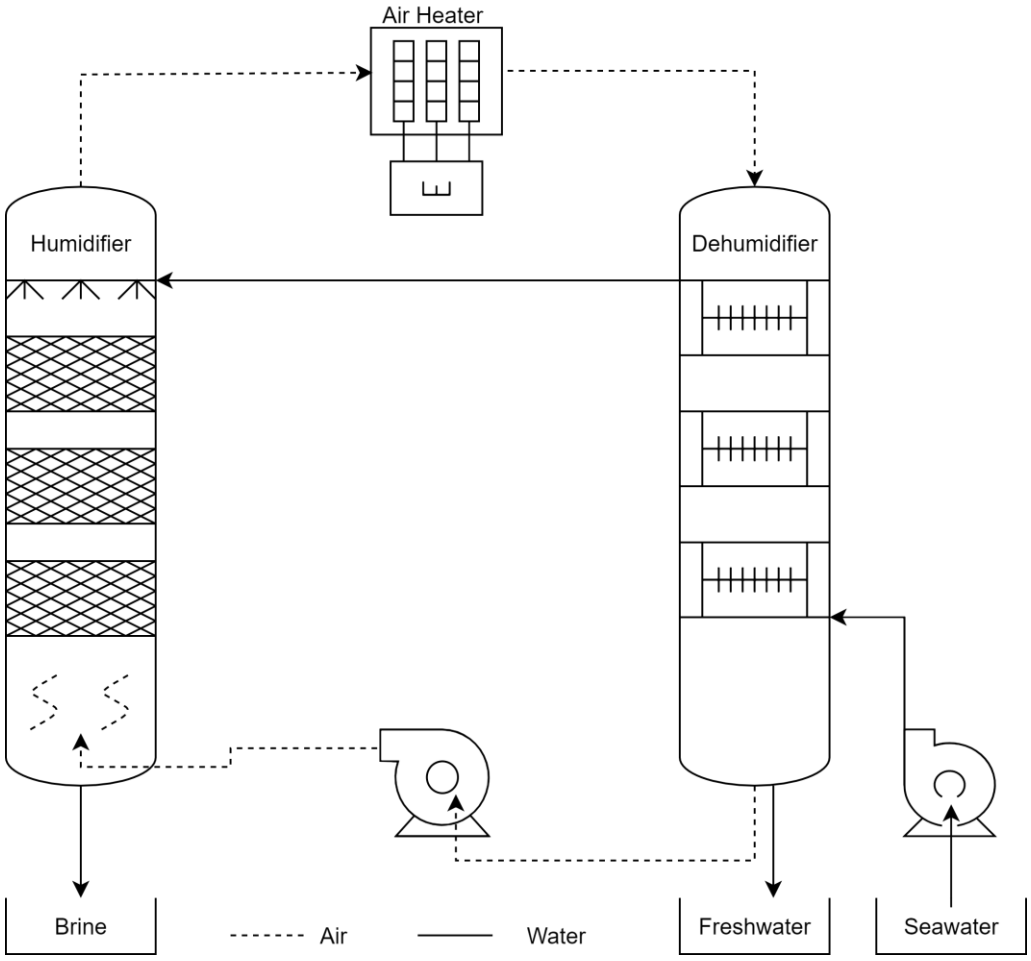

Figure 2.4 Schematic layout of the modified Air Heated HDH Cycle

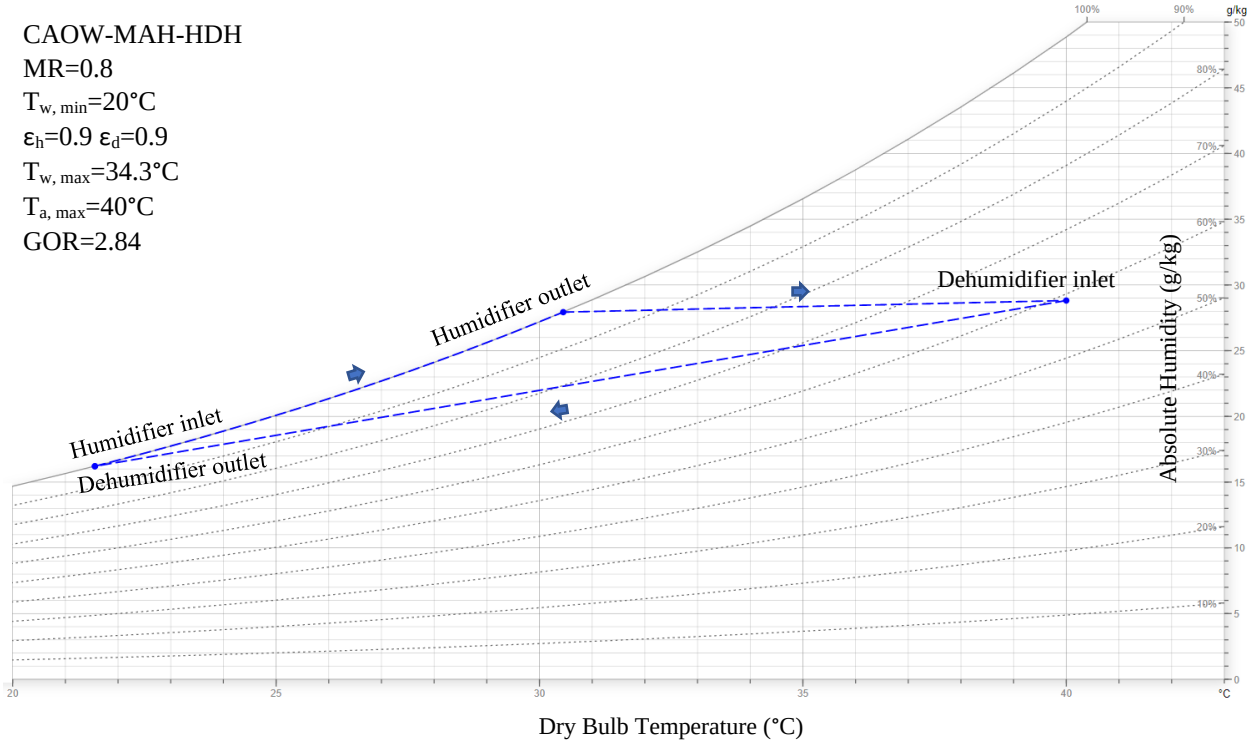

Figure 2.5 Representation of CAOW-MAH-HDH cycle on psychrometric chart

efficient than the basic AH cycle and 25% more effective with respect to performance when compared with the WH cycle. It was deduced that a balanced dehumidifier is of greater significance to the MAH cycle than a balanced humidifier. Their analysis recorded that varying the humidifier and dehumidifier effectiveness values have near to similar effect on the performance of the modified air heated cycle.

Sharqawy et al. [56] investigated multiple design parameters of a CAOW modified air heated HDH desalination cycle, analytically. Their study showed that greater values of the humidifier effectiveness results into a higher degree of increment in the gain output ratio (GOR). However, increasing the dehumidifier effectiveness proved to be significant for GOR at higher humidifier effectiveness only. Additionally, the percentage recovery ratio (RR) increased by increasing both components effectiveness. Furthermore, it was observed that the GOR increased by increasing the maximum cycle temperature only if the initial seawater temperature is also kept low. Otherwise, dehumidification of humid air became less effective when inlet seawater temperature was high. On the same note, RR was reported to decrease with increasing minimum temperature and increasing maximum temperature of the cycle. Authors also devised a number of transfer units (NTU) model to approximate the mass flowrates, heat input and component sizes from desired values of performance parameters (GOR, MR, RR). Another significant conclusion was that an optimum MR for the modified air heated cycle is always less than 1.

He et al. [57] did a parametric study on a closed air-open water modified air heated cycle. The carrier gas was heated after humidification in plate heat exchangers (PHEs), using recovered waste heat. The authors used specific entropy generation of individual components to analyze the viability of theoretical setup. Under system conditions, it was

concluded that the case of maximum GOR at modified heat capacity rate ratio (HCR_d) of 1 was not practical due to the negative specific entropy generation in dehumidifier. Using fixed effectiveness model, it was deduced that increasing humidifier effectiveness (by keeping other system parameters the same), lead to an increased gain output ratio (GOR), decreased minimum heat transfer rate and heat transfer area of plate heat exchange. An effective humidifier would emit the humid air at a higher temperature, which consequently resulted into a decrease in the required waste heat input and thus higher GOR. Similarly, increasing the effectiveness of dehumidifier caused the seawater to leave at a higher temperature and eventually resulted into better system performance. The study also concluded that decreasing the operating pressure and increasing the initial seawater temperature marked an increase in the system performance. In another study conducted by the same research group [58], it was found that pressure drop in PHEs has limited impact on the performance of a modified air heated cycle. They also listed that the freshwater production drops due to decrement in the humidity ratio at humidifier's exit which was attributed to decrease in the corresponding air outlet temperature in humidifier. Meanwhile, the humid air temperature at the exit of evaporator fell due to increment in the seawater flowrate.

Sulaiman et al. [59] conducted a detailed analysis to compare the basic air heated and modified air heated HDH desalination cycles in an open air open water configuration using the parabolic trough solar collectors as air heater. It was shown that the monthly average GOR value for modified air heated cycle (4.7) was considerable higher than the basic air heated system (1.5). Due to their steady performance, parabolic troughs were recommended for the consistent operation of the cycle in Dhahran, Saudi Arabia. Under

their design specifications, averaged daily freshwater productivity was recorded to be 238 kg/day for the basic system compared to 954 kg/day for the modified air heated system, based on 8 h/day of production time. Based on their thermodynamic analysis, the authors concluded that the post-humidification air heating was much better in terms of performance and productivity as compared to the conventional pre-humidification air heating.

Lawal et al. [42] theoretically investigated the performance of a closed air open water MAH humidification and dehumidification cycle powered by heat pump. Evaporator of the heat pump was used to decrease the temperature of inlet seawater and the respective condenser was utilized in heating the air after humidification. The study noticed reduced energy requirements for the cycle because moist air was easier to heat than water due to the difference in their respective thermal capacities. For specified conditions, they reported the GOR of 8.88 at an optimum MR of 0.63 in the case of MAH cycle which was relatively higher than that of the WH cycle (GOR of 7.63 at MR_{opt} of 1.7). Moreover, increasing the dehumidifier effectiveness recorded greater improvement in the GOR as compared to increasing the humidifier effectiveness. Meanwhile, increment in both components effectiveness posed an improvement in performance of the system. They also observed that for fixed components effectiveness and seawater flowrate, increasing the MR resulted into higher maximum cycle temperatures. For fixed MR however, decreasing the water flowrate lead to an increase in the maximum temperature. Finally, the study concluded that freshwater cost for the modified air heated cycle was far less than the water heated cycle.

He et al. [60] analytically examined a CAOW hybrid desalination plant, cogenerating the power and desalinized water simultaneously. Their model integrated the organic rankine cycle with an air heated HDH system. Discharged hypersaline from evaporator was routed

to the boiler and then heated brine was utilized to vaporize the working fluid in the rankine cycle. Residual thermal energy from the concentrated brine was recuperated by the seawater before it enters the dehumidifier. Air in the cycle was heated after humidification. Numerical analysis resulted into the peak distillate productivity of 19.53 kg/h and the gain output ratio of 2.82 from the HDH system, power cycle output peaked at 6.04 kW for MR of 9. They deduced that the desired freshwater production and power generation have to be optimized based on the realistic data, because both output variables showed conflicting behavior with increasing MR.

Qasem and Zubair [61] simulated a modified air heated HDH system, integrated with an adsorption cycle, in two different suggested schemes. First layout pre-cooled the seawater in evaporator, before it entered the dehumidifier and there was no subsequent cooling effect associated to the hybrid system. Therefore, the product was freshwater only. Meanwhile, second scheme utilized saline water to cool the adsorption bed and cooling effect generated by the evaporator was made available. Thus, freshwater and space-conditioning were the products in this later case. Under similar conditions, they reported fresh productivity of 22 kg/h with GOR of 8 for the first system where the seawater got cooled in evaporator. However, these figures slightly decreased for the system where seawater was used to cool the adsorption bed. The authors also noted that the distillate production of modified AH-HDH cycle, without hybridization was 69 kg/h but the GOR was low. Reason cited was the heat distribution that was focused solely for air in this case. The overall cooling effect of 0.45 (COP) was generated by the second system.

2.1.4 Air and Water Heated HDH Cycle

An HDH system where both the fluid streams, that is air and seawater are heated simultaneously, is termed as the dual heated cycle. Performance dynamics of such kind of cycle, are still to be explored in detail. Till now, we understand that dehumidifier balancing is critical, if minimal entropy generation is required. The entropy in the dehumidifier of a modified air heated cycle is generated by the difference between maximum temperature (of air) T_{max} and minimum temperature (of seawater) T_{min}. In addition, the entropy generation in dehumidifier of a WH cycle is much less than that of an air heated cycle. Despite better performance, the entropy generation factor, worsens the case for air heated cycle [62]. With dual heating, in suitable proportions, entropy generation can possibly be minimized. This variation in system could prove beneficial to the HDH cycle's integration with renewable energy resources, as well. Figure 2.6 presents a CAOW, water and air heated HDH system where the water is heated before humidification process and the air is being heated after its humidification in the humidifier. Its psychrometric representation is similar to the MAH cycle.

Efaf and Ameri [63] thermodynamically studied an open water dual (air and water) heated HDH desalination system. This cycle featured a pre-humidifier water heating and post humidifier air heating. Air was introduced to the cycle in different configurations; open, semi-open and closed loops. These configurations were investigated in detail to analyze their impact on the system performance and design parameters. At higher ambient temperatures, they suggested the use of closed air loop for optimal performance. It was concluded that the dual heated cycle will achieve maximum performance when the rate of

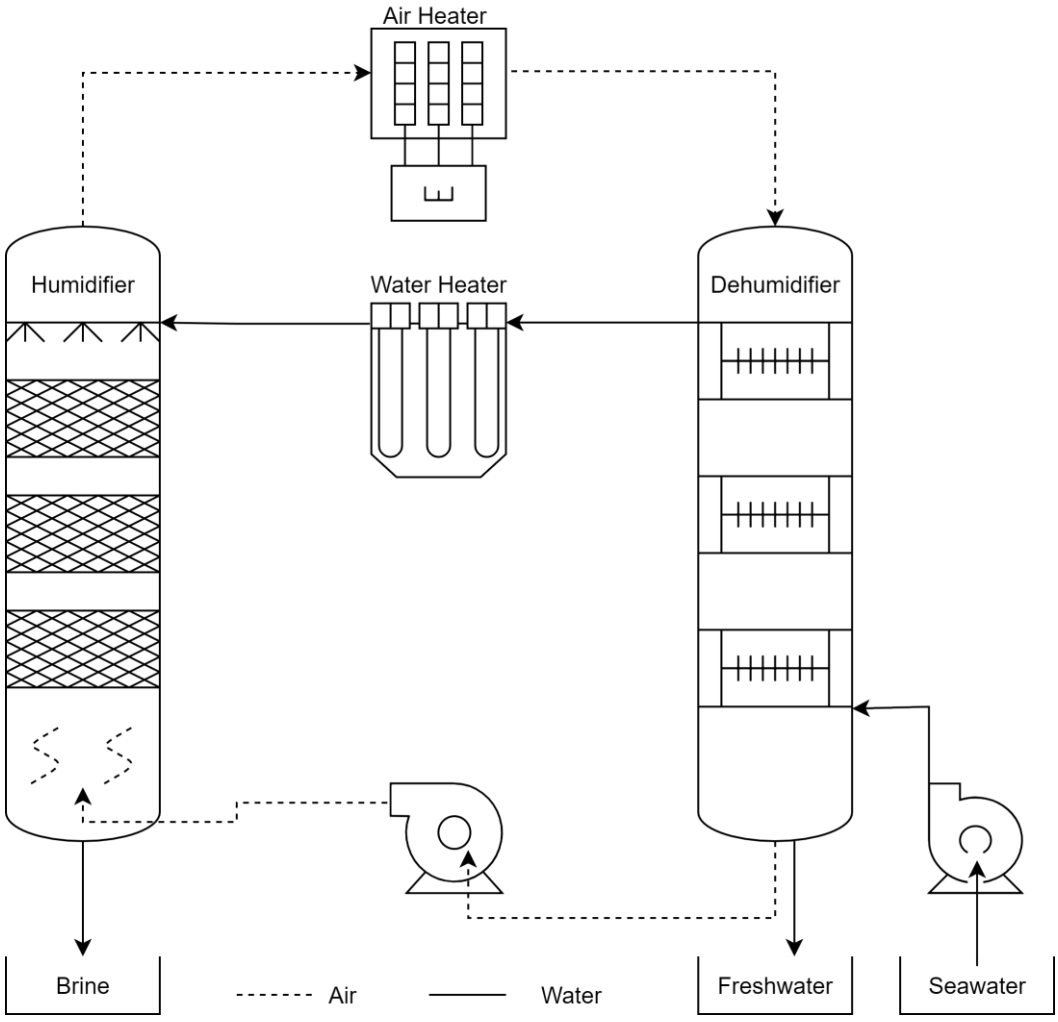

Figure 2.6 Schematic layout of the Air and Water Heated HDH Cycle

energy added to both, air and water streams become almost equal. Furthermore, theoretical model showed that the dehumidifier of an HDH cycle is a major contributor towards system irreversibility. Also, the total specific entropy generation in dual heated system was found to be minimum for either completely open or closed air loops.

Nafey et al. [64] numerically examined an HDH system. The system possessed concentrating solar collector as water heater and solar flat plate collector as air heater. Both streams were heated before the humidification process. Air stream was circulated in a closed loop. However, the water stream was made to flow in two different loops; an open loop for dehumidifier and another closed loop passing through the cooling tower, water heater and brine storage tank. Solar irradiation, air flowrate, seawater and cooling water flowrate were recorded as the factors affecting the overall productivity. Ambient temperature was found to be the least impacting factor for variations in freshwater flowrate. Experiments were conducted by the authors in Suez, Egypt to verify the numerical results [65]. Distillate flowrate among other factors, was also found to be affected by the seawater temperature at humidifier's inlet. They also found that increasing the inlet temperatures of both streams in humidifier increases the vapor content entrained by the air. With specific system design, the setup achieved highest experimental productivity of 1.2 kg/h in the month of July.

Yildirim and Solmus [66] performed a parametric analysis on the solar powered, dual heated open air HDH system for Antalya, Turkey. In system layout, humidifier recycled the water from a storage tank via flat plate water heater whereas the condenser operated the cooling water in an open loop. Double pass solar air heater was used to heat the air before humidification. This study outlined the significance of an optimum air flowrate at

which the highest freshwater production can be achieved. Further, they showed that to maximize distillate flowrate the angle of solar collector should be aligned with angle of latitude at that location. Finally, they concluded that the dual heated configuration increased clean water productivity by 5 to 8 times when compared with the basic air heating layout, due to higher evaporation rate.

Rajaseenivasan and Srithar [67] experimentally investigated a humidification-dehumidification desalination setup energized by using a dual purpose solar collector which was capable of preheating both air and water simultaneously. Carrier gas was made to circulate in an open loop and both component heat and mass exchangers were running two separate closed water loops. Storage tank and cooling water tank were used for the humidifier and dehumidifier, respectively to recycle the water. Increasing the flowrates of air, seawater and cooling water reported an increase in the freshwater productivity. Distillation was also improved by increasing the air and water temperatures in the evaporator. Overall efficiency of the system reached 68% on the utilization of semicircular concave air turbulators inside the solar collector's airfield. Moreover, the highest distillate production rate of 12.36 and 15.23 kg/m^2.day was witnessed without and with concave turbulators, respectively.

Kabeel and Said composed a detailed numerical [68] and an experimental [69] analysis on a solar hybrid, open air, dual heated HDH desalination system adjoined with a flashing chamber. Supporting system components included a mixing chamber, storage tank, collection tank, helical heat exchanger and a condenser to collect flashed vapor. A solar flat plate collector was utilized as a water heater to heat seawater in a helical heat exchanger via nanofluid. Air was heated using another flat plate collector before the humidifier. They

used a packed bed humidifier and a shell and tube type dehumidifier. Experimental results depicted an increase in production by increasing the water temperature and air flowrate. Efficiency of humidifier increased at higher water flowrates and overall performance of the unit was reported to be affected by the variations in cooling water temperature. As per the local operating conditions of Tanta, Egypt, the authors recorded maximum clean water production of 41.8 kg/day.

Yuan et al. [70] conducted an experimental study on a pilot plant located in Dezhou, China. They resourced a comparatively larger solar fields of $100m^2$ for solar air collectors and $12m^2$ for solar water collectors. Pre-humidifier air heating was practiced using an open-air loop. Humidifier and dehumidifier utilized two separate and closed water loops. Water from a cooling pond was recirculated in the condenser whereas the constant temperature tank and water heater recycled the saline water stream for humidifier. Solar insolation was rated as a deciding factor for system temperatures. During October, when solar radiation was 760 W/m^2 the solar airfield recorded an outlet temperature of 118°C. Additionally, the productivity of system was reported to increase with increasing solar irradiation. With an average radiation value of 550 W/m^2, authors reported that the setup could reach freshwater production figure of 1000-1200 liters/day. GOR value ranged between 2 to 2.3 due to high dependency of the system on availability of the solar energy.

Zhani and Bacha [71] experimented with a closed air open water dual heated desalination plant, under the climatological conditions of Sfax, Tunisia. Air and water streams were heated using solar collectors. A pad-type humidifier with viscose packing was used as a cooling tower. Distillation module made of an evaporator/air-humidifier and a condenser/dehumidifier, was deployed to collect freshwater. The components of

distillation module had no separation between them. Saline water, after gaining heat in the dehumidifier was further heated in the solar water collector and it was then parted between the humidifier and evaporator. Meanwhile, the dehumidified air coming out from condenser was allowed to get humidified by exchanging heat and mass within the evaporation chamber. Moist air from evaporation chamber was heated again in the air heater and then humidified in the humidifier. Their prototype in a way realized the multi-effect humidification and dual heating processes, simultaneously. Results showed high solar irradiation during the month of July which eventually turned to high terminal temperatures and maximum productivity. Variations in ambient temperature were reported to be ineffective towards system performance. The system was capable of producing approx. 20 liters/day of freshwater.

From the presented technological overview, it is clear that the previous work on the modified air-heated humidification-dehumidification desalination is largely theoretical. Most of the experimental work on the air heated HDH cycle was conducted on the basic configuration that heats the air before humidification. Furthermore, published articles that discuss air and water heated cycles, have never configured it in a closed air-open water loop with air being heated after the humidification. This gap in the present literature stimulated the need for an experimental study on the modified air heated and dual heated HDH cycles.

Few additional technological references that explain the performance of HDH systems in conventional and modified layouts, are summarized in the table 2.1 here;

Table 2.1 Summary of relevant published work on humidification-dehumidification desalination				
Heating Mode	Max. Yield	Highlights	Scope	Reference
Water Heating	0.013 kg/s	Solar collector used as water heater. Closed air and open water loop used natural convection to circulate the humid air. Heat and mass transfer coefficients from previously conducted experiments were modeled to achieve viability.	Analytical	Farid et al. [72]
Water Heating	505 liters/day	Humidifier and dehumidifier were located in a thermally insulated chamber which used natural convection for circulation of air. The system proposed a solar collector field of $38m^2$ as water heater and a thermal storage tank of $2m^3$ to increase the online duration of plant.	Analytical-Experimental	Holst et al. [73] [74]
Water Heating	8 liters/m^2.day	Closed air open water HDH system with optional electrical or solar heating. Forced air circulation showed significant improvements at the low cycle temperatures.	Experimental	Hallaj et al. [75]
Water Heating	6.2 kg/m^2.day	Water vapor from boiler was used as heating source. Humidifier of the OACW cycle was packed with honeycomb material. An optimum mass flowrate existed under the given conditions to attain maximum productivity.	Experimental	Dai and Zhang [76]
Water Heating	19 liters/day	Distillation module containing evaporator and condenser was separated using the chamber wall. Setup was designed and modeled to be integrated with either solar or geothermal energy. System utilized a closed water loop configuration with natural draft of air.	Analytical-Experimental	Bacha et al. [77]
Water Heating	3.3 kg/h	CAOW utilized coiled heat exchanger as condenser and metal packed cooling tower as evaporator. 2.4 kW of electrical energy provided water heating and it achieved maximum temperature of about 62°C.	Analytical-Experimental	Moumouh et al. [78]

Heating Mode	Max. Yield	Highlights	Scope	Reference
Air Heating	0.17 kg/m^2.h	An open air-open water desalination system was tested by heating the air before humidification in a solar collector. Variations in the inlet air temperature were dependent on the solar radiation. Exergy efficiency increased by decreasing inlet air temperature, increasing humidifier diameter and decreasing humidifier length.	Analytical-Experimental	Nematollahi et al. [79]
Air Heating	4.63 kg/h	An HDH system integrated with the conventional vapor compression air-conditioning unit was studied. Recovered hot air from condenser was used as carrier gas in the humidifier and in dehumidifier a cold-water circuit extracted freshwater out from the moist air. Productivity was highly dependent on the ambient conditions.	Analytical-Experimental	Santosh et al. [80]
Air Heating	2.28 liters/m^2day	CAOW-HDH system integrated with a photovoltaic (PV) panel was simulated. PV panel was cooled, and air was heated through an intermediate gap in the panel. PV-HDH system was reported to have better environmental impact than the PV-RO setup.	Analytical	Giwa et al. [81]
Air Heating	3.5 kg/m^2.day	Numerical study featured a closed air open water desalination cycle using solar air heater before humidification. Increasing air flowrate beyond a certain value didn't improve the productivity further. Effectiveness of dehumidifier, an air-cooled heat exchanger had minimal effect on freshwater production.	Analytical	Fath and Ghazy [82]
Water and Air Heating	15 liters/m^2.day	Parametric study featured an open water cycle and an optional open or closed loop for air circulation. Results showed that by optimizing the system at each hour for solar radiation and corresponding MR, the productivity can be maximized. Open air circulation showed slightly better performance as compared to the closed loop.	Analytical	Orfi et al. [83]

Heating Mode	Max. Yield	Highlights	Scope	Reference
Water and Air Heating	2.5 liters/h	Open air cycle with multi-stage humidification and dehumidification. Inlet water flowrate and air flowrate were kept 300 liters/h and 10 m^3/h, respectively. The 2-stage humidification and air preheating used hot seawater from solar water heaters, in a closed loop. And each dehumidifier operated its respective open water loop.	Experimental	Chiranjeevi and Srinivas [84]
Water and Air Heating	4.74 kg/h	An OAOW desalination system integrated with an air-cooled condenser was tested. Air was preheated with an inline duct mounted electric heater whereas steam boiler was used to heat the saline water. Productivity increased by increasing air flowrate and specific humidity.	Experimental	Nada et al. [85]
Water and Air Heating	68.3 liters/m^2.day	Comparison between water heated and dual heated cycle was made with an open-air loop. System incorporated pre-humidifier heating of air and water using a combination of solar and electric heaters. Productivity increased by increasing the air flowrate. Dual heating gave better performance than the water heating mode.	Experimental	Siddiqui et al. [86]
Water and Air Heating	20 liters/day	Closed air layout used a humidifier and another evaporator inside a distillation module to increase humidification and consequently the productivity. Solar energy was used to preheat the air and water streams. High solar intensity impacted the experimental outputs positively. An increment in the air and water flowrates lead to a decrease in output parameters.	Analytical-Experimental	Bacha [87]
Water and Air Heating	1.117 kg/h	Solar energy was utilized as heating source for both streams. Air followed a single pass configuration. Water through humidifier and dehumidifier was circulated in a closed and open loop, respectively. PV panel was used to drive the electrical equipment. Freshwater yield increased by increasing inlet air and water temperatures to the humidifier.	Experimental	Deniz and Cinar [88]

CHAPTER : 3

EXPERIMENTAL APPARATUS

3.1 Experimental Setup

Experiments for the humidification-dehumidification desalination system were conducted at the desalination lab in KFUPM. In this study, motive is to analyze the off-design performance of an HDH system. Experimental apparatus with fixed system dimensions and (sizing) constraints, is tested to analyze the thermal performance of cycle in two different configurations namely MAH and DH-HDH systems.

3.1.1 Equipment and Framework

A pilot scale experimental setup is made of multiple components and instruments, that are mounted on a rigid frame made of iron-steel. Its structure is supported on a set of four caster wheels which makes it possible for the unit to move or shift from its rooted position. The support structure is 2.3 meters in height and its width is 1.5 meters.

Humidifier is a direct heat and mass exchanging component of the system and possesses a cross-sectional area of 0.09 m^2, 30 cm wide and 30 cm across. The module is made from 1mm thick sheet of galvanized stainless steel and it is 1.7 m in height. Different sections of humidifying tower are assembled together by flanges. Therefore, it can easily be dismantled into its sub-components. An array of spray nozzles is affixed at the upper

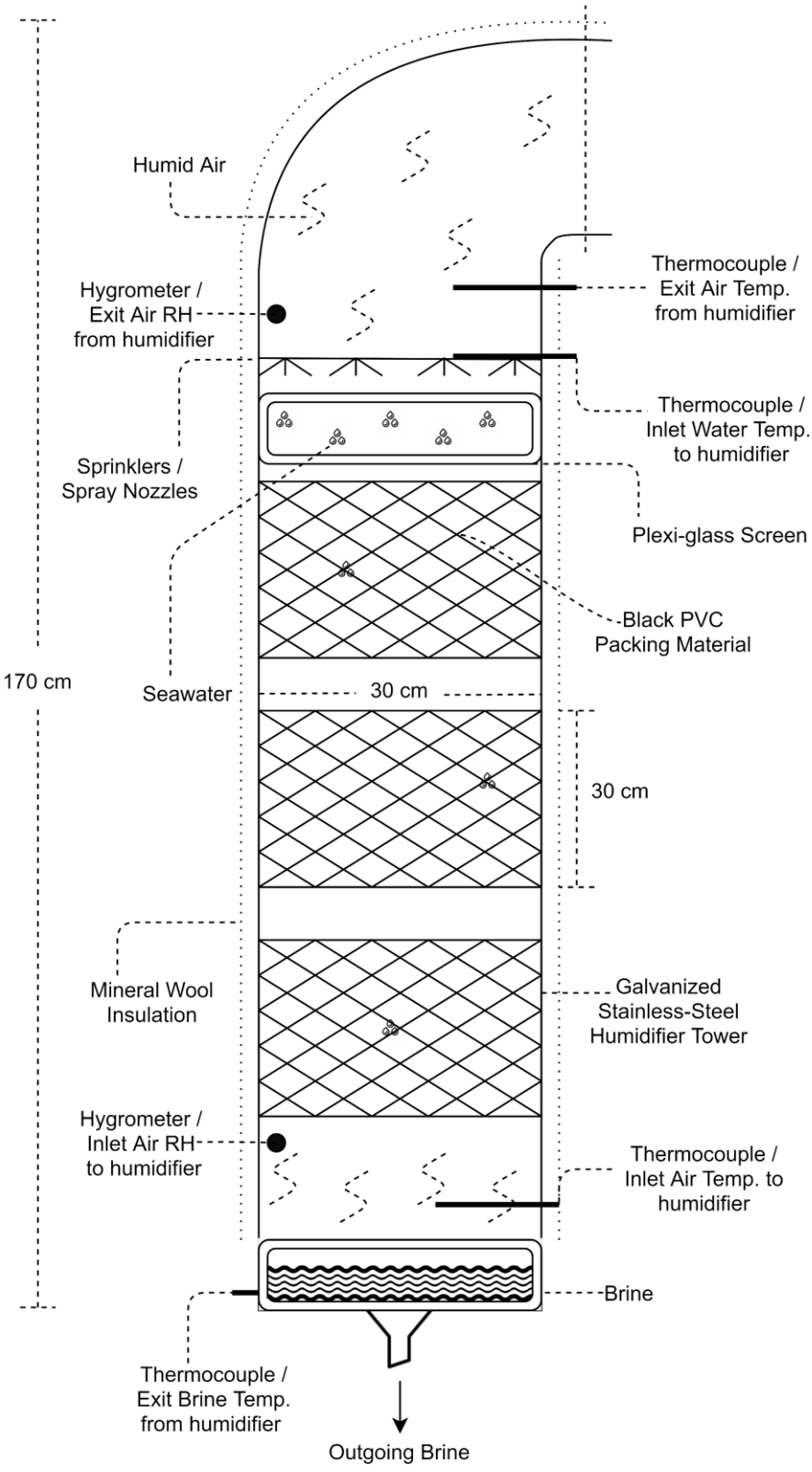

Figure 3.1 Component Layout of Humidifier

end of the cooling tower to disperse pre-heated seawater coming out from the dehumidifier. In addition to that, the central portion of this humidifying tower is filled with packing material to increase direct heat and mass exchange between the two interacting fluid streams. Each cube of packing material has a height of 30 cm and same transversal area as of humidifier's duct. Three blocks of the fill material are equally spaced apart from each other with an intermediate distance of 15 cm, to prevent the formation of larger drops along the edges and to distribute the falling water evenly across the packing decks. Underneath the packing material is a small collector that accumulates and eventually discharges saline water out from the humidifier. Figure 3.1 shows a schematic layout of humidifier.

Dehumidifier is made from the same galvanized stainless-steel sheet of 1 mm thickness. The height and cross-sectional area of dehumidifier are similar to that of the humidifier. Its constructional built also gives flexibility in disassembling the unit, when needed. But instead of fill material, the condensing tower is equipped with a set of 3 finned tube heat exchangers (HE) that serve as condensers. Squared fins of each finned tube exchanger have the area dimensions of dehumidifier module with partial clearance to fix it inside the steel duct. Circular tubes of heat exchanger are 0.25 inch in diameter and made of copper. Moreover, the height of a single exchanger is 15.24 cm. The main purpose of finned tube exchangers is to condense the freshwater out from hot and humid air coming in from the humidifier. Other than cooling the moist air down, these indirect heat and mass exchangers also recover the heat from hot air by heating the incoming seawater. Bottom portion of dehumidifying compartment carries a similar collection trap with an opening to discharge freshwater into the distillate tank. Figure 3.2 presents a layout of the dehumidifying tower.

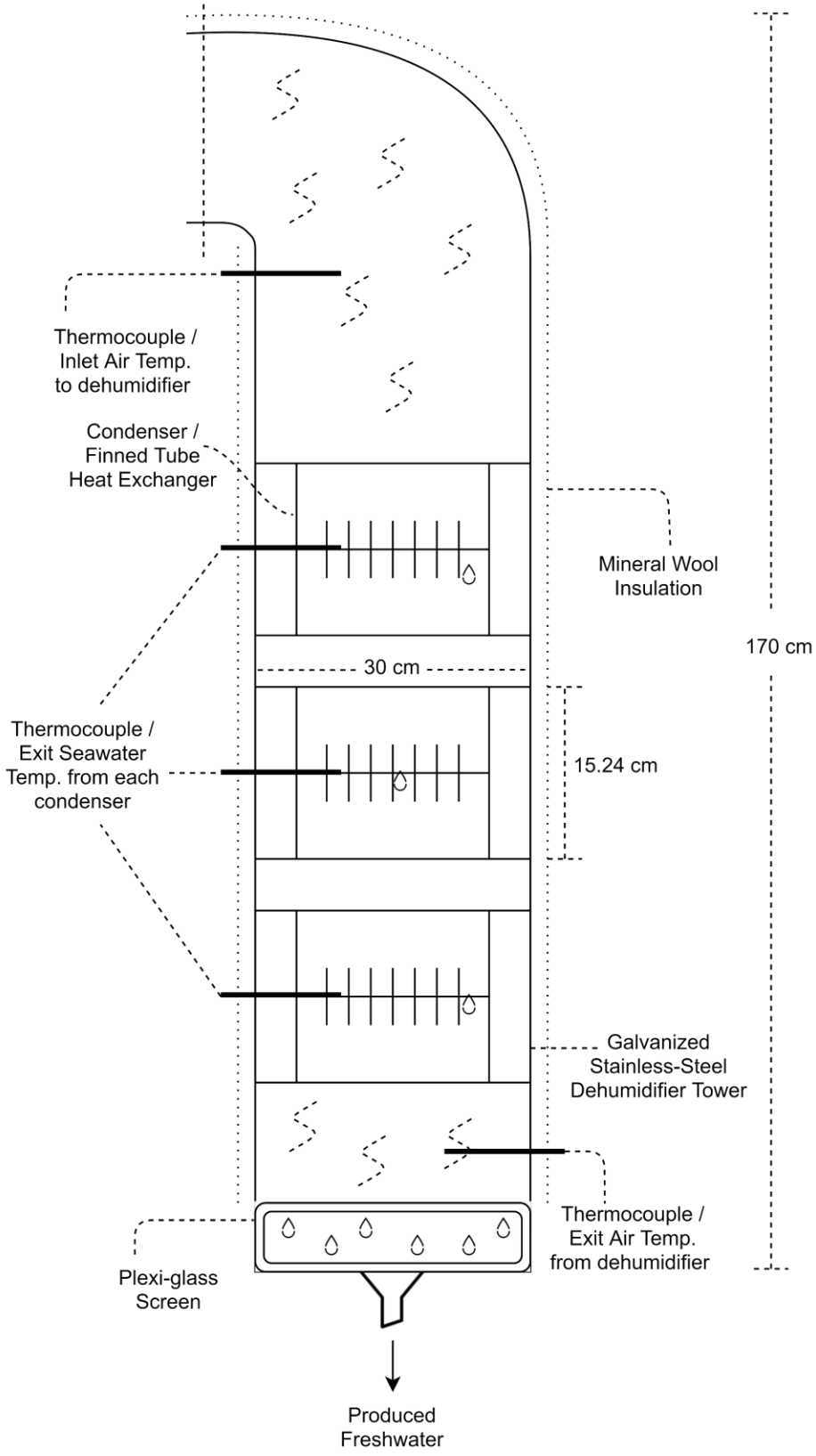

Figure 3.2 Component Layout of Dehumidifier

Heating unit is incorporated between the humidifier and dehumidifier. This desalination system is capable of heating air and/or water in separate electric heaters. Air stream can be heated after humidification in air duct heaters whereas the water stream is configured to get heated before the humidification process using water coil heaters. Each electric heater is adjusted with multiple heating elements and separate switches to vary the amount of heat transferred to a particular fluid.

Table 3.1 below enlists the details about sub-components of humidifier, dehumidifier and heating unit, from experimental humidification-dehumidification system;

Table 3.1 Specification of sub-components from Experimental HDH Setup

Component Type	Model	Material Specifications	Features	Manufacturer
Packing	CF1200 MA	Black PVC	Specific area 226 m^2/m^3. High thermodynamic performance and low pressure drop.	Brentwood®
Finned tube heat exchanger	-	Aluminum Fins Copper tube coils	Maximized heat transfer surface area.	Zamil®
Air Heater	Open coil heating element	Nickel-Chromium	3.9 kW, 1.6 kW Fast heat up times, provides uniform heat distribution, equipped with a fan relay switch.	Procured from local market
Water Heater	SGW2507-430481 Tubular Heating Element	Nickel-Based Alloy with zinc plating	1.5 kW, 1.5 kW Suitable for use with hard water and in potable water applications.	Grainger®

3.1.2 System Auxiliaries

- Galvanized stainless-steel ducts are heavily insulated with mineral wool thermal insulation to conserve system's internal conditions within its boundaries. Spray nozzles and the bottom end of humidifier and dehumidifier are made visible via transparent plexi-glass screens that are sealed in place with temperature-grade epoxy sealant.
- Horizontal multistage close-coupled pump, model MXPM 202-60 made by Calpeda® is commissioned to pump the seawater from tank to spray nozzles, through dehumidifier and heater. Suction port of the pump lies above its axis and the delivery port is at a radial position. The pump makes very little noise owing to its water filled shroud across stages. Moreover, the position of suction port adds an extra layer of safety to keep it from running dry. Impeller stages are made from Noryl PPO-GF20 material. It can pump water within a flowrate range of 1 - 6 m^3/h (0.6 HP) and is useful for high pressure applications.
- Backward curved centrifugal blower driven by 0.37 kW electric motor, is procured from Saudi Fan Industries®. A V-belt is connecting the blower and motor shaft. The blower is fixed on the rig in a closed air loop configuration. Suction side is connected to the dehumidifier exit and outlet is facing the humidifier inlet. Motor on this unit is equipped with a variable frequency drive by Danfoss® and an analogue switch to vary the speed of rotation of the blower. Model: HRE0B-250-B-2 features aluminum impeller with black steel sheet casing. Due to non-overloading characteristic, it is acceptable for wide range of duct applications.

- On the water side, one-inch polyvinyl chloride (PVC) pipes are utilized to circulate the seawater, freshwater and brine, in and out of the system components. Two flexible pipe hoses are used to discharge brine and by-pass the water from seawater tank. An in-line flow type rotameter Model: FL45100 and turbine flowmeter Model: FTB4605 by Omega® were used to gauge the mass flow rate of feedwater flowing into the dehumidifier.
- Float valve was used in the seawater tank to ensure that an optimal amount of water remains in the tank and the suction side of the pump remains submerged at all times. That was articulated to keep the pump from running dry. Spears® PVC ball valves are used throughout this testing setup to manage the flow of water, to bypass certain components and to change the configuration of cycle if needed.
- Rugged pipe plug K-type thermocouple probes with tapered threads are used to measure temperatures of the seawater in PVC pipes, at the inlet and exit of dehumidifier. Model: TC-K-NPT-G-72-SMP. Wider temperature range, chemical inertness and reliability were primary reasons behind the selection of K-type thermocouple. It is also being used to measure the seawater temperature after the heater, before it gets sprinkled in the humidifier. Brine temperature at the exit of humidifier was also monitored with a standard wire K-type thermocouple.
- Air temperatures across the circuit are tracked with thermocouple probes made by Omega®. Quick disconnect probes are featured with K-type thermocouple wires housed inside a metallic tube made of stainless steel and inconel. Model: KMQSS-125G-6. These probes are equipped with mini connectors to make them fix steadily inside the duct. Moist air temperatures are recorded at the inlet and exit of

humidifier and dehumidifier, respectively. In addition to that, the temperatures of carrier gas across the air heater and through dehumidifier are followed with the same probes.

- Duct type hygrometers or relative humidity sensors are being used to record relative humidity at the inlet and exit of the humidifier. Model HX94V by Omega® is fixed with flanged connection into duct housing. Monitoring setup consists of a transmitter and a high temperature relative humidity remote duct-type probe, made of stainless steel.
- Analogue voltmeter and ammeter devices are used to read the voltage and current being supplied to the rig and consequently the power consumed by each electric component of the system. Which includes blower, pump and heaters.
- Data logger 2686A DAQ by Fluke® with 6 card slots of 20 channels each, is used to receive the voltage signals from different recorders including thermocouples, relative humidity sensors and flow meters. It is installed with 128 MB flash memory card and it can read 20-120 channels per chassis. At minimum measurement speed, it is able to record 6-45 readings per second. Its storage and retrieval characteristics make it useful for standalone, networked or non-computer assisted applications. In the current setup, a portable computer is connected to this multichannel data logging system with an ethernet cable to send and receive the measured values, in fractional amount of time.
- Seawater tank and distillate tank at the base of humidifier and dehumidifier respectively, are made from 10 mm thick sheets of plexi-glass, fixed by using liquid chloroform and clear silicon. Purpose of first tank is to accumulate the seawater

that is to be pumped in the condenser and to collect the by-pass flow of seawater (if any) coming from the water pump. Meanwhile, the second tank is meant to collect the condensing freshwater from dehumidifier. Dimensions of both containers are the same (L=61 cm, W=40 cm, H=40.6 cm).

- Graduated measurement cylinder manufactured by Spectrum® is used to measure the freshwater volume collected at the bottom of dehumidifier. It is made from heavy-duty plastic with wide pentagonal base and non-wetting interior. It can also withstand temperatures of up to 100°C.
- Handheld digital thermocouple reader HH200A by Omega® is used to check the temperatures of exiting brine and entering moist air at the inlet of humidifier.

3.2 Experimental Procedure

All experimental work is conducted in desalination lab that features an air-conditioning system, water drainage system, necessary hand tools, fire extinguishers, first aid kit and an uninterrupted supply of municipal water and electricity. Recording a single data point usually requires a minimum duration of three to four hours, excluding the time needed for the preparation or maintenance of setup. The experiments are needed to be performed at constant inlet seawater temperature to study the impact of other varying parameters. Procedure adapted to conduct experimental work is stipulated here;

- First step in experimentation is to accumulate feedwater in a large storage tank. The water sits in the tank for about 20 to 24 hours, in order to achieve the specified

constant temperature. It is understood that seasonal variations in real life application may not always result into constant inlet water temperature, but this study is conceived to focus on assessing the performance of system under different operating parameters, not different ambient conditions. Furthermore, varying the temperatures at dehumidifier inlet would change the collected volume of distillate and hinder details on direct impact of MR on various performance parameters.

- Water from the storage tank is brought down to a smaller seawater tank that is integrated with a water pump as shown in figure 3.3. Pump sucks water and delivers it to condenser tubes in the dehumidifier.
- The blower is powered on, to force the air circulation in a closed loop. As soon as suction port gets submerged under water in seawater tank, the water pump is switched on as well. It gets water running through the dehumidifier followed by spray nozzles and then finally out from the humidifier into the drain.
- Mass flowrates of air and water are adjusted to a set value using variable speed drive and gate valve, respectively. Further on, both streams are kept flowing inside the insulated chambers for approx. 15 min time period to ensure flowrate stability.
- Data acquisition system is set up by connecting an ethernet cable to a laptop computer and then running system's interface. Afterwards, the heating unit is turned on. In heating unit, air or water heaters can be operated individually or simultaneously based on the cycle requirements.
- The experimental rig takes around 60-90 min of duration to stabilize and to reach a steady state. The stability in system is reached when all monitored temperatures and flowrates of both carrier gas and liquid stream become steady and unwavering.

- Once steady state is reached, the data logger is put down to record incoming voltage signals from all sensors. Currently, the data logging system is set to track about 36 readings per minute from every instrument. Numeric data from the system is collected for over 1-hour duration. Subsequently, freshwater collected over the corresponding period is measured with graduated cylinder.
- For each location in the system, quantitative values of variables (temperatures, flowrates, etc.) are averaged and then processed to calculate the performance parameters.
- The voltmeters and ammeters are read thrice during each functioning cycle, to get a value for power that is being consumed by heating elements.
- This experimental procedure is repeated at least twice on a single value of mass flowrate ratio. Moreover, to study the effect of MR in a certain cycle configuration, multiple experiments are performed by changing mass flowrate ratio and heat energy supplied to the system.
- Finally, extracted quantitative data is then processed using excel and engineering equation solver. Graphical figures are plotted to study performance metrics in different cycle arrangements.

Schematic layout of the experimental rig is shown in figure 3.3 below. Additionally, an image of lab setup is also illustrated in figure 3.4.

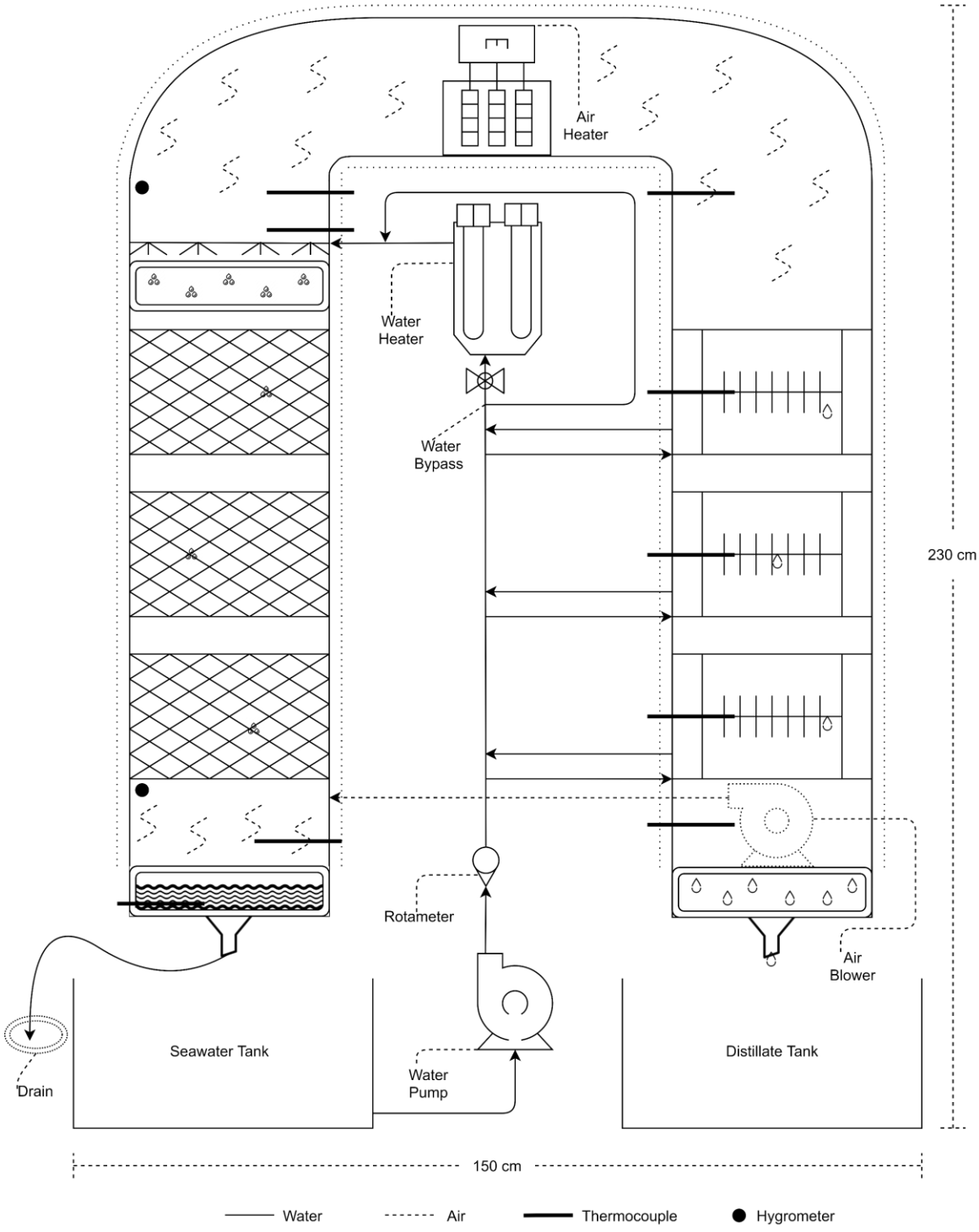

Figure 3.3 Schematic layout of Experimental Testing Rig

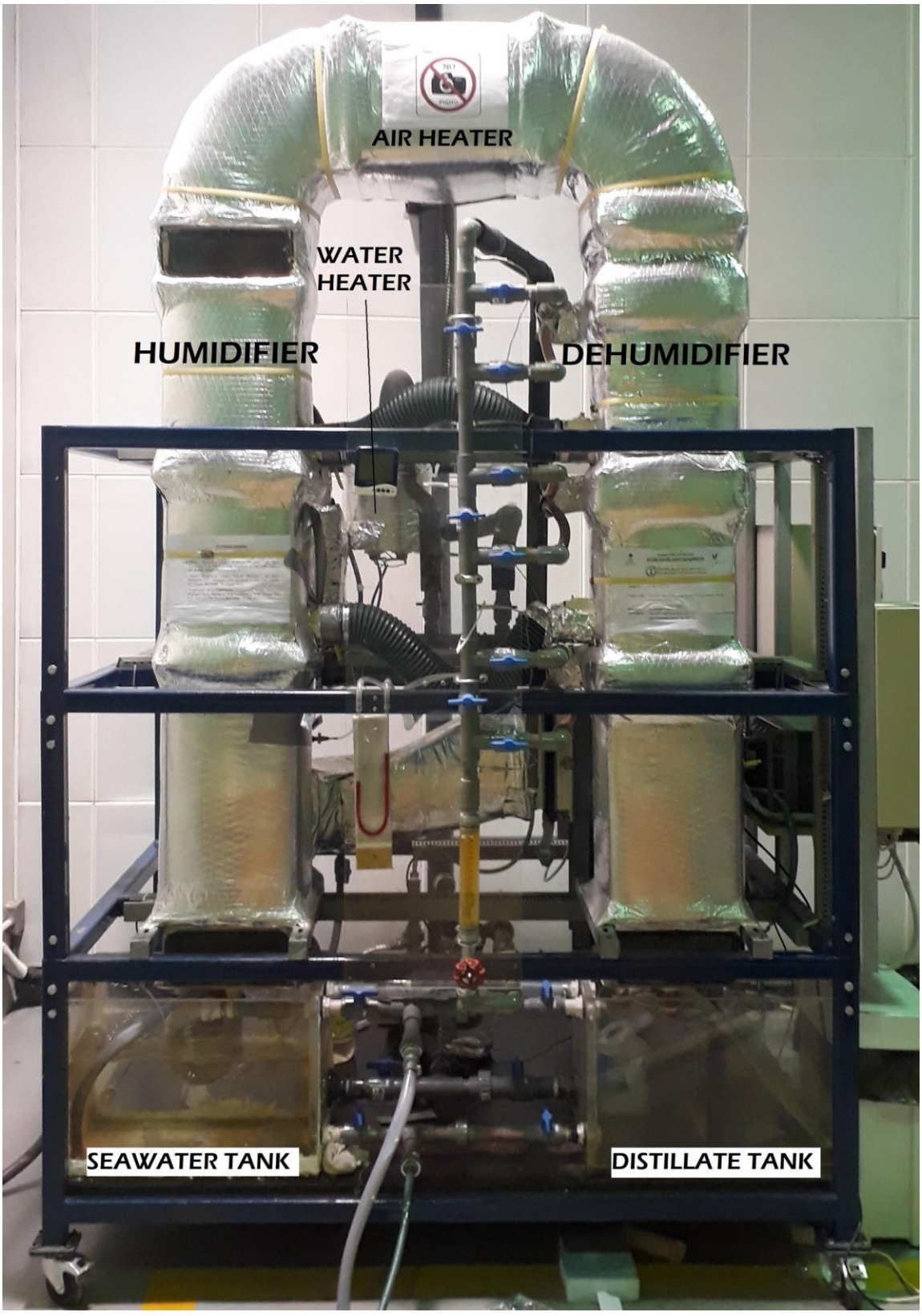

Figure 3.4 Photograph of the Experimental Setup

3.3 Measurement Uncertainties

Air and water temperature, flowrate and relative humidity values are recorded using instruments at various locations, on the experimental rig. Details about the equipment are given in section 3.1.2. All of these devices are hosted by a DAS platform, that is connected to a computer. Parameters in an operating cycle are monitored using FLUKE® Software. Measuring instruments have inaccuracies that need to be addressed in a way that their effect on performance parameters is made known. Table 3.2 presents the instrument details, their measuring ranges, accuracies and uncertainties. Measurement uncertainties can be evaluated with a relation that is used by Zhang et al. [89]. It expresses clearly that instrumental uncertainty (U) is dependent on accuracy (a) of that equipment, given as;

$$U = \frac{a}{\sqrt{3}} \tag{1}$$

Table 3.2 Technical specifications of measuring devices

Instrument	Parameter	Range	Accuracy	Uncertainty
Thermocouple K-type	Temperature	0-1250 °C	±0.75%	±0.4331 %
Relative Humidity / Temperature Transmitter	Relative humidity / Temperature	3-95 % (RH) 0-100 °C (T)	±2.0 % ±0.6 °C	±1.1547 % ±0.3464 °C
Rotameter	Volume Flowrate	2-38 LPM	±1.5 %	±0.8660 %
Graduated Cylinder	Volume Collected	200-2000 ml	±20.0 ml	±11.5470 ml
Stopwatch	Cycle duration	0-99 h	±0.010 s	±0.0058 s

Instrument uncertainty has indirect effect on the derived performance indicators. These uncertainties are attributed to the calculated parameters using an expression given by Kline and McClintock [90]. If δ_C is the uncertainty of computed result (C), then equation is expressed as;

$$\delta_C = \left[\left(\frac{\partial C}{\partial x_1}\delta_1\right)^2 + \left(\frac{\partial C}{\partial x_2}\delta_2\right)^2 + \cdots + \left(\frac{\partial C}{\partial x_n}\delta_n\right)^2\right]^{\frac{1}{2}} \quad (2)$$

The uncertainties associated with performance parameters are given in Table 3.3;

Table 3.3 Uncertainties associated with derived parameters

Calculated Parameter	Uncertainty
Gain output ratio (GOR)	±0.00202
Humidifier effectiveness (ε_h)	±0.03196
Dehumidifier effectiveness (ε_d)	±0.01109
Mass flowrate ratio (MR)	±0.01194
Recovery ratio (RR)	±0.005206
Humidifier heat capacity ratio (HCR_h)	±0.0149
Dehumidifier heat capacity ratio (HCR_d)	±0.046

CHAPTER : 4

EXPERIMENTAL RESULTS AND DISCUSSION

4.1 Performance Parameters

The first step in analyzing HDH systems, is to understand the performance scales. They set a criterion and specify the performance of an individual desalination system. Performance parameters are also crucial to a comparative study as they allow the user to compare between different system layouts.

4.1.1 Gain Output Ratio

Gained Output Ratio (GOR) is computed as the enthalpy of evaporation multiplied by the distillate water flow rate to the total thermal energy input. It outlines the efficacy of system in producing fresh water and gives an estimate about the reinstated heat recovery, in a desalination cycle.

$$GOR = \frac{\dot{m}_{pw} \times h_{fg}}{\dot{Q}_{in}} \quad (3)$$

4.1.2 Recovery Ratio

Recovery Ratio (RR) is calculated as the ratio between mass flowrate of product water to the feed flowrate of inlet seawater to a desalination unit.

$$RR = \frac{\dot{m}_{pw}}{\dot{m}_w} \tag{4}$$

4.1.3 Mass Flowrate Ratio

Mass Flow Rate Ratio (MR) is calculated by dividing the mass flowrate of inlet saline water to the air being circulated in the cycle. At an optimum value of MR, the GOR is maximum. Optimum value ensures that for a given humidifier size, appropriate amount of seawater flows in to humidify the air.

$$MR = \frac{\dot{m}_w}{\dot{m}_a} \tag{5}$$

4.1.4 Specific Electrical Energy Consumption

Specific Electrical Energy Consumption (SEEC) is presented as total electrical energy consumed by the desalination system in kilowatt-hour per kilogram of freshwater production. It is expressed as;

$$SEEC = \frac{\dot{Q}_{in,heater} + \dot{Q}_{blower} + \dot{Q}_{pump}}{\dot{m}_{pw}} \tag{6}$$

4.2 Operating Parameters

Some primary operating variables are defined here, that hold significance towards effective understanding of an HDH cycle;

4.2.1 Modified Heat Capacity Ratio

Heat Capacity Ratio is defined as the minimum to maximum capacity rates of heat exchanging fluids in a heat exchanger [$\dot{m}_c C_c$ / $\dot{m}_h C_h$]. However, in simultaneous heat and mass exchangers, absolute humidity of air stream affects the moist air enthalpy. Therefore, a modified capacity ratio is devised based on total enthalpy change to include the variations in humidity and temperatures of heat and mass exchanging fluid streams.

Modified Heat Capacity Ratio (HCR) is defined as maximum enthalpy variation in the cold stream to the maximum enthalpy change of the heated stream. For specified initial conditions, the irreversibility or imbalance in a system component can be minimized, depending on the value of HCR.

$$HCR = \frac{\Delta H_{max,cold}}{\Delta H_{max,hot}} \tag{7}$$

4.2.2 Effectiveness

Effectiveness (ε) is calculated as total enthalpy change to the maximum possible enthalpy change in a system component. This definition is based on the total energy variation of each fluid stream that participates in the process. Based on definition [91], maximum value of either fluid stream effectiveness is assigned to the heat and mass exchanging component. It is given as;

$$\varepsilon = max\left(\frac{\Delta H}{\Delta H_{max}}\right)_{w/a} \tag{8}$$

4.2.3 Terminal Temperature Difference

Terminal Temperature Difference (TTD) is the difference of temperature between flow streams at the tail end of either system subcomponent in an HDH unit.

4.2.4 Top Cycle Temperature

Top Cycle Temperature (T_{max}) is defined as the maximum temperature of either fluid at the exit of air or water heater after it has been heated.

4.2.5 Bottom Cycle Temperature

Bottom Cycle Temperature (T_{min}) is the temperature of seawater entering the cycle at inlet to the dehumidifier, it is minimum temperature in a cycle.

4.3 Cost of Desalinated Water

The cost of freshwater production from current setup is evaluated by using relations given in this section, El-Dessouky and Ettouney [92]. Analysis is performed by considering cost factors that include; capital, electrical energy, labor, maintenance and management costs. Fixed cost of system components is given in table 4.1. In addition, there are few input variables that are needed to calculate the unit product cost in $/kg. These inputs are sourced from different references and are tabulated in table 4.2. To calculate the capital cost, amortization or capital recovery factor is needed, it is formulated as;

$$\alpha = \frac{i\,(1+i)^n}{(1+i)^n - 1} \tag{9}$$

Where i is the interest rate and n represent the life expectancy of desalination plant.

Table 4.1 Capital investment cost of main components of desalination system

Description	Price ($)
Packed bed humidifier	235
Finned tube dehumidifier	725
VFD & centrifugal blower	900
Water pump	320
Flowmeters	250
Pipes and fittings	50
Water tanks	200
Accessories	40
Water heaters	120
Air heaters	230

Table 4.2 Inputs for cost analysis

Inputs	Values	Reference
Pretreatment Cost	Zero	[91]
Electricity cost (COE)	0.045 $/kWh	[90] [92]
Plant life expectancy (n)	20 years.	[92]
Plant availability (A)	90%	[92]
Interest rate (i)	5%	[92]
Operating labor specific cost (L)	0.0001 $/kg	[93]

Annual capital cost;

$$\dot{C}_i = \gamma \times \alpha \tag{10}$$

Where γ specifies total direct capital investment, α is amortization factor, L is operating labor specific cost.

Annual electric power cost;

$$\dot{C}_{elec} = COE \times SEEC \times A \times \dot{m}_{pw} \tag{11}$$

Annual labor cost;

$$\dot{C}_{lb} = L \times A \times \dot{m}_{pw} \times 365 \tag{12}$$

Annual maintenance cost ($\dot{C}_{mnt}$) is computed as 1.5% of capital cost and annual management cost ($\dot{C}_{mgt}$) is 20% of the labor cost. Sum of all five factors give total annual cost in ($/yr) as;

$$\dot{C}_T = \dot{C}_i + \dot{C}_{elec} + \dot{C}_{lb} + \dot{C}_{mnt} + \dot{C}_{mgt} \tag{13}$$

Corresponding to that, the unit product cost (C_p) in ($/kg) is calculated from the following relation;

$$C_p = \frac{\dot{C}_T}{A \times \dot{m}_{pw} \times 365} \tag{14}$$

These formulations are utilized to perform economic analysis of modified air heated and air and water heated humidification-dehumidification desalination systems studied in this work. Cost of plant components is based on the actual purchased prices from retail vendors.

4.4 Experimental Results of CAOW-MAH-HDH Cycle

Modified air heated humidification-dehumidification desalination cycle with closed air and open water loop is experimentally examined. In the air heating unit, air stream is heated before it enters the dehumidifier. Furthermore, heat input to air stream is kept constant at 3.8 kW. Temperature of feedwater is maintained at nearly a constant value of 25.4 ± 0.23 °C. Notable characteristic of an experimental study in humidification-dehumidification desalination is floating effectiveness values of system components. Unlike fixed effectiveness models that are studied theoretically, the effectiveness values in experimental analysis are destined to vary with mass flowrate ratio owing to fixed size of the system.

4.4.1 Effect of MR on Gain Output Ratio

Gain output ratio (GOR) of the modified air heated cycle is witnessed to get affected by variation in mass flowrate ratio (MR). A graphical interpretation from experimental analysis is shown in the figure 4.1. Temperature of seawater at the inlet of dehumidifier is kept nearly constant at 25.4 °C. With fixed mass flowrate of circulating air, MR in this analysis is solely dependent on the water mass flowrate. From definition of MR, it is obvious that there is a direct relation between MR and mass flowrate of water. Therefore, with constant air flowrate, increasing the water mass flowrate translates to increased MR. It can be noticed that GOR initially projects an increasing trend with MR values. This increase in productivity can be associated to a consistent increment in humidity levels of carrier gas at the exit of humidifier.

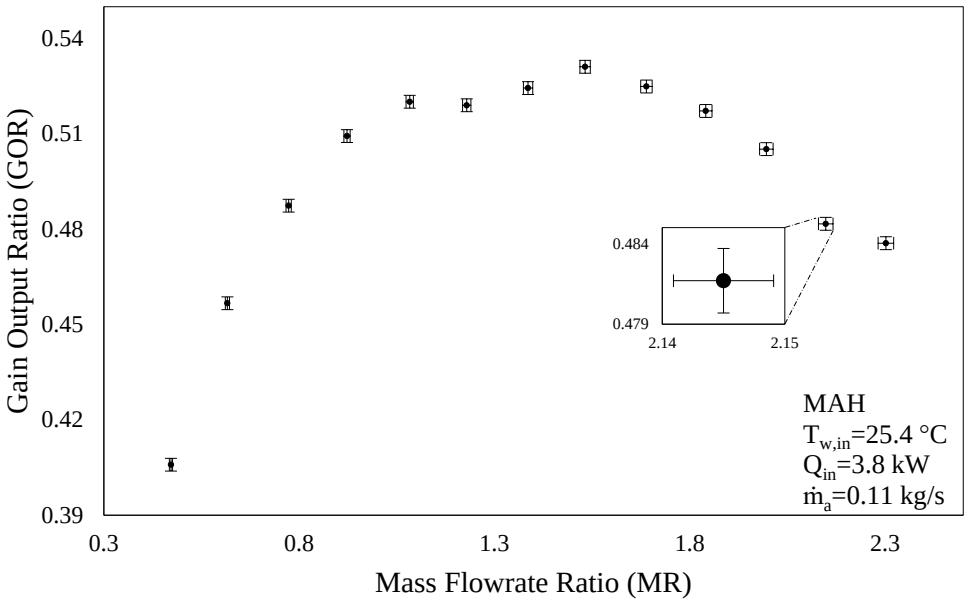

Figure 4.1 MAH Cycle: Mass flowrate ratio vs gain output ratio

Increasing the quantity of preheated water in humidifier results into an effective heat and mass exchange between interacting streams but this improvement sustains to an optimum point. Beyond optimum MR, further increase in feedwater flowrate brings a decline in thermal performance of the system. Justification for this behavior is the inability of feedwater to diffuse additional moisture content in air stream. Furthermore, with fixed flowrate, air is also unable to carry the extra vapor content that water stream has to offer at corresponding temperatures. Subsequently, the loss of recovered heat with outgoing brine causes poor energy performance and leads to reduction in GOR. In the current setting, maximum GOR value of 0.53 is recorded at MR of 1.53. Similarly, it minimized at MR of 0.47. The GOR values are impacted mainly by the freshwater flowrate that varied with the respective changes in MR.

4.4.2 Effect of MR on Productivity

Figure 4.2 indicates the variation in freshwater production rate over mass flowrate ratio. It highlights the existence of a strong relation between productivity and water flowrate. The distillate production surges upon increasing the water flowrate to an optimum value. It can be explained by an increase in both heat and mass transfer coefficients at high water flowrates. Moist air in the dehumidifier is able to condense greater amount of freshwater with increasing MR values. At the same time, high feedwater flowrates offer greater quantity of vapor content to air in humidifier. However past that optimum value, the freshwater production dips with further increase in water flowrate. This reduction in productivity can be associated to the state of air in humidifier.

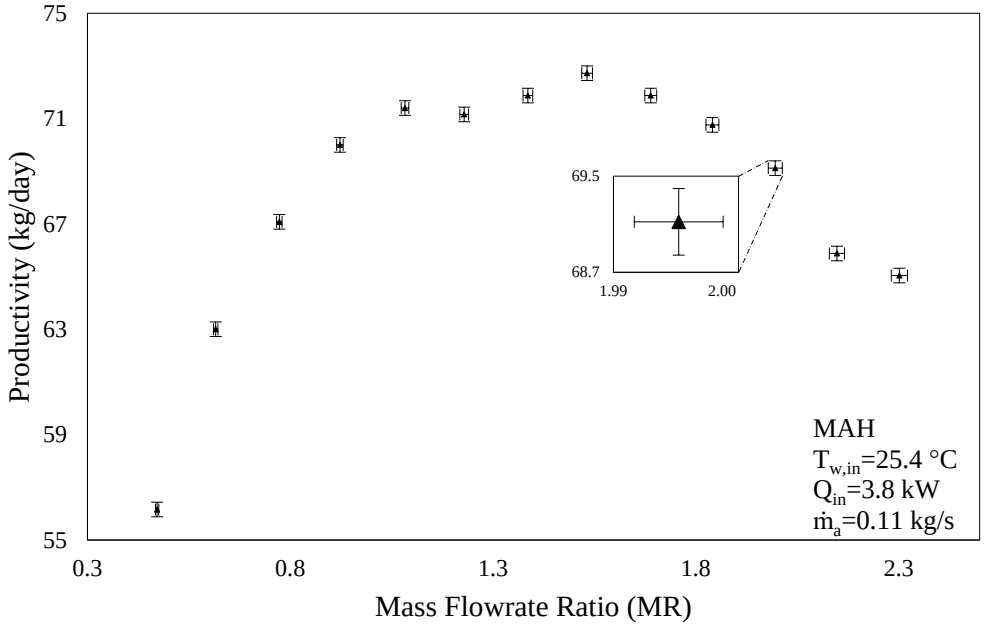

Figure 4.2 MAH Cycle: Mass flowrate ratio vs productivity

Once the air gets saturated in humidifier, additional water supply goes unused and simply gets rejected as brine. Meanwhile, increasing water flowrate decreases its temperature gain in dehumidifier which lowers the operating water temperature in the unit. Subsequently the evaporation and condensation efficiencies are decreased, and it brings down the system productivity. At MR value of 1.53, the highest amount of distillate 72.7 kg/day is recorded.

4.4.3 Effect of MR on Recovery Ratio

The percentage recovery ratio is witnessed to be decreasing with an increase in mass flowrate ratio, as depicted in figure 4.3. It stipulates that greater quantity of distillate can be recovered from the preheated seawater at lower values of MR.

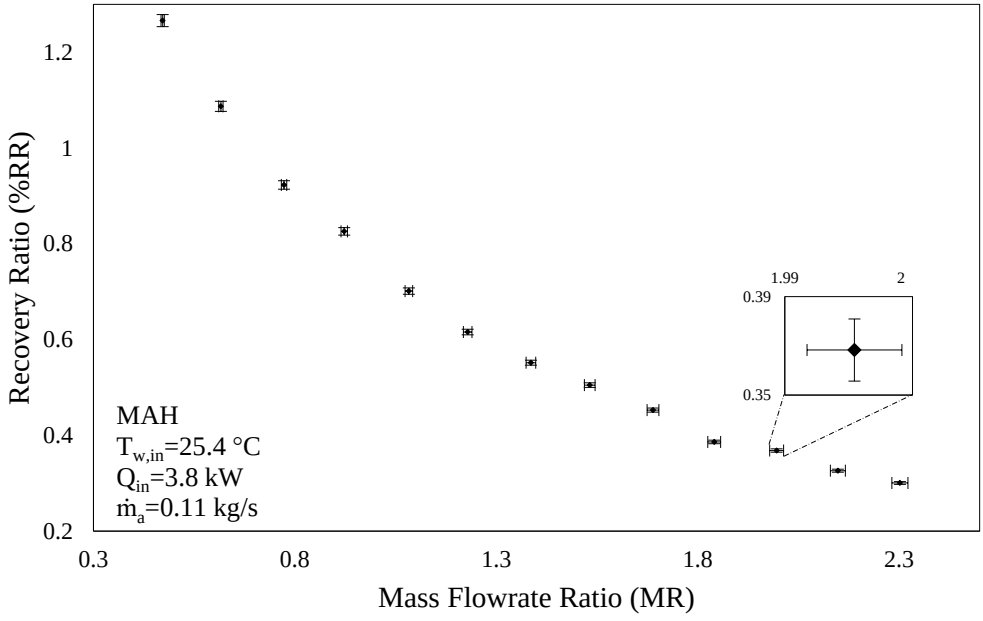

Figure 4.3 MAH Cycle: Mass flowrate ratio vs recovery ratio

This behavior can be accredited to the fact that air has the capacity to take in large amount of the sprayed water at low MR. Water with reduced flowrate is able to recover relatively more heat in dehumidifier and eventually heats up the air to a similar scale in humidifier. Consequently, air becomes capable of accepting more vapor content at low water flowrates. In contrast, less quantity of freshwater is collected with further increase in feedwater flowrate. Increasing water flowrate does not guarantee greater humidity levels in air. It may be ascribed to water temperature at the inlet of humidifier that decreases with increasing flowrate and thus air achieves saturated state at lower temperatures as well. Once the carrier gas attains saturation, seawater becomes supplementary. Hence, lesser quantity of distillate is collected at high mass flowrate ratio. In other words, the air has a certain capacity to absorb moisture depending on its temperature and absolute humidity and this trait decides the quantity of vapor it carries. Maximum and minimum values for the recovery ratio are recorded as 1.26 % and 0.31 % at feed flowrates of 3 liters per minute (lpm) and 15 lpm, respectively. Feed flowrate is a primary factor influencing these values. Generally, low RR values are desirable in the sense that unlike major centralized technologies, the cost of pre- and post-treatment is minimized in desalination plants.

4.4.4 Effect of MR on Maximum Cycle Temperature

Impact of changing MR on the maximum temperature of the cycle is illustrated in figure 4.4. The maximum temperature in a modified air heated cycle specifies the temperature of humid air after it has passed through the heater and before it enters the dehumidifier. It is evident that $T_{max,air}$ is higher at low MR and then it gradually follows a downward trend

with increasing mass flowrate ratio. This tendency can be explained by the respective variations in humidity levels of the air-vapor mixture. When MR is less than 1, incoming air flow in the humidifier exceeds the amount of water being sprayed. Furthermore, low feedwater flowrate enables the water to recover large amount of thermal energy in dehumidifier. When this water gets sprayed in the humidifier it elevates the temperature of air at the exit of humidifying tower.

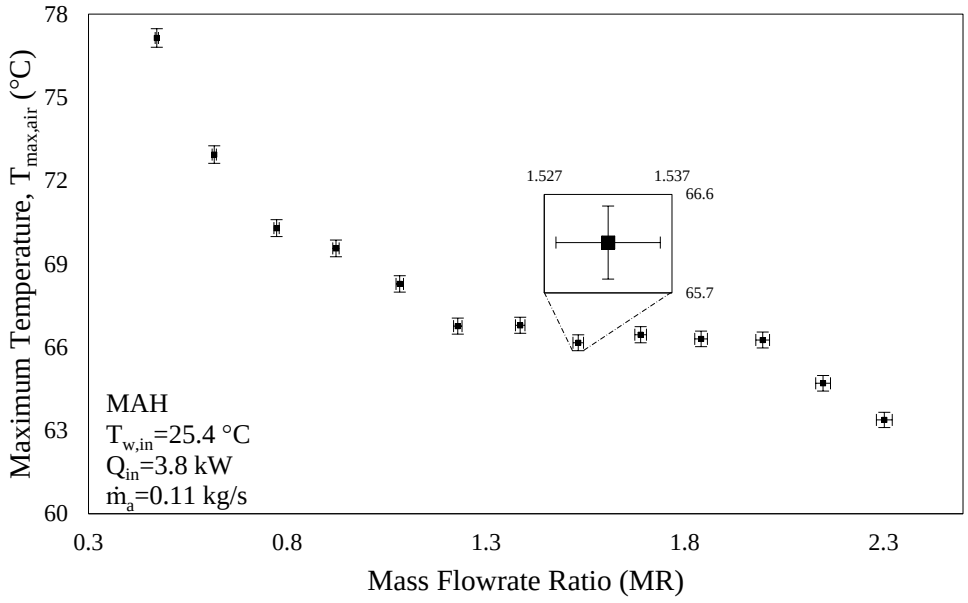

Figure 4.4 MAH Cycle: Mass flowrate ratio vs maximum temperature

Secondly, low water flowrate and high air temperature implies that the air can carry additional moisture if it is made available. Accordingly, the moist air at humidifier's exit is destined to have low specific heat capacity. Hence, heater becomes capable of heating the relatively less moist air to higher temperatures. As the mass flowrate ratio increases, the amount of water that is being made available in the humidifier also increases. This oversupply dips the inlet temperature of water stream at humidifier inlet, leading to a

subsequent fall in air temperature at humidifier exit. Therefore, the air stream is saturated and has low temperature. Due to constant heat input and high specific heat capacity of humid air, the temperatures would fall. The maximum $T_{max,air}$ is noted to be 77.1 °C, at mass flowrate ratio of 0.47.

4.4.5 Effect of MR on Water Temperature

Figure 4.5 interprets inlet and outlet temperatures of feedwater passing through dehumidifier at different mass flowrate ratios. The inlet temperature of feedwater to dehumidifier is kept nearly constant at around 25.4 °C to study the impact of changing MR on the exit water temperature. As represented in the graph, the exit feedwater temperature is greater at low values of MR. It can be ascribed to the reduced feedwater flowrate in dehumidifier, which gives water appropriate residence time to recover heat from the incoming flow of hot and humid air. Water with elevated temperature then enters the humidifier and heats up the air thus increasing its capacity to absorb moisture. On the contrary, increase in MR leads to high water flowrates. Resultantly, the water stream flowing through condenser tubes will have relatively small amount of time to exchange heat with the moist air. It drives the reduction in water temperature at dehumidifier exit. From the illustration of productivity and GOR, it can be deduced that achieving the maximum cycle temperature and feedwater temperature does not promise an increase in freshwater production. However, managing the mass flowrate ratio in such a way that the portions of interacting streams become optimal for each other can assure maximum distillate collection, even at intermediate temperatures.

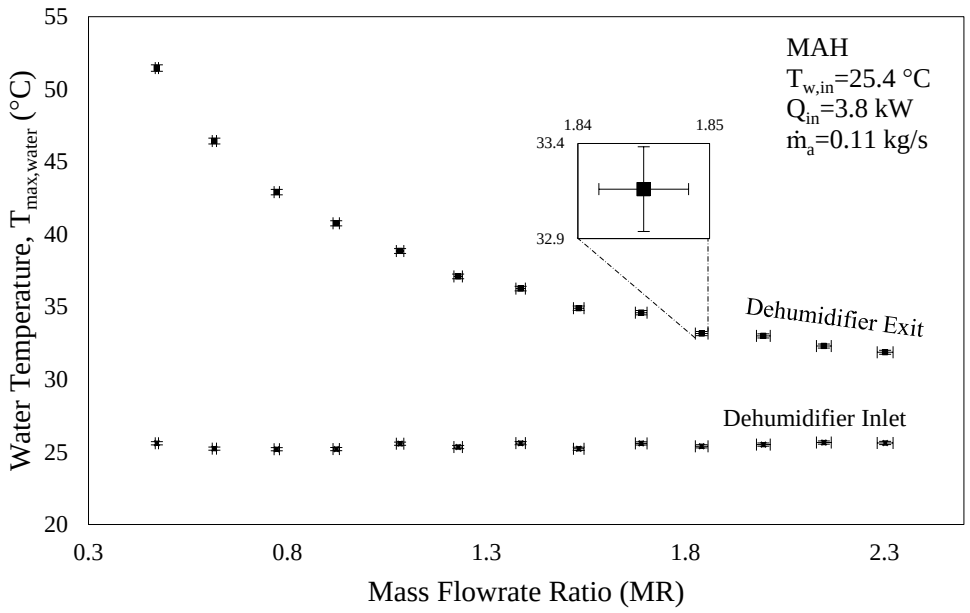

Figure 4.5 MAH Cycle: *Mass flowrate ratio vs water temperature*

4.4.6 Effect of Minimum Cycle Temperature of Water on Maximum Cycle Temperature of Air

The effect of varying feedwater temperature on maximum cycle temperature and productivity is demonstrated in figures 4.6 and 4.7. MR is fixed at 0.77 with seawater flowrate of 5 lpm. The temperature of feedwater at dehumidifier inlet is the variable. As shown, increasing feedwater temperature elevates the maximum cycle temperature. It can be explicated by the resultant increase in water temperature at dehumidifier exit and humid air temperature at humidifier exit. Likewise, when this relatively hotter air enters the heater, it gets heated to a higher degree. Meanwhile, productivity also surged with increasing feedwater temperature.

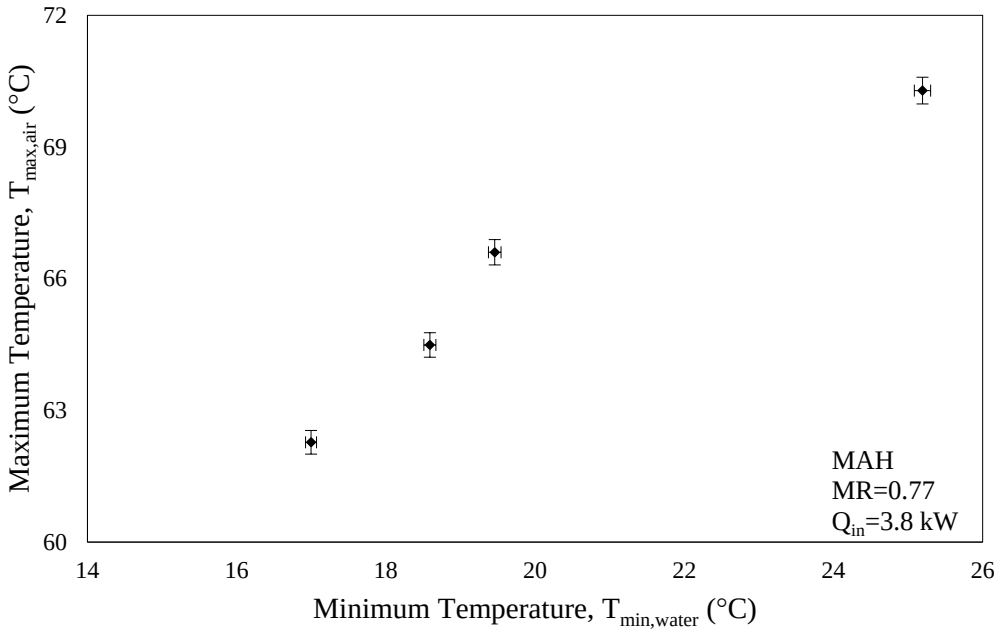

Figure 4.6 MAH Cycle: Minimum temperature vs maximum temperature

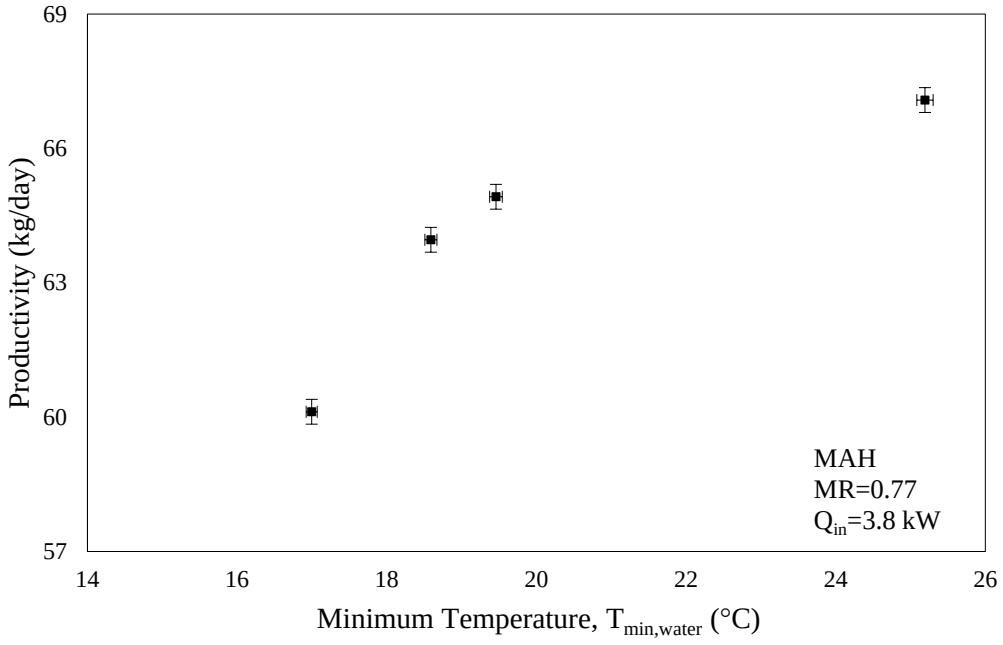

Figure 4.7 MAH Cycle: Minimum temperature vs productivity

Because high air temperature in humidifier has led the carrier gas to gain more water vapor therefore, resulting into a better heat and mass exchange. Distillate production peaked at 25.2 °C. It is to be noted that the temperature range represented here can be maintained in the lab by space conditioning. Moreover, the data presented previously at different MR values is recorded at an average temperature of 25.4 °C because such conditions are possible to maintain and are nearer to the atmospheric state. Undoubtedly, feedwater temperature cannot be increased beyond a certain limit. Increasing it further would pull the productivity down, due to ineffective condensation in dehumidifier [56]. Decreased temperature gradient would hinder the moist air from dropping its vapor content and producing freshwater. As a consequence, the distillate flowrate is lowered.

4.4.7 Effect of MR on Component Effectiveness

Figure 4.8 presents the change in the effectiveness of components with mass flowrate ratio, for a fix-sized humidification-dehumidification unit. Prior to discussing this trend, it is worth mentioning that out of limited studies that are available on the MAH-HDH cycle, nearly all of them considered the component effectiveness to be constant even for analysis that included examining the impact of MR on other operational parameters [56], [57], [93]. Such investigations are acceptable for analytical understanding of wider perspective. These studies are substantial in the design process where a system has to be erected from the scratch. Considering effectiveness to be constant at different mass flowrate ratios would let the size of components to float, from one MR value to the other. To address this

limitation, an experimental evaluation was needed where physical size of the system remained fixed.

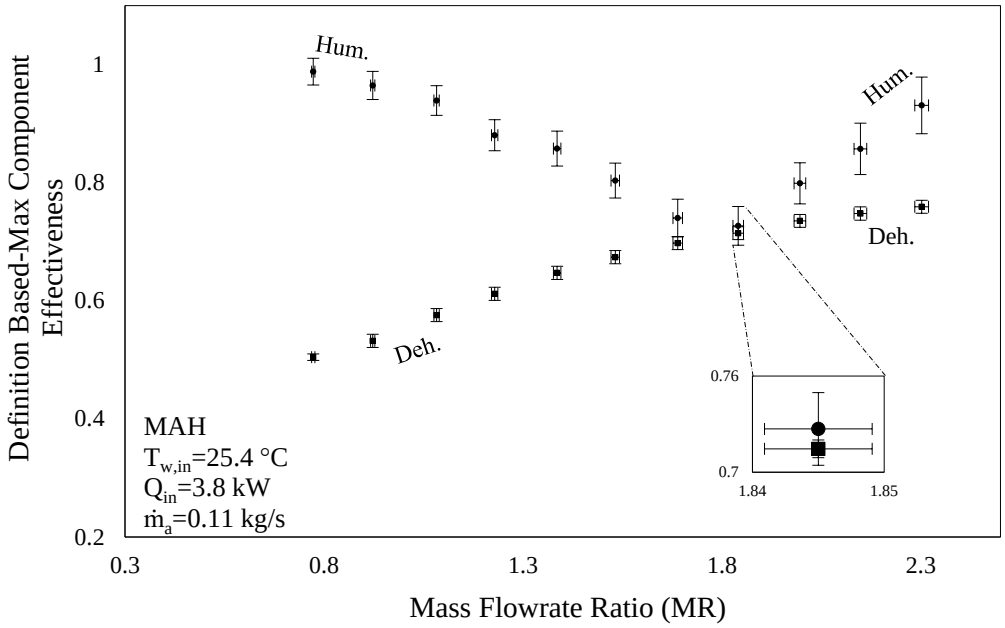

Figure 4.8 MAH Cycle: Mass flowrate ratio vs maximum component effectiveness

However, varying MR in the latter case would affect component effectiveness. Therefore, effectiveness values of the humidifier and the dehumidifier are expected to be different for each individual mass flowrate ratio. As explained earlier, shifting feed flowrates from one value to another, has an influence on temperatures across the system. Finally, changing these temperatures would change enthalpies or the energy content carried by the streams which eventually leads to the variation in effectiveness of system components. The above scatter diagram presents this change in effectiveness for a fix-sized system. It can be witnessed that increasing the mass flowrate ratio under specified initial conditions, surged dehumidifier effectiveness but it remained well below the mark of one. From theoretical viewpoint, it is understood that an optimally balanced dehumidifier (HCR_d=1) is of more

significance than a balanced humidifier, in the case of modified air heated cycle [55] [91]. Dehumidifier, at thermally balanced state attains minimum entropy generation and it can contribute towards achieving the maximum GOR value. Nonetheless, sizing and operational constraints in current experimental setting do not allow the condensing component to achieve the desired state. ε_D maximized at mass flowrate ratio of 2.30. In contrast, humidifier effectiveness is noticed to be diminishing with MR over the range where the water side effectiveness prevails but then it changes the course at $\dot{m}_w$=11 lpm and starts to increase from there onwards, as the air side effectiveness takes over. Definition of ε_H is given in equation (8). This behavior can further be analyzed in figure 4.9. In addition to that, figure 4.10 shows the stream-wise effectiveness in dehumidifier. It can be observed that air side has kept its precedence in this case.

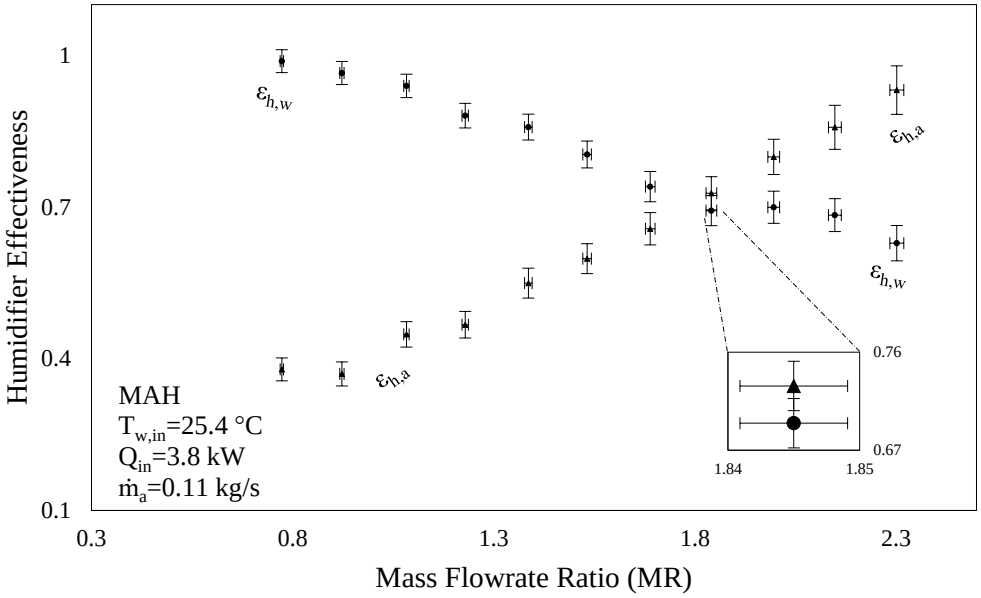

Figure 4.9 MAH Cycle: Mass flowrate ratio vs humidifier effectiveness

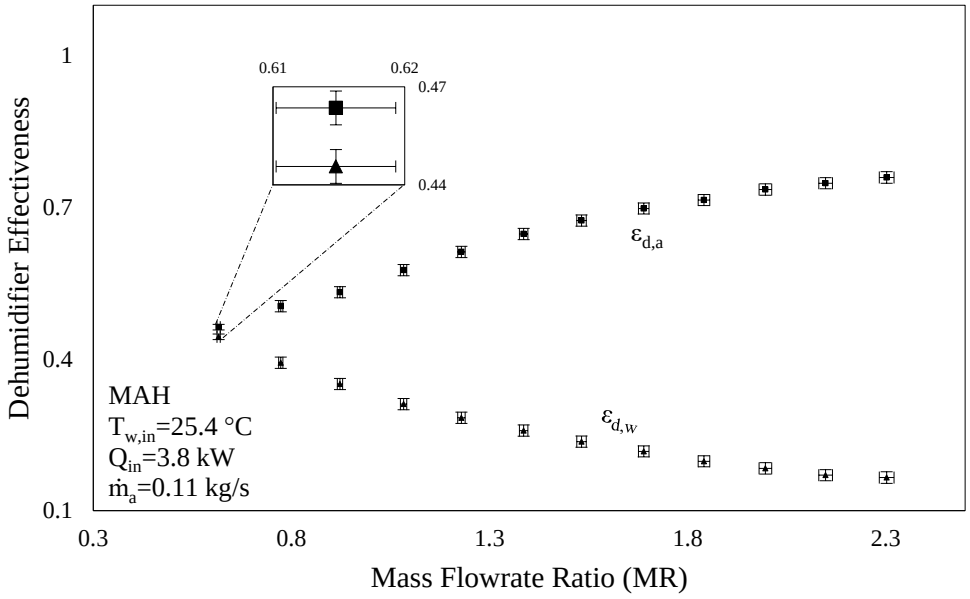

Figure 4.10 MAH Cycle: Mass flowrate ratio vs dehumidifier effectiveness

4.4.8 Effect of MR on Heat Capacity Ratio

Modified heat capacity rate ratio (HCR) is of significance in determining the thermally balanced condition for heat and mass exchangers. It is defined as the ratio of maximum possible change in enthalpy of cold fluid stream to the maximum possible change in enthalpy of hot fluid stream. Narayan [94] has shown previously that for various values of component effectiveness, the entropy generation gets minimized at an HCR value of 1. However, that study kept component effectiveness, pressure, relative humidity, fixed at a single value and then changed operating parameters like $\dot{m}_w$, MR and $T_{w,i}$ to observe the behavior. In present study, effectiveness is a function of MR since the physical size of the system is fixed. Figure 4.11 shows the variation in modified heat capacity ratio with mass

flowrate ratio. In the humidifier, it decreases with increasing MR. As value of HCR_h is noted to be 1.06 at MR of 1.39. It signifies that for this particular MR value ($\dot{m}_w$=9 lpm), the humidifying component in the system is balanced.

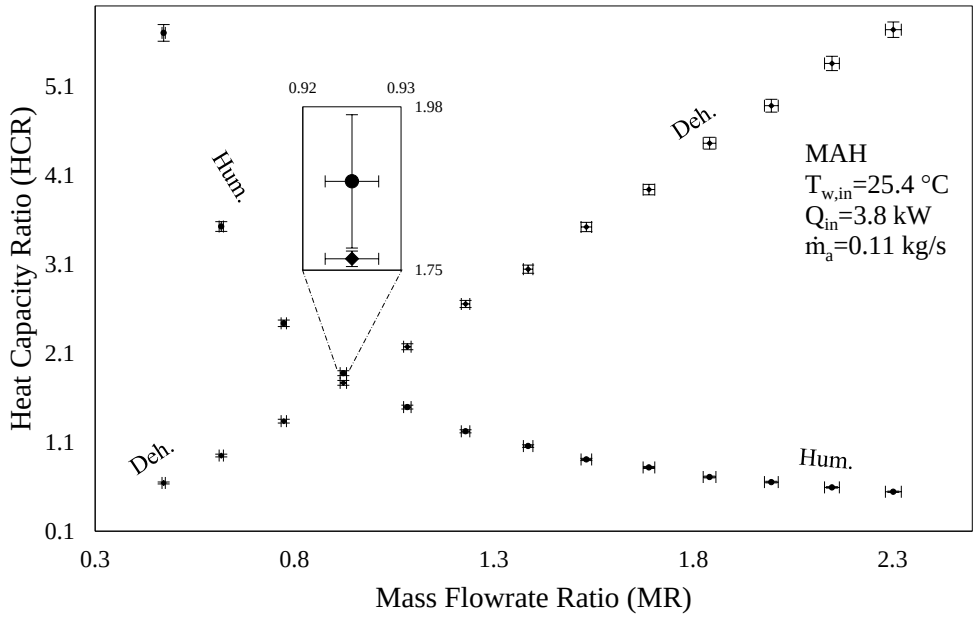

Figure 4.11 MAH Cycle: Mass flowrate ratio vs heat capacity ratio

It also describes that if system conditions remain rooted to this state then this is the point where the evaporator will perform with minimum performance losses. But it has been known from analytical deductions that a balanced dehumidifier is of more significance to the overall performance of modified air heated cycle than a balanced humidifier. Likewise, for the dehumidifier, the heat capacity rate ratio is witnessed to be increasing with MR. Again, it is reminded here that the effectiveness of the physical component is not fixed, and it changes with stream flowrates. The HCR_d reaches a value of one at the point where $\dot{m}_w$ is slightly higher than 4 lpm. It identifies that the physical size of dehumidifier is optimal when operated at this condition. If all system conditions are locked at this point

and inlet stream temperatures are varied, as Narayan [94] did in his study then distillate produce would peak at this point. Whereas in the present case with floating effectiveness, freshwater productivity is not expected to peak at MR=0.7. Because there are other effectiveness values at which even an unbalanced dehumidifier has more output. Highest production rate in experimental setting was recorded at MR of 1.53 where the HCR_d is not one. It tells that even higher produce would have been possible had the dehumidifier is designed to have a heat capacity ratio of one at mass flowrate ratio of 1.53. In most cases, the size of individual components, especially of dehumidifier in the present case would need to be increased to a larger extent, in order to reach the desired operational state. In figure 4.11, HCR_h is witnessed to decrease from 5.70 to 0.54, over the MR range of 0.47 - 2.30. Whereas, the HCR_d showed an incremental trend with values varying between 0.64 and 5.73.

4.4.9 Effect of MR on Specific Electrical Energy Consumption and Production Cost

Figure 4.12 illustrates the effect of mass flowrate ratio on specific electrical energy consumption of the system. SEEC represents the amount energy expended by air heater, pump and blower to produce one kilogram of water in one hour. As depicted, the SEEC decreases with increasing MR till an optimum point is reached, where it is minimum indicating least utilization of electrical energy by the system and improvement in the rate of distillate production. Note that minimum SEEC occurs at an optimum MR value where the productivity and GOR of cycle are maximum. The SEEC decreases initially with increasing MR, because at low MR values water recovers more heat in dehumidifier and consequently exchanges more of its energy content with air stream in humidifier. As a

result, the carrier gas exits humidifier at higher absolute humidity leading to better overall performance. Increasing MR beyond optimum value gives low feedwater temperature at humidifier inlet, causing low humid air temperature and specific humidity at the humidifier exit. It yields high specific electrical energy consumption by decreasing productivity. Increasing feedwater flowrate from 3 to 15 lpm, varies SEEC from 1.99 kWh/kg to 1.72 kWh/kg. At the $\dot{m}_w$ of 10 lpm, the SEEC is recorded to be minimum with value of 1.54 kWh/kg. Figure 4.13 presents the cost of freshwater production with changing mass flowrate ratios. Electricity cost is a major factor in evaluating the cost of freshwater from the system. The effect of MR on production cost is consistent with other performance parameters. Minimum cost of producing freshwater at optimum mass flowrate ratio is 0.079 $/kg. Meanwhile at specified initial conditions, the average distillate production cost with MR ranging from 0.47 to 2.30 is 0.085 $/kg.

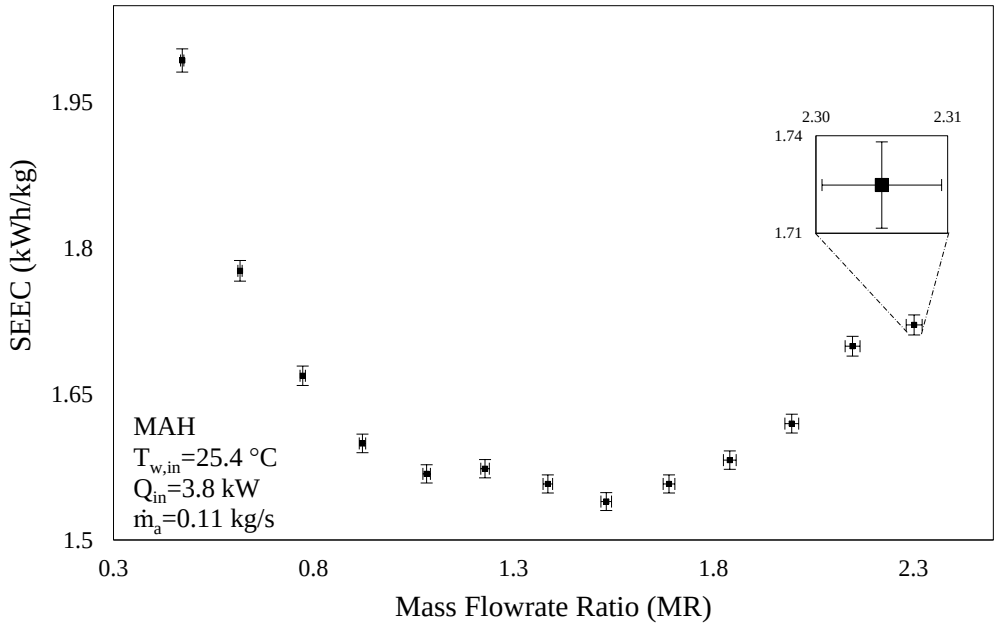

Figure 4.12 MAH Cycle Mass flowrate ratio vs specific electrical energy consumption

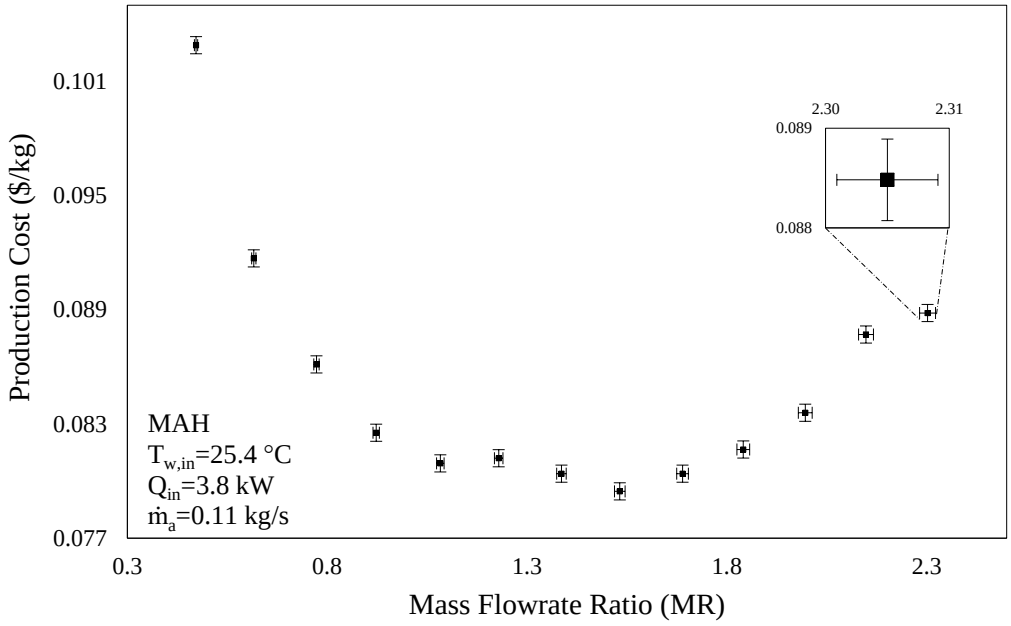

Figure 4.13 MAH Cycle: Mass flowrate ratio vs production cost

4.5 Experimental Results of CAOW-DH-HDH Cycle

The dual heated humidification-dehumidification cycle with closed air and open water loop is investigated, experimentally. As explained in the previous chapter, physical properties of the module allow it to configure into different heating modes. In dual heating mode, water stream is heated before it enters the humidifier and air stream is heated after it leaves the humidifier. Two different cases are studied to understand the impact of heat rate on system performance and energy input differentiates one case from the other. Consequently, heat input to the air stream is kept constant in both cases at 1.59 kW. However, the water stream is provided with different energy inputs in each case. In the first case (DH-I), 1.42 kW of input energy is provided to the water exiting from dehumidifier and for second case

(DH-II), it is kept at 2.82 kW. Temperature of feedwater is maintained at nearly a constant value in both settings i.e. 25.7 ± 0.1 °C and 25.6 ± 0.07 °C for DH-I and DH-II, respectively.

4.5.1 Effect of MR on Gain Output Ratio

The influence of changing mass flowrate ratio on gain output ratio, in the case of dual heated cycle is presented in figures 4.14 and 4.15. It is noteworthy here that in addition to post-humidification air heating, the preheated water coming out from dehumidifier is also being heated before it enters humidifier. GOR of DH-I cycle with total Q_{in} of 3.0 kW is illustrated in figure 4.14, which identifies variation in system performance with MR. It can be perceived that increasing the MR, increases GOR. This increase in thermal performance can be explained with increased moist-air capacity to absorb water vapor.

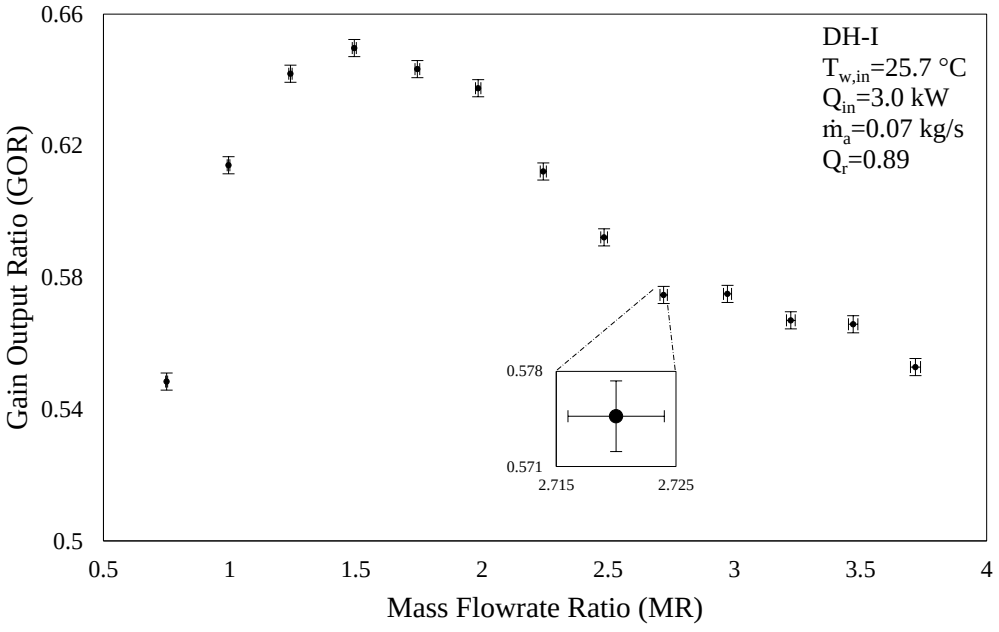

Figure 4.14 DH-I Cycle: Mass flowrate ratio vs gain output ratio

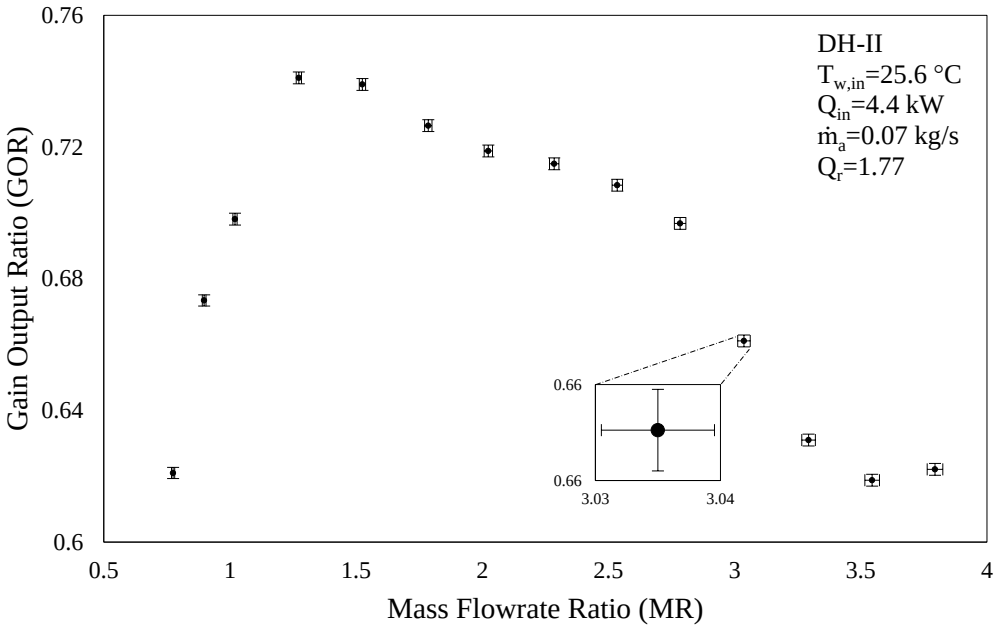

Figure 4.15 DH-II Cycle: Mass flowrate ratio vs gain output ratio

Moreover, GOR in dual heated cycle seems to surge at a relatively greater pace, that is because water is being heated in a water heater and when this hot water interacts with air, it increases the air temperature more rapidly thus enabling it to carry more moisture at humidifier exit. However, this upward trend breaks at an optimum point, where the GOR is maximum. This point signifies that under the given conditions both water and air streams are reasonably adequate for each other. Such that maximum heat and mass exchange takes place between them. For DH-I, the optimum performance with GOR of 0.65 is reached at mass flowrate ratio of 1.49. After that the performance sloped downwards because air does not take in additional water that eventually drains out of the system with its added energy. Thus, decreasing the GOR. Similarly, figure 4.15 shows the relation between GOR and MR at heat rate ratio of 1.77. It is obvious that the performance in later case is better than the previous one. GOR maximizes at 0.74 with an MR value of 1.27. Despite higher

expense of energy, the GOR in DH-II case comes out to be greater which signifies the impact of heating water stream on the overall cycle performance. The rational explanation for curve behavior is same as explained earlier. However, it is evident that increasing heat rate has added to overall performance of the system. One exception is that the post-optimum performance fall is not as steep for DH-II as it is in the case DH-I. It can be attributed to the fact that water at same $\dot{m}_w$ has more added energy content in DH-II and its temperature is also higher. Resultantly, it would be able to heat the air more in humidifier which could then carry more vapor than it carried at the same $\dot{m}_w$ in DH-I case.

4.5.2 Effect of MR on Productivity

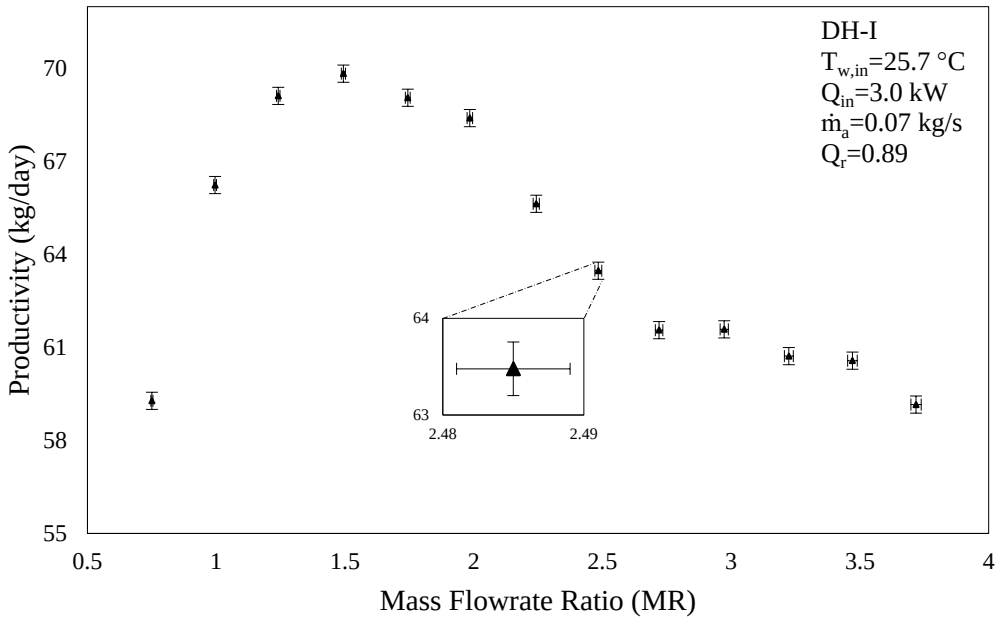

Figure 4.16 DH-I Cycle: Mass flowrate ratio vs productivity

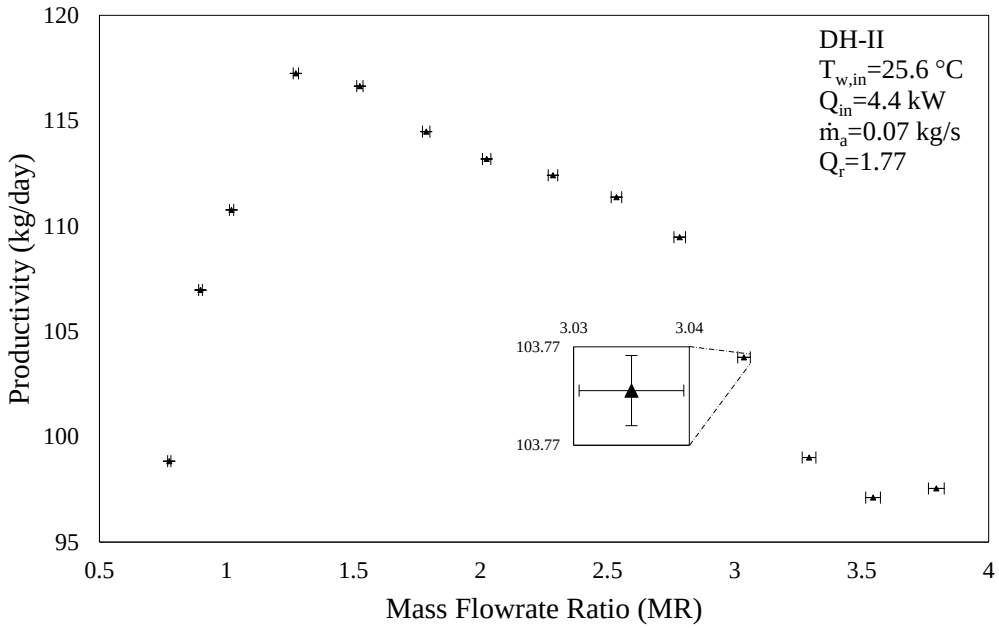

Figure 4.17 DH-II Cycle: Mass flowrate ratio vs productivity

Productivity of the dual heated cycle is plotted with mass flowrate ratio at two different heating inputs, in figures 4.16 and 4.17. Productivity variance follows the trail of GOR and rightly so, because it is directly related to GOR. The increasing and decreasing trends in distillate production are quite similar to that of GOR, for the same reasons, given in the previous section. For DH-I with Q_{in} of 3.0 kW, the maximum recorded production rate is 69.8 kg/day. It is only 3.99 % less than the maximum output from modified air heated cycle. Meanwhile, to achieve maximum productivity, the MAH cycle consumed 27.7 % more energy than the dual heated-I cycle. This inclination can be associated to the specific heat capacity of water. Once heated, water stream has better ability to ingest and retain its energy owning to its thermal capacity. Similarly, uplifting the heat input to 4.4 kW results into a maximum productivity of 117.2 kg/day, that is 40.4 % higher than the DH-I case. In fact, the minimum production output from DH-II mode is even higher than the maximum

product water outflow from modified air heated or DH-I cycle. It implies that adding more heat to the water stream does payoff in higher outflux of freshwater from the unit. Energy added to DH-II is 14.6 % and 46.3 % higher than the modified air heated and dual heated-I cycles, respectively. Consequently, the maximum freshwater produce from the cycle is 61.2 % and 67.9 % higher when compared to the MAH and DH-I systems, respectively. From stipulated experimental data, it is obvious that for a fix-sized system, dual heating is beneficial in general in terms of thermal performance and the productivity from this configuration is expected to increase with the heat rate.

4.5.3 Effect of MR on Recovery Ratio

Figures 4.18 and 4.19 present the effect of changing mass flowrate ratio on recovery ratio for dual heated humidification-dehumidification cycle in DH-I and DH-II mode, respectively. Percentage recovery ratio traces the amount of freshwater produced per feedwater consumption. As expected, RR decreases with increasing MR in both cases. RR only tracks the material gain in an operational cycle. It does not count energy recovery during the process. Likewise, at low mass flowrates of feedwater the quantity of distillate collected is higher. It is anticipated because air stream has the capacity at low mass flowrate ratio to take in vapor from sprayed water. Also, the heated water stream in the humidifier elevates air temperature, enabling it to gain surplus moisture content. As mass flowrate ratio increases, the respective temperatures of water at dehumidifier exit and humidifier inlet decrease, due to decrease in the residence time of water in condenser and heater.

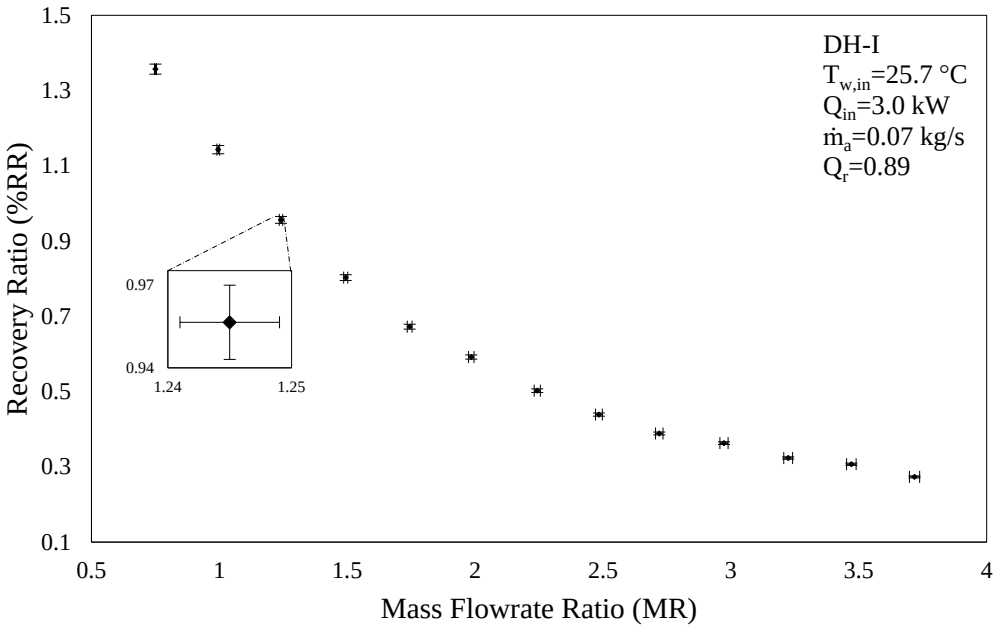

Figure 4.18 DH-I Cycle: Mass flowrate ratio vs recovery ratio

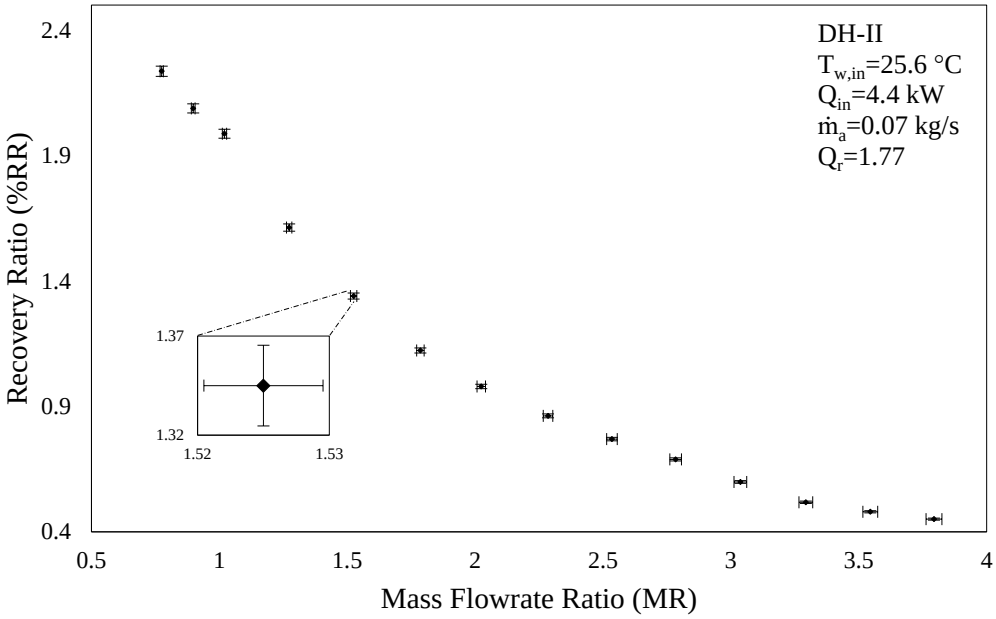

Figure 4.19 DH-II Cycle: Mass flowrate ratio vs recovery ratio

Moreover, it is evident from the energy balance that higher feedwater flowrates lead to smaller energy gains. At higher feed flowrates, brine discharge from humidifier increases which implies that air stream has nearly reached its saturation state and would not accept supplementary humidity that water stream has to offer. Maximum RR of 1.36 is recorded for the dual heated cycle when heat rate ratio is 0.89. Increasing the heat rate ratio to 1.77 results into an increased value for maximum RR that is 2.24. In either case, the maximum recovery ratio reported for dual heated cycle is higher than the corresponding maximum value observed in the modified air heated system. Average values of RR in DH-I and DH-II case are 0.62 and 1.12, respectively. Whereas for MAH system, the average is noted to be 0.64. Meanwhile, total energy input provided to DH-I is 28 % less than MAH cycle.

4.5.4 Effect of MR on Maximum Cycle Temperature

Variation in maximum temperature with mass flowrate ratio is illustrated in figure 4.20 and 4.21 for the case of dual heated cycle. Air stream exiting the heating unit is observed to hold the maximum cycle temperature. Figure 4.20 pronounces the change when total heat input to the cycle is 3.0 kW, out of which 1.59 kW is being used to heat the air. The proclivity of cycle's maximum temperature towards air despite water heating can be attributed to its low specific heat capacity. Water, on the contrary has relatively high thermal capacity therefore it takes more energy to raise its temperature. In the dual heated cycle, maximum temperature of air is reached at the lowest mass flowrate ratio. Firstly, because water with low flowrate is destined to recover more energy in dehumidifier.

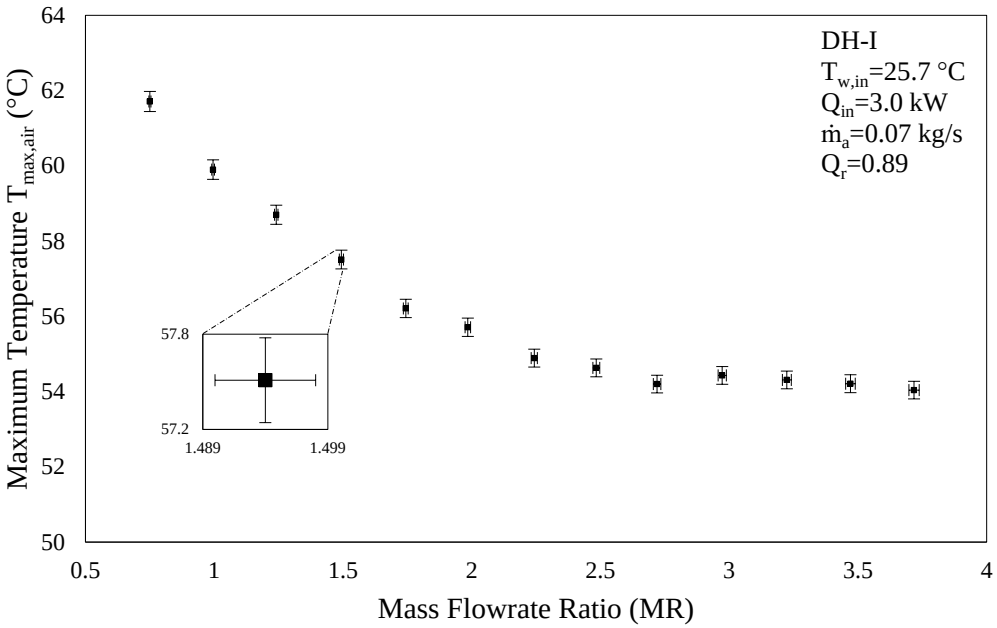

Figure 4.20 DH-I Cycle: Mass flowrate ratio vs maximum temperature

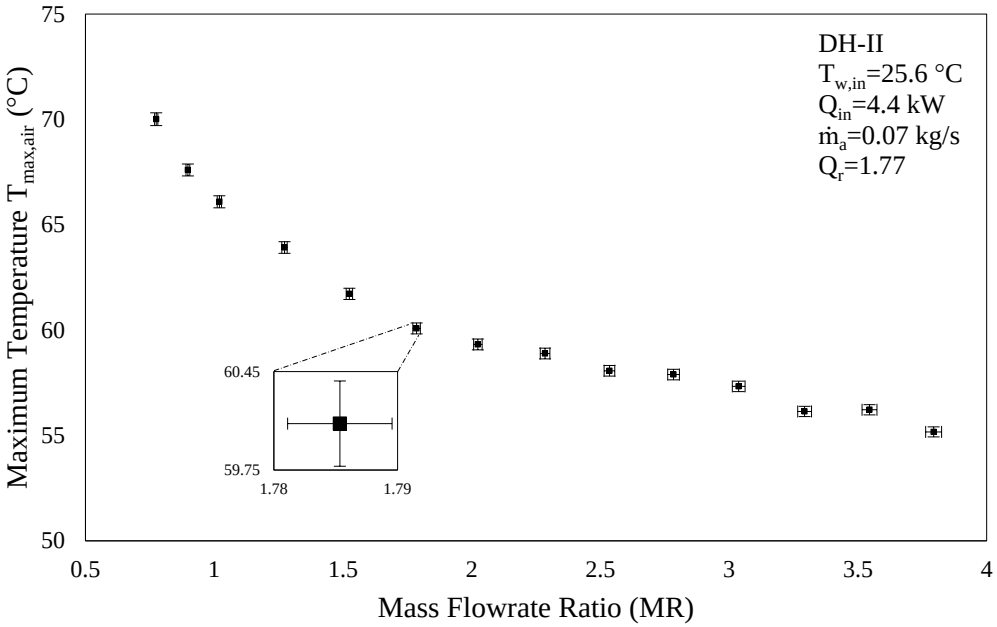

Figure 4.21 DH-II Cycle: Mass flowrate ratio vs maximum temperature

Following that, it enters the water heating unit where is absorbs additional energy with effective duration for heat exchange. Subsequently, it enters humidifier at higher temperature and heats up the air to the same extent. Secondly at low MR values, air exiting the humidifier is at a higher temperature, owning to its heat and mass exchange with water stream. Additional energy gained by the air-vapor mixture in air heating unit further elevates the temperature of humid air at the inlet of dehumidifier. Hence, it ends up with highest $T_{max,air}$ at lowest MR value. In DH-I mode, the highest and lowest values of $T_{max,air}$ are observed to be 61.7°C and 54.0°C, at feedwater flowrates of 3 and 15 lpm. Similarly, DH-II mode with more energy input to the water stream showed greater $T_{max,air}$. High inlet water temperatures would increase the exit air temperature in humidifier. Sequentially in air heater, energy would be added to the air stream that is already at a higher temperature. In this mode, the maximum temperature of dual heated HDH cycle peaked at 70.0 °C and it dipped to 55.2 °C, as MR increased from 0.77 to 3.79. Average maximum cycle temperature is recorded to be 56.2 °C and 60.6 °C for DH-I and DH-II cases, respectively.

4.5.5 Effect of MR on Water Temperature

Effect of changing MR on temperature of water passing through a dual heated HDH cycle, is presented in this section. In both set of experimental runs, temperature of water at the inlet to dehumidifier is kept constant at around 25 °C. As water ascends through the dehumidifier, it condenses freshwater out from the moist air and recovers the heat of condensation from the humid air stream.

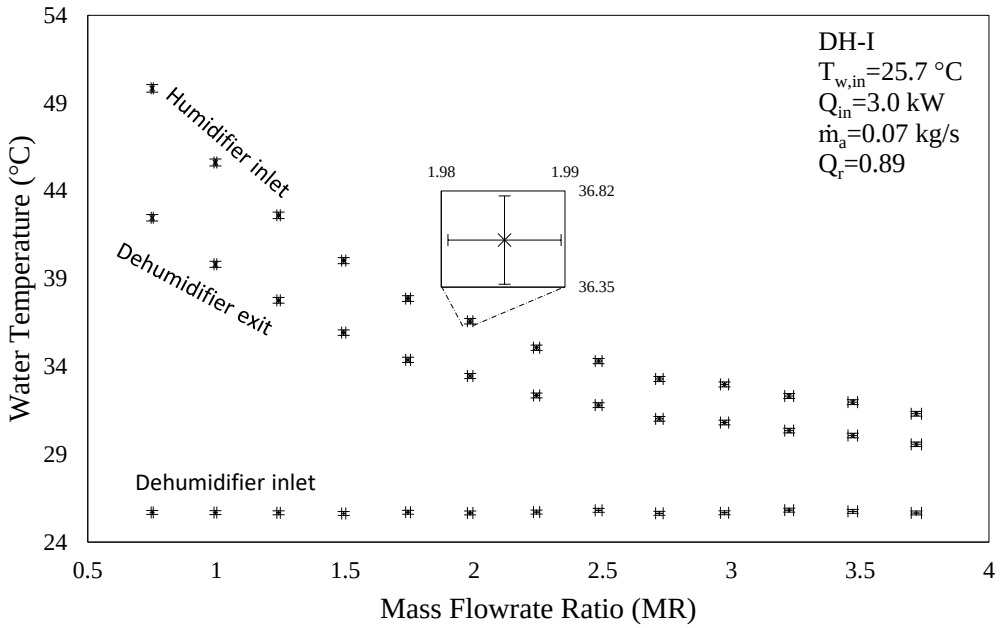

Figure 4.22 DH-I Cycle: Mass flowrate ratio vs water temperature

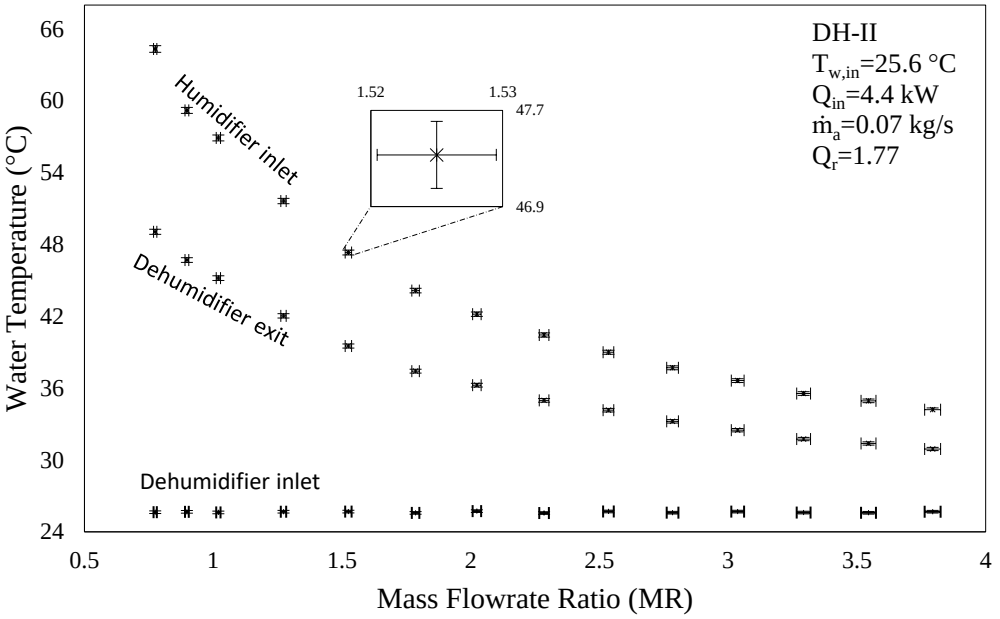

Figure 4.23 DH-II Cycle: Mass flowrate ratio vs water temperature

In due course, when it reaches the exit of dehumidifier, its temperature has been elevated. The degree of temperature increase is dependent on the temperature of interacting air stream and feed flowrate. Carrier gas in the dehumidifier is coming in from the air heating unit, it is at the maximum cycle temperature when it enters the dehumidifier. Its conduct is explained in the preceding section. Meanwhile at sunken feed flowrates, water flowing through the condenser tubes is able to exchange heat more effectively than the case when $\dot{m}_w$ is high. It explains the decreasing trend in water temperature at dehumidifier exit with increase in the mass flowrate ratio. In dual heated HDH cycle, water at exit of dehumidifier is directed towards water heater where it gains additional thermal energy and then enters humidifier. Since consistent amount of energy is provided to the water heater, temperature at humidifier inlet mainly depends on the temperature of water at dehumidifier exit. Another noticeable detail is that the gap between temperatures at dehumidifier exit and humidifier inlet, decreases with the increase in MR. It is destined to happen because feed flowrate surges with MR, which evidently limits the time period during which heat transfer can occur from heating elements to the water. Figure 4.22 illustrates the case for DH-I cycle where Q_{in} is 3.0 kW and the maximum temperature reached by water stream is 49.8 °C, at $\dot{m}_w$ of 3 lpm. Comparably, when the heat input is increased to 4.4 kW with same MR value, the highest temperature at humidifier inlet is recorded at 64.3 °C, as shown in figure 4.23. Finally, it should be observed here that like modified air heated cycle, water enters the humidifier at a higher temperature than air. It ensures an effective heat and mass exchange and improves overall system performance.

4.5.6 Effect of MR on Component Effectiveness of DH-I Cycle

In a dual heated HDH system, figures 4.24, 4.25 and 4.26 show the influence of changing MR on the effectiveness of components, in a fix-sized experimental unit. Both humidifier dehumidifier effectiveness values are computed at specified initial conditions. General trend between MR and ε is expected to remain same, as the physical size of system components remain unchanged in the dual heated configuration.

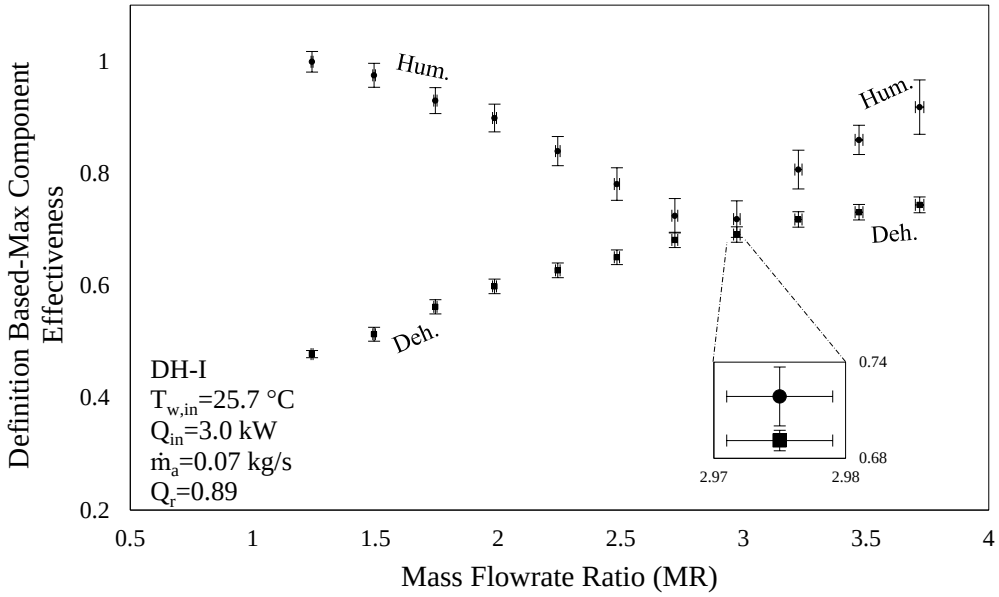

Figure 4.24 DH-I Cycle: Mass flowrate ratio vs maximum component effectiveness

In first segment of curve, the effectiveness of the humidifier is witnessed to decrease with increasing MR, as shown in figure 4.24. This decreasing section shows that the $\Delta H_{max,water}$ in humidifier has the minimum value during this period. At mass flowrate ratio of 2.97, the maximum effectiveness value switches from water to air stream. From this point onwards, $\Delta H_{max,air}$ becomes minimum value of maximum possible enthalpy change.

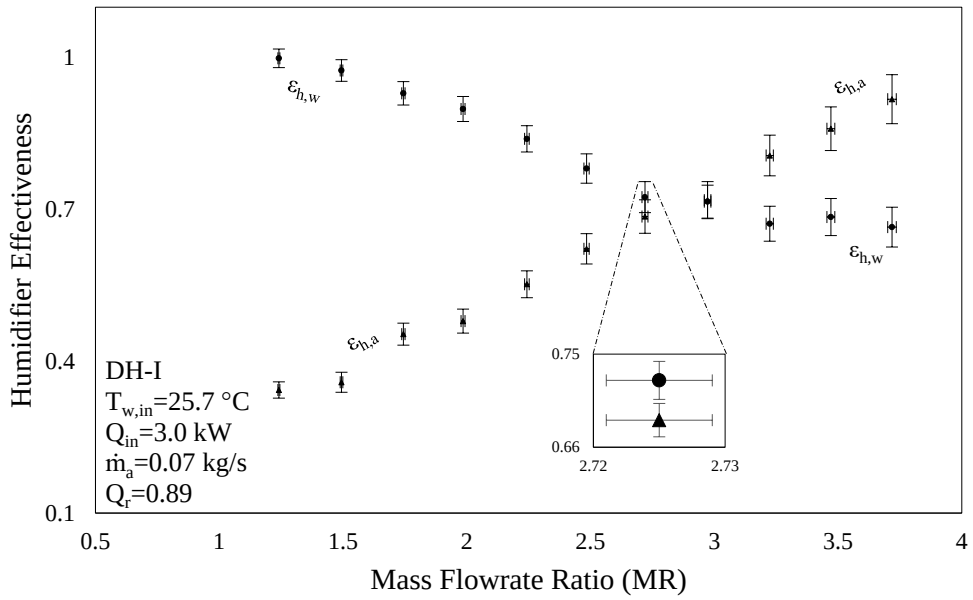

Figure 4.25 DH-I Cycle: Mass flowrate ratio vs humidifier effectiveness

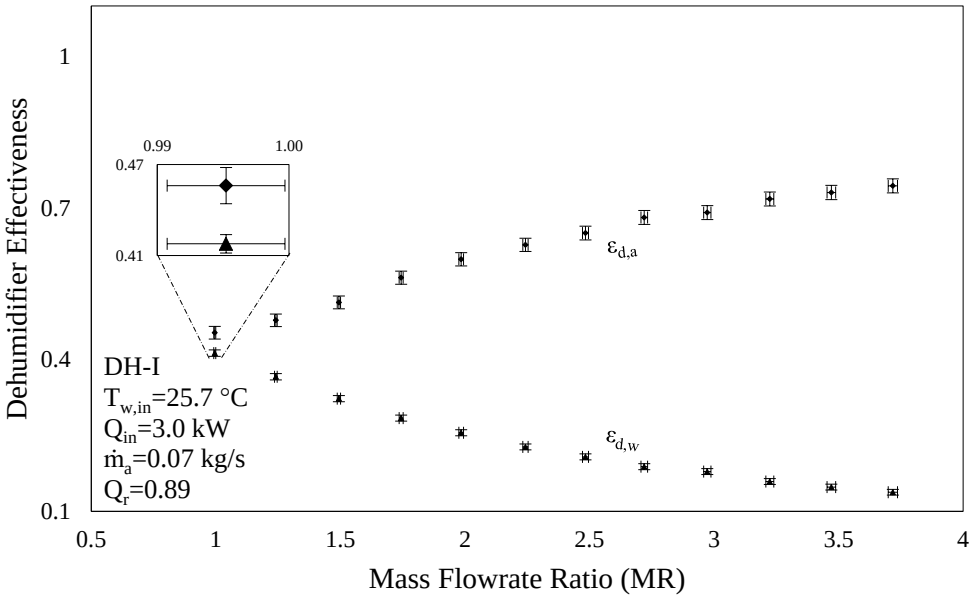

Figure 4.26 DH-I Cycle: Mass flowrate ratio vs dehumidifier effectiveness

Figure 4.25 represents this transformation by demonstrating the change in effectiveness values for individual fluid streams. Effectiveness of humidifier remained higher than dehumidifier, throughout the experimental observation. Whereas, dehumidifier effectiveness ranged between 0.48 and 0.74 over the feed flowrate ranging from 3 lpm to 15 lpm. Effect of discrete behavior of flowing streams on the effectiveness of the dehumidifier is depicted in figure 4.26. As demonstrated, air side effectiveness has kept its primacy with the change in MR. In dehumidifier, as water flowrate $\dot{m}_w$ increases, ΔT_{water} between dehumidifier inlet and exit decreases. As discussed in figure 4.22 previously, it implies that average temperature of water side in dehumidifier has decreased with MR even though the rate of heat input has not been changed. Furthermore, the temperature difference between points along the length of condenser is proportional to the rate of heat transfer between them. Lowering the average water temperature by increasing MR means better heat transfer from hot and humid air to the now relatively cooler water stream. Consequently, the carrier gas gets an effective heat and mass exchange as it passes through the condensing component of the system. Maximum effectiveness of dehumidifier 0.74 is reached at $\dot{m}_w$ of 15 lpm.

4.5.7 Effect of MR on Component Effectiveness of DH-II Cycle

Figures 4.27 to 4.29 illustrate the change in effectiveness of experimental HDH setup with mass flowrate ratio. In the present case, a similar dual heated cycle is under consideration except for the fact that heat input has been elevated to 4.4 kW. Figure 4.27 shows that humidifier effectiveness remains relatively higher than dehumidifier, as in the preceding

case. However, once the ε_{max} has converted from water to air-based definition in humidifier, the values didn't hike as they did in the previous case and remained close to the dehumidifier effectiveness. It can be attributed to the relative increase in water temperature at inlet of the humidifier. Variation range in the case of dehumidifier also remained unchanged, partly because size of the component is fixed and testing range in terms of mass flowrate ratio is same as it was in DH-I mode. Perceptible representation of maximum humidifier effectiveness is given in figure 4.28. It delineates the path that ε_h follows, as it alters its definition based on minimum value for either $\Delta H_{max,air}$ or $\Delta H_{max,water}$.

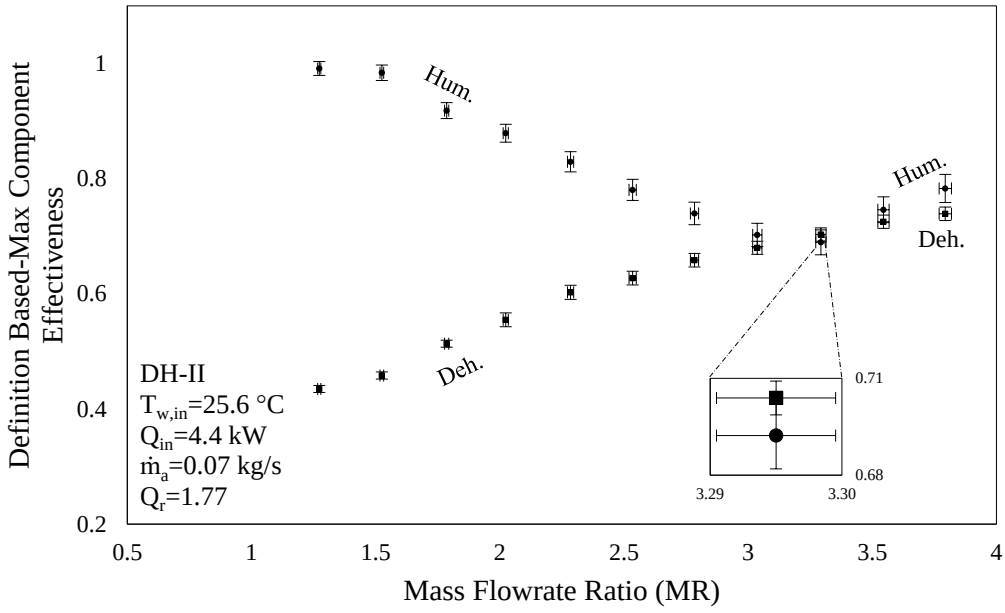

Figure 4.27 DH-II Cycle: Mass flowrate ratio vs maximum component effectiveness

Finally, figure 4.29 shows the occurrences in dehumidifier. Increasing the MR lead to an increase in the overall effectiveness of dehumidifier. But it still remained less than the humidifier. Over the range of ε_d variance with MR, air has the minimum value of maximum

possible enthalpy change $\Delta H_{max,air}$. Maximum value of ε_d is reported to be 0.75 at $\dot{m}_w$ of 15 lpm.

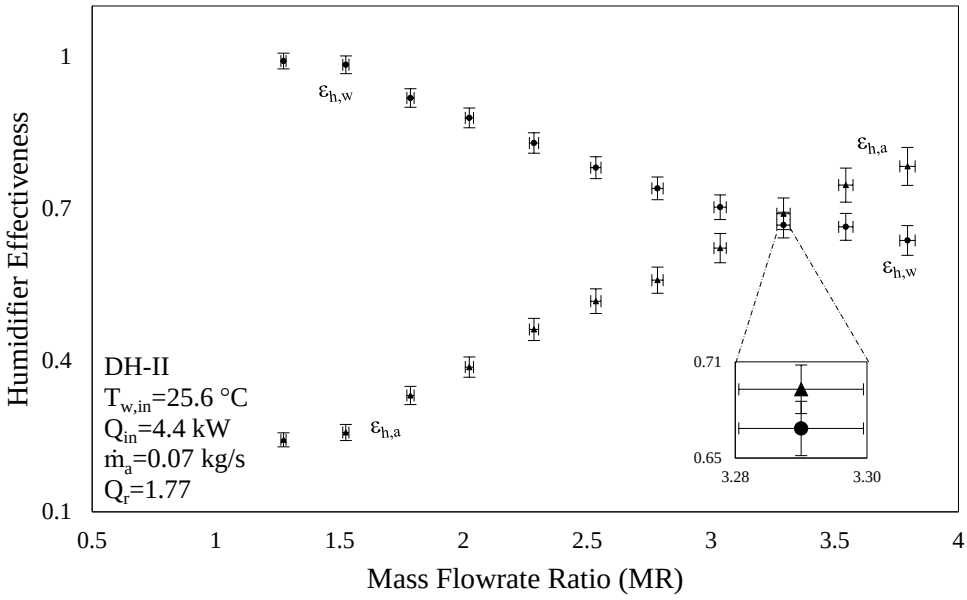

Figure 4.28 DH-II Cycle: Mass flowrate ratio vs humidifier effectiveness

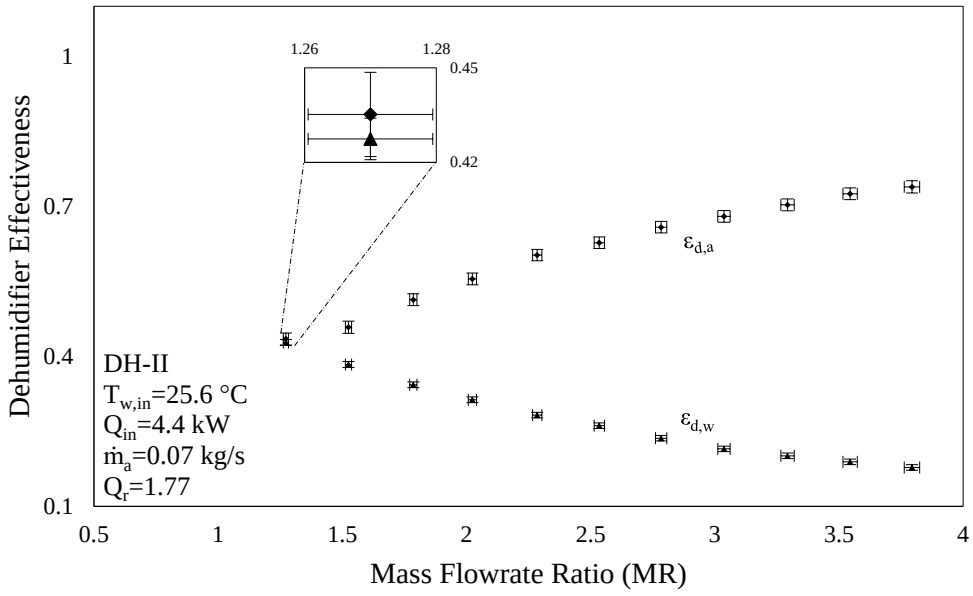

Figure 4.29 DH-II Cycle: Mass flowrate ratio vs dehumidifier effectiveness

4.5.8 Effect of MR on Heat Capacity Ratio

Impact of changing mass flowrate ratio on modified heat capacity ratio is illustrated in figures 4.30 and 4.31 at heat rate ratios of 0.89 and 1.77, respectively. Present experimental analysis is executed on a system that has set dimensions. Therefore, unlike reported work in literature, the effectiveness of individual components cannot be fixed. In theory, fixing the effectiveness allows the size of components to float. Not enough consideration is given to the practical aspect of this issue.

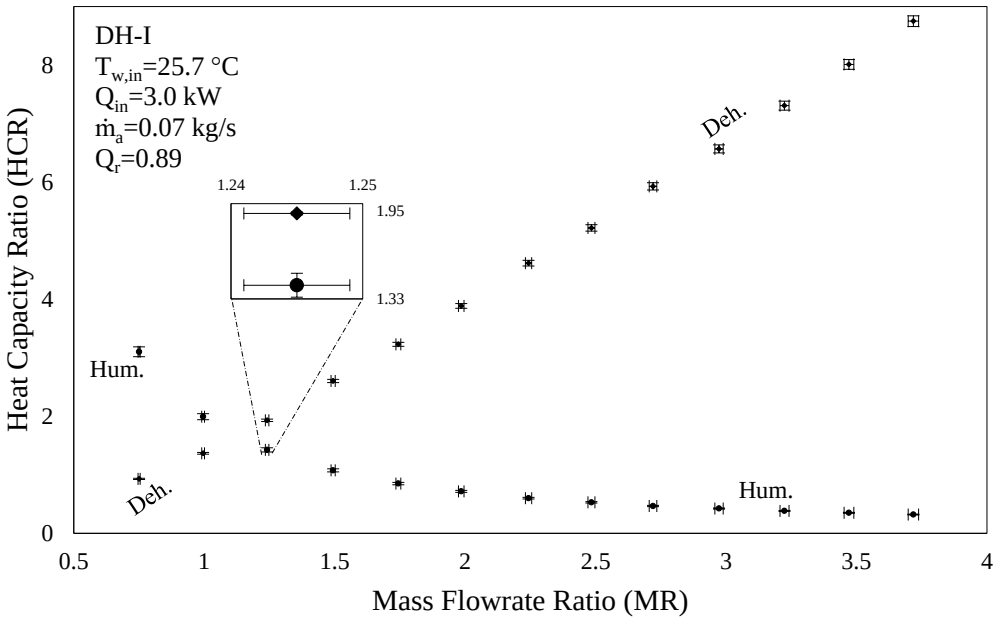

Figure 4.30 DH-I Cycle: Mass flowrate ratio vs heat capacity ratio

On the contrary, in this practical study, equipment sizes are fixed, and effectiveness values are allowed to float since they are dependent on the mass flowrate ratio. This pragmatic approach is inherently more rational, as in any operational plant the size is not expected to change with input variables. In this context, HCR in humidifier is shown to be decreasing with the increasing mass flowrate ratio. Increasing MR, decreases maximum cycle

temperatures which has an indirect effect on the feedwater temperature at humidifier inlet. The drop in $T_{water,in}$ leads to reduced air temperature at humidifier exit. As a consequence, $\Delta H_{max,air}$ decreases and since air is the cold fluid in humidifier, it escorts the HCR_h down with mass flowrate ratio. Graphical data presented in both figures show similar trends. In figure 4.30, HCR_h variations can be observed for DH-I cycle.

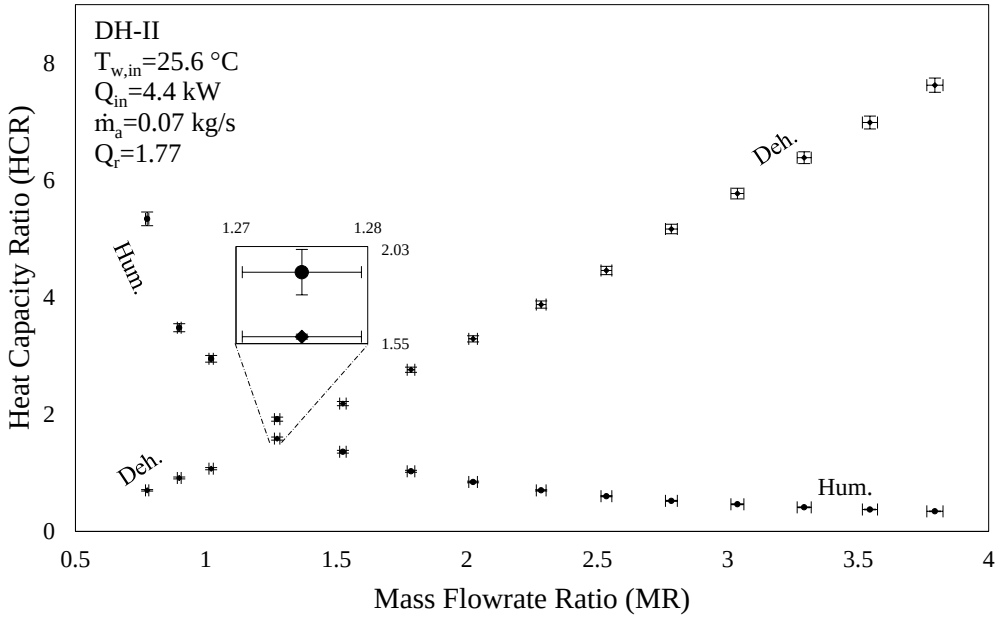

Figure 4.31 DH-II Cycle: Mass flowrate ratio vs heat capacity ratio

Whereas figure 4.31 presents the relationship for DH-II mode. In contrast, dehumidifier possesses water as the cold fluid and air as the hot fluid. Likewise, HCR_d is shown to be increasing with MR. Numeric value of HCR also signifies the balanced condition of component. For instance, an HCR values equals to one indicates that entropy generation is minimum. However, in theoretical sense this inference is made at constant component effectiveness by making temperature variations. In data presented above, HCR of one

stipulates that component is thermally stable if that effectiveness value is maintained at respective initial conditions.

4.5.9 Effect of MR on Specific Electrical Energy Consumption and Production Cost

The effect of varying mass flowrate ratio on specific electrical energy consumption of dual heated humidification-dehumidification desalination cycle is presented in figures 4.32 and 4.33. SEEC is witnessed to decrease with the increase in MR until an optimum point is reached. Beyond that optimum MR, the SEEC is observed to surge with MR. Decrease in SEEC indicates less consumption of electrical energy by blower, pump and heater. Simultaneously, it also specifies improved freshwater production rate. In DH-I case, SEEC recorded its maximum value of 1.55 kWh/kg at MR of 3.72. On contrary, the minimum reported value for specific energy consumption is 1.32 kWh/kg at mass flowrate ratio of 1.49. At high mass flowrate ratios, water temperature at dehumidifier exit and humidifier inlet is relatively lower, indicating less heat recovery in dehumidifier. Moreover, a large proportion of feedwater exits humidifier as brine with some available energy content. These factors tend to pull the productivity downwards, resulting into an increase in SEEC. Increasing the heat rate ratio 1.77 resulted into an overall decrease in SEEC values. Average specific consumption over MR ranging from 0.77 to 3.79 is recorded to be 1.17 kWh/kg. Minimum and maximum values of SEEC are noted to be 1.07 and 1.29 at feedwater flowrates of 5 and 14 lpm, respectively. Variation trends in SEEC are consistent with other performance metrics and indicate that specific electrical energy consumption is least when maximum cycle performance is achieved at optimum flowrate ratio.

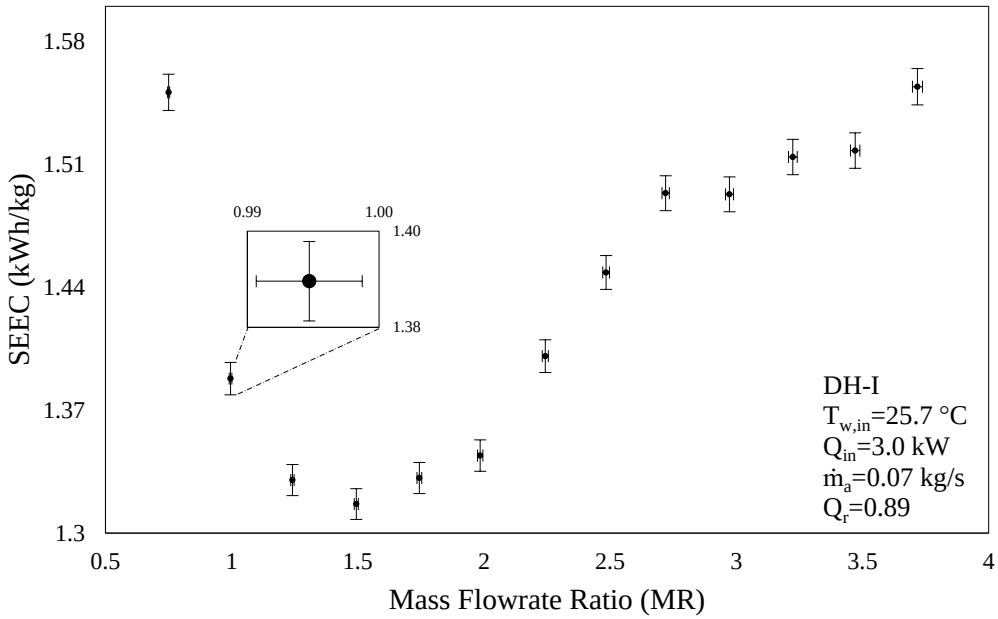

Figure 4.32 DH-I Cycle: Mass flowrate ratio vs specific electrical energy consumption

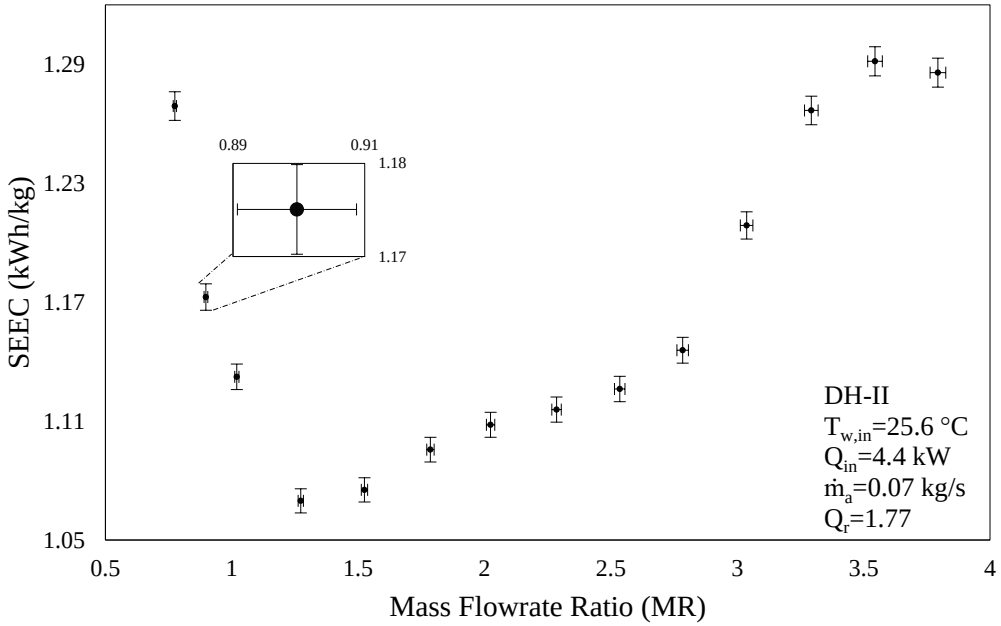

Figure 4.33 DH-II Cycle: Mass flowrate ratio vs specific electrical energy consumption

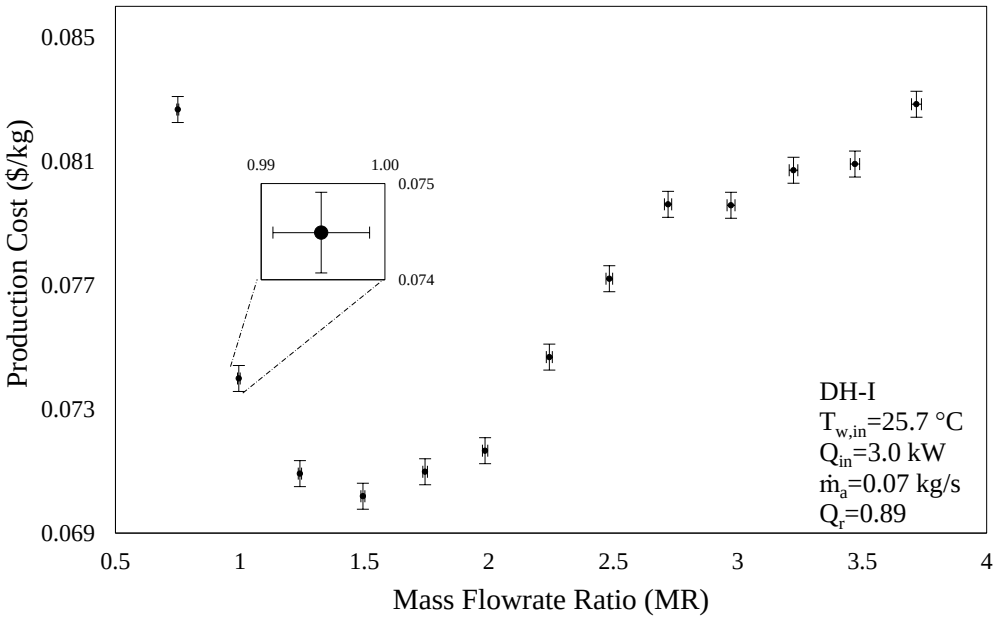

Figure 4.34 DH-I Cycle: Mass flowrate ratio vs production cost

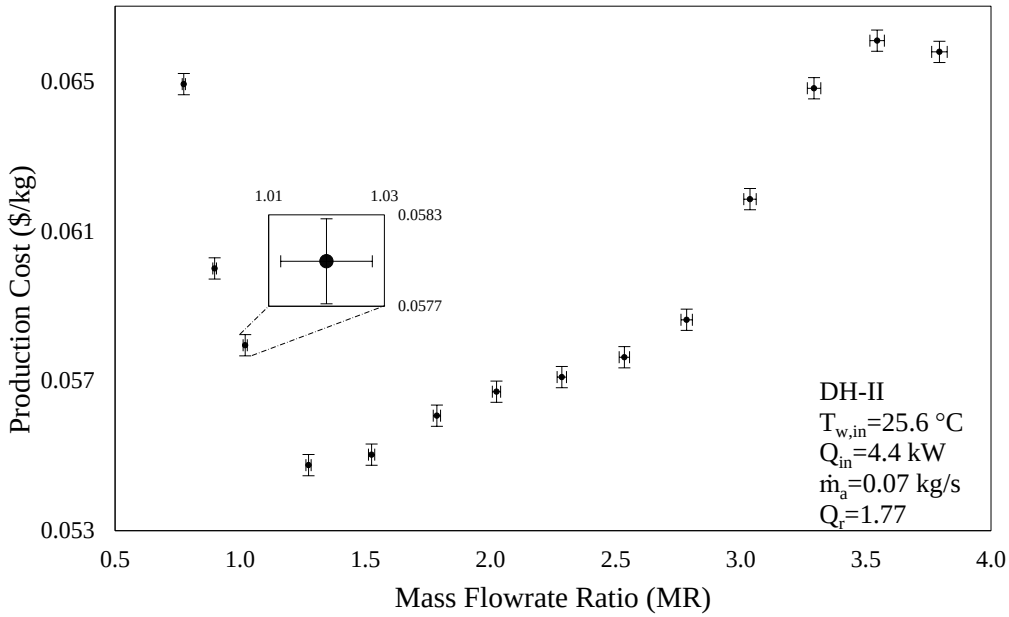

Figure 4.35 DH-II Cycle: Mass flowrate ratio vs production cost

Figures 4.34 and 4.35 illustrate the cost of freshwater production with the change in mass flowrate ratios. Both DH-I and DH-II cycles show minimum production cost at mass flowrate ratios where specific electrical energy consumption of the cycle is also minimum. Increasing the mass flowrate ratio from 0.7 to 3.7, resulted into an average production cost of 0.077 $/kg for the DH-I case whereas the average value for DH-II cycle is noted to be 0.060 $/kg. With Q_r of 0.89, minimum production cost of DH-I cycle is reported to be 0.070 $/kg at MR of 1.49. However, increasing Q_r to 1.77 resulted into 21.42% decrease in the cost of freshwater production. In DH-II cycle, the minimum is 0.055 $/kg at mass flowrate ratio of 1.27. Table 4.3 below is subjected to compare presented HDH system configurations with other HDH systems reported in the literature, for freshwater cost;

Table 4.3 Cost comparison of the current system with existing references

Reference	Features	Heating Source	Production Cost ($/kg)
Zubair et al. [41]	CAOW-HDH system with evacuated tube water heaters.	Solar energy	0.032-0.038
Hamed et al. [95]	CAOW-WH-HDH system with evacuated tubes for water heating.	Solar energy	0.0578
El-Agouz [96]	OAOW-WH-HDH system with water heating elements and separate loop for dehumidifier.	Electrical energy	0.052 - 0.095
Zhani and Bacha [71]	CAOW-DH-HDH system with flat plat collectors and an evaporator.	Solar energy	0.087
Deniz et al. [88]	OACW AH and WH-HDH cycle with PV panel and flat plate heaters.	Solar energy	0.098
Bacha [87]	CAOW-DH-HDH system with evaporation-condensation tower and flat plate collectors.	Solar energy	0.156
Muthusamy et al. [97]	OACW-DH-HDH system using air heater with circular inserts, band water heater and double pipe condenser.	Electrical energy	0.180
Current Study	CAOW-HDH system in modified air heated and dual heated configuration	Electrical energy	MAH: 0.085 DH:0.060-0.077

CHAPTER : 5

MATHEMATICAL MODELING AND VALIDATION

5.1 Analytical Model: Modified Air Heated HDH Cycle

The model devised here is a thermodynamic explanation of MAH-HDH system. Following the 1st law of thermodynamics, energy and mass balances are executed to system elements. As described earlier, in a CAOW modified AH HDH system, pre-heated water is diffused in humidifier that is hotter than the air. Warm water comes in direct contact with the incoming air and this air gets humidified and heated, in the humidifier. This hot and moist air exits humidifier and flow towards an air heater, where sensible heat is added before it advances to the dehumidifier. As it moves in the condensing unit, feedwater is heated through an indirect contact with air and vapor condenses out of the humid air stream. At the end of the cycle, dehumidified air is forced to flow back into the humidifier, by a blower. Figure 5.1 presents working layout of a modified air heated HDH cycle.

Assumptions

Following assumptions are made in order to study the analytical model:

- The processes involved in the cycle operate at steady state conditions.
- Negligible heat loss occurs through the subcomponents, in the cycle.
- Power needed to operate the pump and fan is minimal in comparison to the input required by heating unit.
- Produced freshwater is expected to leave the dehumidifier at a mean temperature, averaged between the temperature of humid air at the entrance and temperature of air at the exit.
- Relative humidity of air that leaves both the system subcomponents is assumed to be > 90 %. Since, air gets heated and humidified simultaneously in an evaporator. Similarly, air loses heat and moisture as it flows through the dehumidifier.

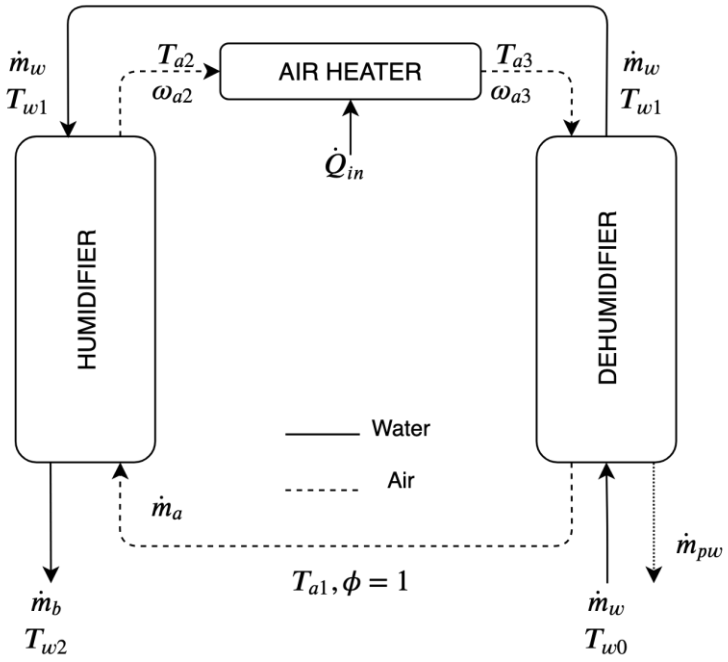

Figure 5.1 Working Diagram of a Modified Air Heated HDH Cycle

Governing Equations

Primary governing equations that represent mathematical model of a closed air-open water, modified air heated HDH cycle, are represented in this section.

Mass and energy balance of the humidifier is expressed in equations, respectively as;

$$\dot{m}_a \omega_{a1} + \dot{m}_w = \dot{m}_b + \dot{m}_a \omega_{a2} \tag{15}$$

$$\dot{m}_a h_{a1} + \dot{m}_w h_{w1} = \dot{m}_b h_{w2} + \dot{m}_a h_{a2} \tag{16}$$

Entropy balance of the humidifier is given as,

$$\dot{S}_{gen,hum.} = \dot{m}_a s_{a2} + \dot{m}_b s_{w2} - \dot{m}_a s_{a1} - \dot{m}_w s_{w1} \geq 0 \tag{17}$$

Effectiveness of humidifier is defined as;

$$\varepsilon_{hum.} = max \left\langle \frac{\dot{m}_w h_{w1} - \dot{m}_b h_{w2}}{\dot{m}_w h_{w1} - \dot{m}_b h_{w2,ideal}}, \frac{(h_{a2} - h_{a1})}{(h_{a2,ideal} - h_{a1})} \right\rangle \tag{18}$$

Mass and energy balance of the dehumidifier are noted below;

$$\dot{m}_w + \dot{m}_a \omega_{a3} = \dot{m}_w + \dot{m}_a \omega_{a1} + \dot{m}_{pw} \tag{19}$$

Or equation (9) can be rewritten as;

$$\dot{m}_{pw} = \dot{m}_a (\omega_{a3} - \omega_{a1}) \tag{20}$$

$$\dot{m}_w h_{hw0} + \dot{m}_a h_{a3} = \dot{m}_w h_{w1} + \dot{m}_a h_{a1} + \dot{m}_{pw} h_{pw} \quad (21)$$

Entropy balance of the dehumidifier is stated as,

$$\dot{S}_{gen,dehum.} = \dot{m}_w s_{w1} + \dot{m}_a s_{a1} + \dot{m}_{pw} s_{pw} - \dot{m}_w s_{w0} - \dot{m}_a s_{a3} \geq 0 \quad (22)$$

Effectiveness of dehumidifier is expressed as,

$$\varepsilon_{dehum.} = max \langle \frac{h_{w1} - h_{w0}}{h_{w1,ideal} - h_{w0}}, \frac{h_{a3} - h_{a1}}{h_{a3} - h_{a1,ideal}} \rangle \quad (23)$$

Energy and entropy balance for the air heater is given respectively as,

$$\dot{Q}_{in,air=} \dot{m}_a (h_{a3} - h_{a2}) \quad (24)$$

$$\dot{S}_{gen,heater} = \dot{m}_a (s_{a3} - s_{a2}) - \frac{Q}{T} \geq 0 \quad (25)$$

Validation

With reference to analytical model presented above for a CAOW modified AH-HDH system. This section is aimed at validating the current model. Commercial Software EES has been utilized here to develop and run the system equations. EES is a computational aid for numerical solutions, it utilizes iterative methods to get a solution for non-linear

equations [98]. The fluid property data functions are available in the EES directories. Specific ones that were employed to carry out this particular study are listed here:

1. Properties of water are computed by EES using formulation by the (IAPWS)-International Association for the Properties of Water and Steam [99].
2. The moist air property functions are computed by considering an ideal mixture between water vapor and air, using formulation given by Hyland [100].
3. Seawater properties were taken from an EES directory which utilizes the formulations presented by Nayar and Sharqawy [101].

The stated mathematical model is solved with following input variables; T_{max}=80°C, T_{min}=30°C, $\varepsilon_h=\varepsilon_d$=0.9, ϕ=1 and (salinity) S=35g/kg. These are the exact same values used in Narayan's reference article [55]. Relation between HCR and GOR is considered here to check for the validity of developed analytical model. As illustrated in figure 5.2 and 5.3, developed model clearly exhibits a good match with existing one in the literature. Figure 5.2 and 5.3 shows the impact of HCR_d and HCR_h on performance (GOR) of the cycle, respectively. Overall maximum GOR occurs at HCR_h value of 5.20. Under given conditions, maximum GOR is unlikely to achieve due to the 2nd law violation, at the specified point. In figure 3.2, the kink at HCR_d=2.41 represents the point at which HCR_h is equals to 1. Likewise, the deflection in figure 3.3 at HCR_h=5.20 indicates HCR_d of 1. It implies that for set initial conditions, dehumidifier cannot be balanced except for that the 2nd law is violated, since entropy generation for such cases would be less than zero.

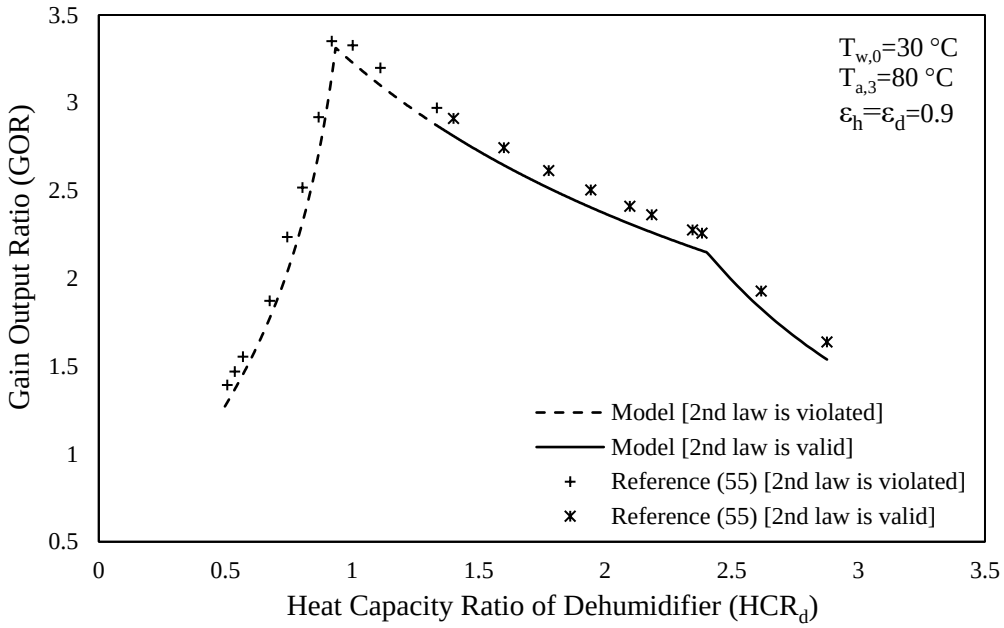

Figure 5.2 Model validation: HCR_d vs GOR

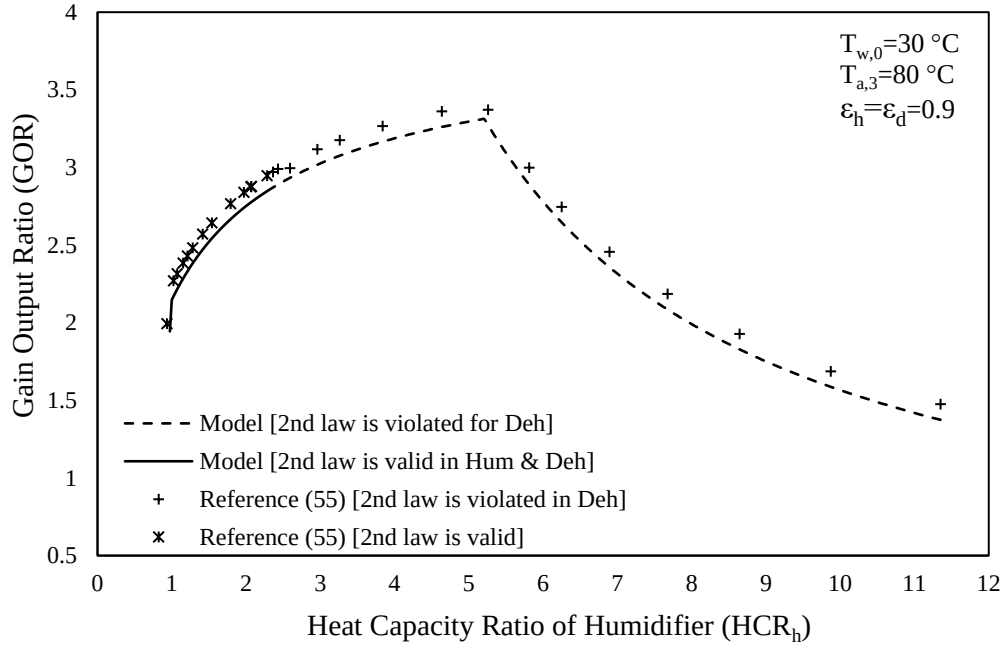

Figure 5.3 Model validation: HCR_h vs GOR

Specific entropy generation in the present model, at initial conditions in each component of the system is shown in figure 5.4. It can be noticed that over a certain range of mass flowrate ratio, $\dot{s}_{gen,deh}$ is negative which denotes that those operating points are inconceivable. Also, the $\dot{s}_{gen}$ of each component rather than whole system, decides whether the system is realistic or not [57]. It can be deduced from here that a balanced dehumidifier ($\Delta H_{max,cold}=\Delta H_{max,hot}$) is of greater significance to the cycle than a balanced humidifier.

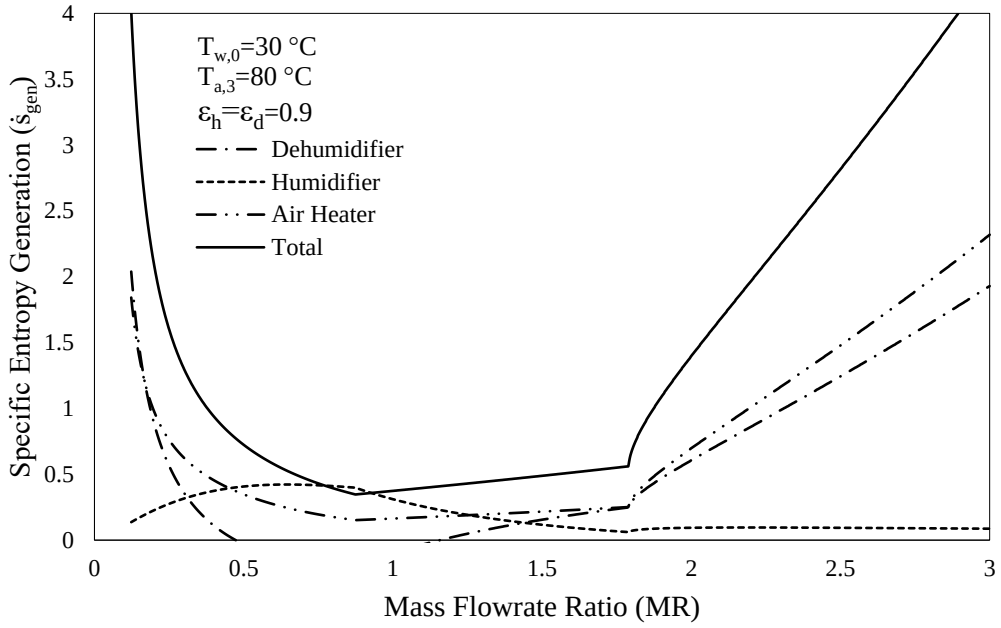

Figure 5.4 Model Validation: Specific Entropy Generation vs MR

Apart from validation of mathematical model, there are other initial conditions where the 2nd law is valid at HCR_d=1. Correspondingly, the maximum cycle GOR at stipulated input conditions is achievable and specific entropy generation $\dot{s}_{gen}$ in cycle is positive. Two such cases with mass flowrate ratio ranging between 0.5 and 3 at different initial states are presented in table 5.1 here;

Table 5.1 Cases where second law is valid for MAH-HDH model at HCR_d=1				
Case	Parameters	HCR_d=1	HCR_h=1	Initial Conditions
I	MR (-)	0.64	1.45	T_{max}=65°C, T_{min}=30°C, ε_h=0.76, ε_d=0.74
	$\dot{s}_{gen,total}$ (kJ/kg K)	0.71	1.58	
	GOR (-)	1.25	0.60	
II	MR (-)	0.74	1.60	T_{max}=80°C, T_{min}=30°C, ε_h=0.85, ε_d=0.74
	$\dot{s}_{gen,total}$ (kJ/kg K)	0.70	1.78	
	GOR (-)	1.60	0.67	

In case I, HCR_d=1 at MR of 0.64 and $\dot{s}_{gen,total}$ is 0.71 at this condition which is less than the total specific entropy generation at HCR_h=1. On similar note, the cycle performance peaks when total entropy generation is minimum. It signifies the importance of a balanced dehumidifier (HCR_d=1). Meanwhile, the value of $\dot{s}_{gen,total}$ is relatively high in case II. Consequently, the system GOR is low when MR is staged to achieve HCR_h=1. Therefore, inferences made from figures 3.2 and 3.3 are in compliance with the dynamics of cycle.

5.2 Analytical Model: Air and Water Heated HDH Cycle

Analytical model for closed air-open water loop, air and water heated HDH desalination cycle is staged in this section. Mathematical framework of verified MAH-HDH cycle is reformed and extended to formulate the theoretical representation of a dual heated HDH cycle. First law energy balances are applied to substantiate the heat and mass exchange processes. Feedwater enters the dehumidifier at an ambient temperature. It ascends through condenser tubes and takes in the heat of condensation during its upward trail. Meanwhile, outgoing heated air in dehumidifier interacts with the incoming water indirectly via fins to

discharge the moisture it is holding, as freshwater. Preheated feedwater from dehumidifier enters a water heating unit where its temperature gets raised further.

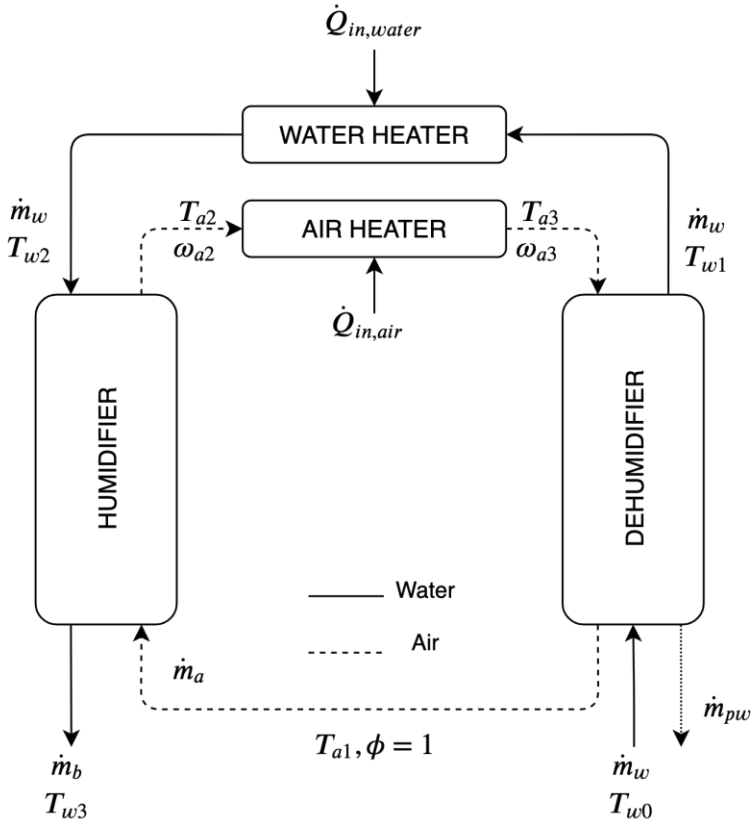

Figure 5.5 Working Diagram of a Dual Heated HDH Cycle

Heated water is then sprayed in humidifier using sprinklers. Similar to the MAH cycle, water in humidifier enters hotter than the air. In humidifier, direct heat and mass exchange take place between the two interacting streams. Air gets heated and humidified and then advances into the air heating unit, where sensible heat is added to the preheated moist air stream. Sequentially, air then circulates in a closed loop and re-enters the humidifier after losing its moisture content in condenser. Figure 5.5 illustrates a functioning layout of a CAOW-DH-HDH cycle.

Governing Equations

Mass balance and energy balance in humidifier of a DH-HDH cycle is expressed in the respective equations below;

$$\dot{m}_w = \dot{m}_b + \dot{m}_{pw} \tag{26}$$

$$\dot{m}_a h_{a1} + \dot{m}_w h_{w2} = \dot{m}_b h_{w3} + \dot{m}_a h_{a2} \tag{27}$$

Effectiveness of humidifier is defined as;

$$\varepsilon_{hum.} = max\left\langle \frac{\dot{m}_w h_{w2} - \dot{m}_b h_{w3}}{\dot{m}_w h_{w2} - \dot{m}_b h_{w3,ideal}}, \frac{(h_{a2} - h_{a1})}{(h_{a2,ideal} - h_{a1})} \right\rangle \tag{28}$$

Similarly, mass balance equation for dehumidifier is formulated below. It remains same as represented in the previous case of MAH cycle, given by equations (9) and (10). Sequentially, the representation of energy balance in the dehumidifier also remains unchanged due to similar nomenclature and is expressed in equation (11);

$$\dot{m}_w + \dot{m}_a \omega_{a3} = \dot{m}_w + \dot{m}_a \omega_{a1} + \dot{m}_{pw} \tag{29}$$

$$\dot{m}_{pw} = \dot{m}_a(\omega_{a3} - \omega_{a1}) \tag{30}$$

$$\dot{m}_w h_{hw0} + \dot{m}_a h_{a3} = \dot{m}_w h_{w1} + \dot{m}_a h_{a1} + \dot{m}_{pw} h_{pw} \tag{31}$$

Effectiveness of dehumidifier is expressed as;

$$\varepsilon_{dehum.} = max\left\langle \frac{h_{w1} - h_{w0}}{h_{w1,ideal} - h_{w0}}, \frac{h_{a3} - h_{a1}}{h_{a3} - h_{a1,ideal}} \right\rangle \quad (32)$$

Energy balance for the air heater is given by equation (14). However, energy balance for the water heater is presented here;

$$\dot{Q}_{in,air=}\dot{m}_a(h_{a3} - h_{a2}) \quad (33)$$

$$\dot{Q}_{in,water=}\dot{m}_w(h_{w2} - h_{w1}) \quad (34)$$

Heat rate ratio is defined as ratio between total energy input to water over air as;

$$Q_r = \frac{\dot{Q}_{in,water}}{\dot{Q}_{in,air}} \quad (35)$$

For fixed component effectiveness and mass flow rate ratio, the dual heated humidification-dehumidification desalination cycle in semi-open air-open water configuration has shown better system performance when heat rate ratio is equal to or greater than unity [63].

5.3 Validation of Experimental Results

This section is subjected to endorse the experimental results of humidification-dehumidification desalination system. Observed performance indicators are validated here, by comparing them with numerical solution from the respective mathematical models.

5.3.1 Modified Air Heated HDH Cycle

The experimental analysis of MAH-HDH system is performed at set initial conditions that have been specified earlier. In this comparative study, certain parameters such as mass flowrate ratio, energy input, initial water temperature, effectiveness and relative humidity are given as input to the mathematical model. The corresponding outcomes are freshwater flowrate, gain output ratio and stream temperatures across the cycle. Therefore, the performance indicators that were previously detected from experimental data are now computed from the model by utilizing system conditions. A primary performance metric in humidification-dehumidification cycle is gain output ratio. Its variation with mass flowrate ratio is illustrated below in figure 5.6 which inspects the experimental and theoretical difference between deduced values.

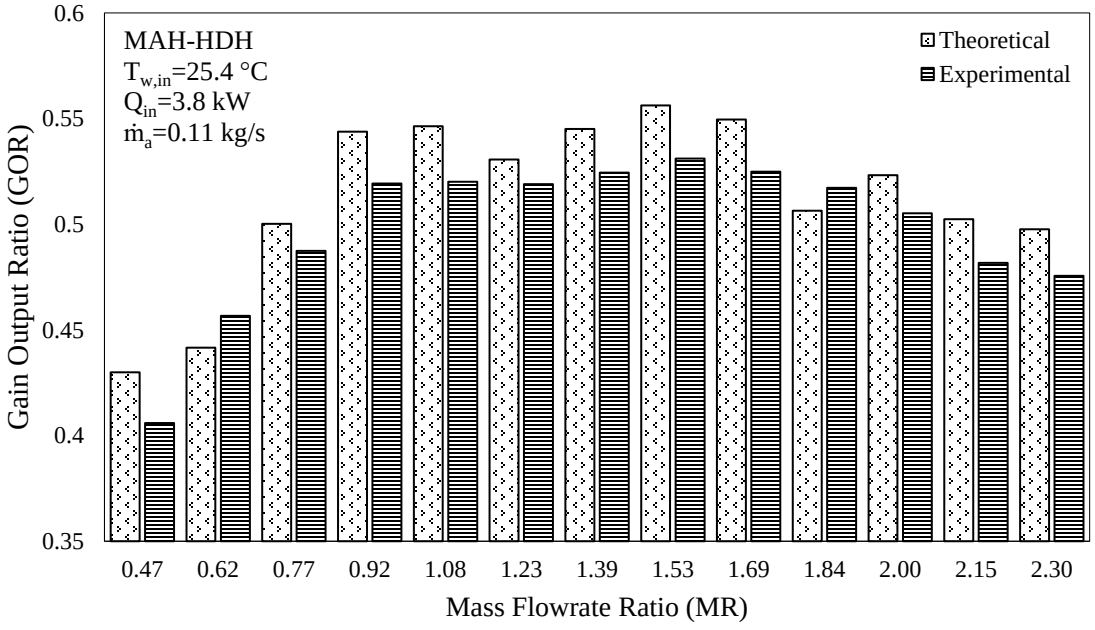

Figure 5.6 MAH Cycle Theo & Exp: Mass flowrate ratio vs gain output ratio

Maximum percentage deviation of experimental GOR from theoretical GOR came out to be 5.58 % at MR of 0.47. The main parameter contributing to this deviation is product water mass flowrate $\dot{m}_{pw}$. It is anticipated because after achieving the steady state, the feedwater coming from storage tank would observe slight temperature variations including minor fluctuation in $\dot{m}_w$ that is controlled via ball valve. But when it comes to computation, the reported data has been averaged to minimize the noise in recorded data. Likewise, the theoretical model is processing these averaged values of recorded parameters that tend to give slight differences in productivity. To further strengthen the case, experimental $T_{max,air}$ is compared with mathematically computed maximum cycle temperature of the modified air heated desalination cycle. It is evident from figure 5.7 that analytical and experimental temperatures are in agreement with maximum percentage error of 0.79 at mass flowrate ratio of 0.62.

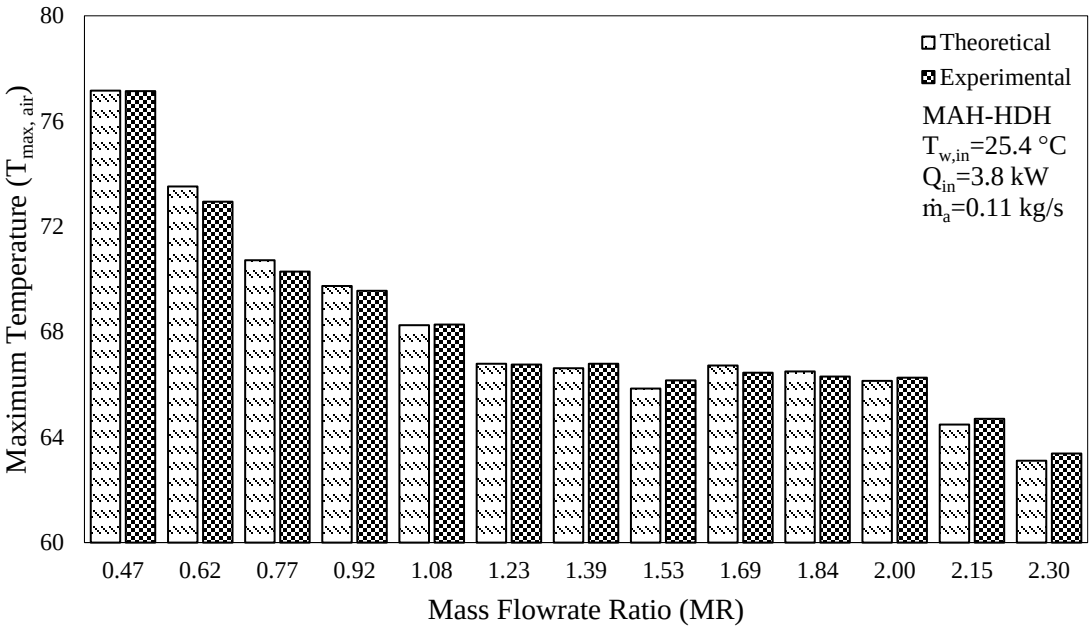

Figure 5.7 MAH Cycle Theo & Exp: Mass flowrate ratio vs maximum temperature

5.3.2 Dual Heated HDH Cycle

In the case of water and air heated HDH cycle with total heat input of 3.0 kW, the comparison between experimental and theoretical evaluation is presented in figure 5.8. It can be deduced from the analysis that overall variation trend of GOR with MR has remained the same in mathematical interpretation as well. Highest difference in GOR of about 6.05 % is recorded at mass flowrate ratio of 2.48. Apparent disparity in $T_{max,air}$ can be witnessed in figure 5.9. The maximum difference between analytical model and experimental runs, at MR of 2.72 is recorded to be 0.88 °C. Likewise, maximum temperature of water after exiting the heating unit and before entering humidifier is also highlighted in figure 5.10. A good agreement between observed and computed values can be witnessed here. At MR of 2.24, experimental value of $T_{max,water}$ exceeded the calculated temperature by 0.25 °C. It is the largest difference recorded between $T_{max,water}$ values.

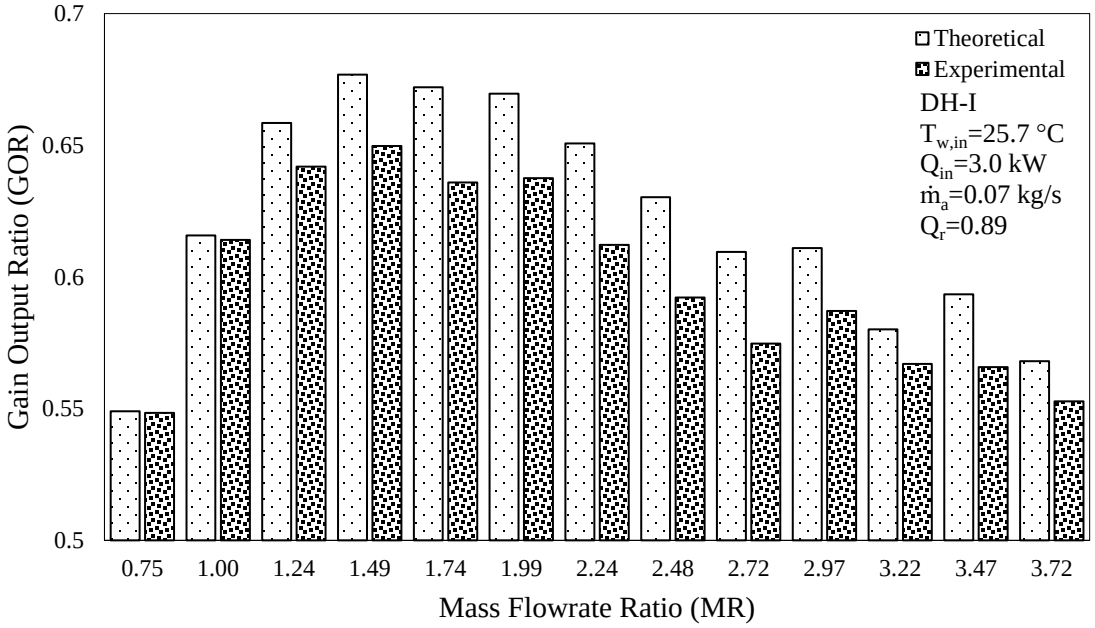

Figure 5.8 DH-I Cycle Theo & Exp: Mass flowrate ratio vs gain output ratio

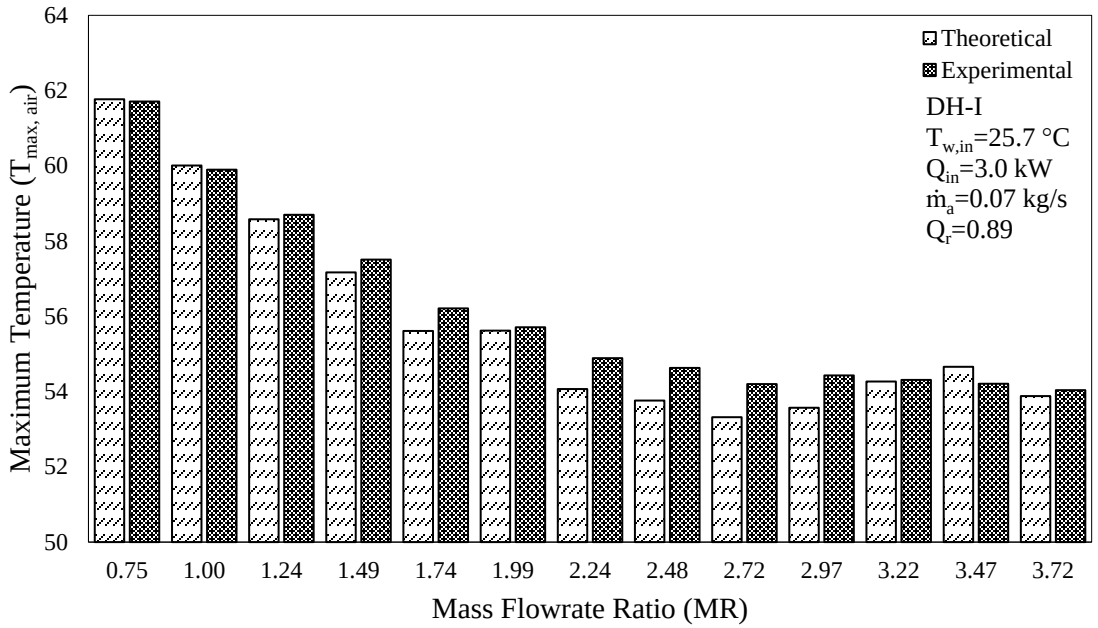

Figure 5.9 DH-I Cycle Theo & Exp: Mass flowrate ratio vs maximum cycle temperature

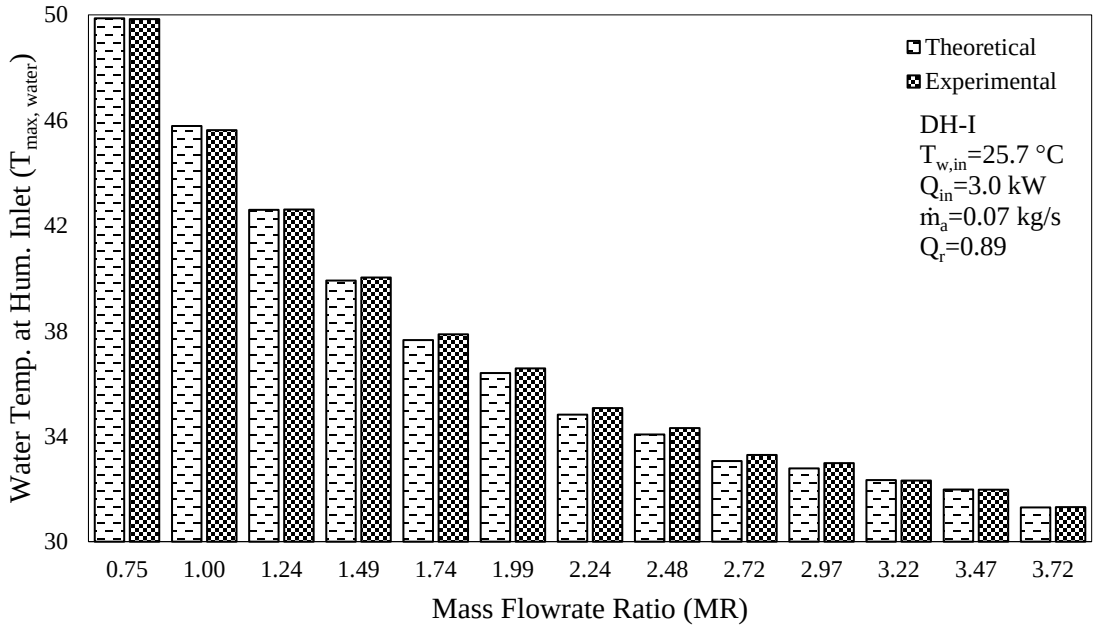

Figure 5.10 DH-I Cycle Theo & Exp: Mass flowrate ratio vs water temp. at hum. inlet

It has been demonstrated experimentally, that increasing the heat rate ratio improves overall performance of closed air open water loop, dual heated HDH system. Figure 5.11 illustrates the comparison between analytical and experimental performance of DH-HDH system with total heat input of 4.4 kW. Maximum error percentage of 3.33 % is noted between theoretical and experimental results at MR of 3.04. The contrast in maximum temperature of cycle $T_{max,air}$ is given in figure 5.12. Largest temperature difference of 0.74 ℃ is recorded between mathematical and experimental values, at mass flowrate ratio of 3.04. Similarly, maximum water temperature in cycle is collated under the specified initial conditions of DH-II system in figure 5.13. It has been found that maximum disparity between experimental and analytical $T_{max,water}$ is only 0.20 ℃, at mass flowrate ratio of 2.78. Overall comparative results from the devised analytical study of all systems under set conditions authenticate the experimental analysis and its conclusions.

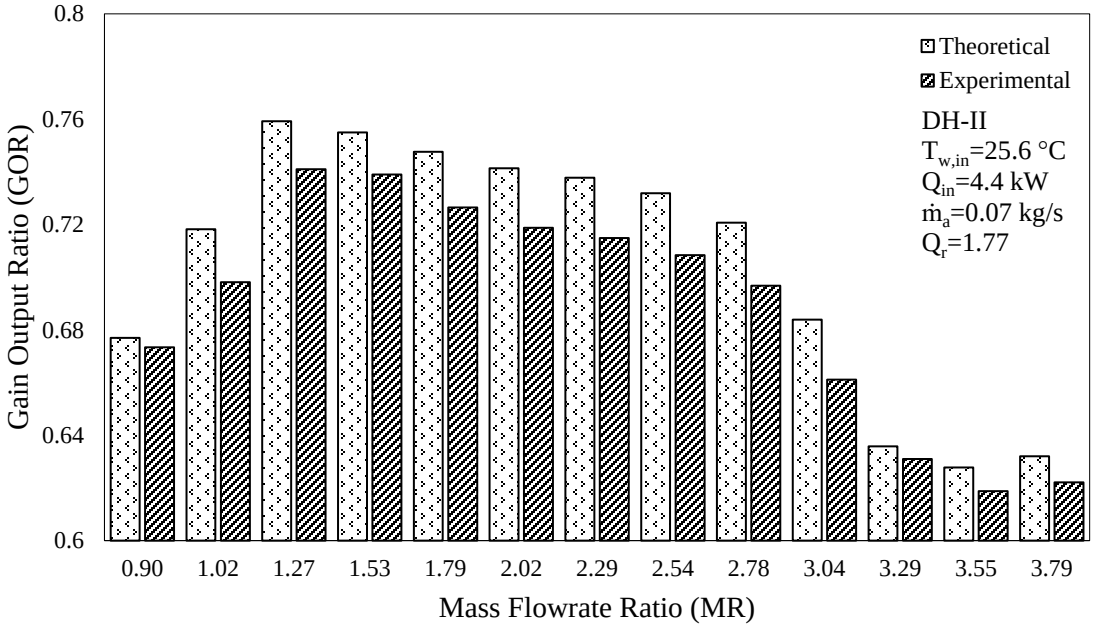

Figure 5.11 DH-II Cycle Theo & Exp: Mass flowrate ratio vs gain output ratio

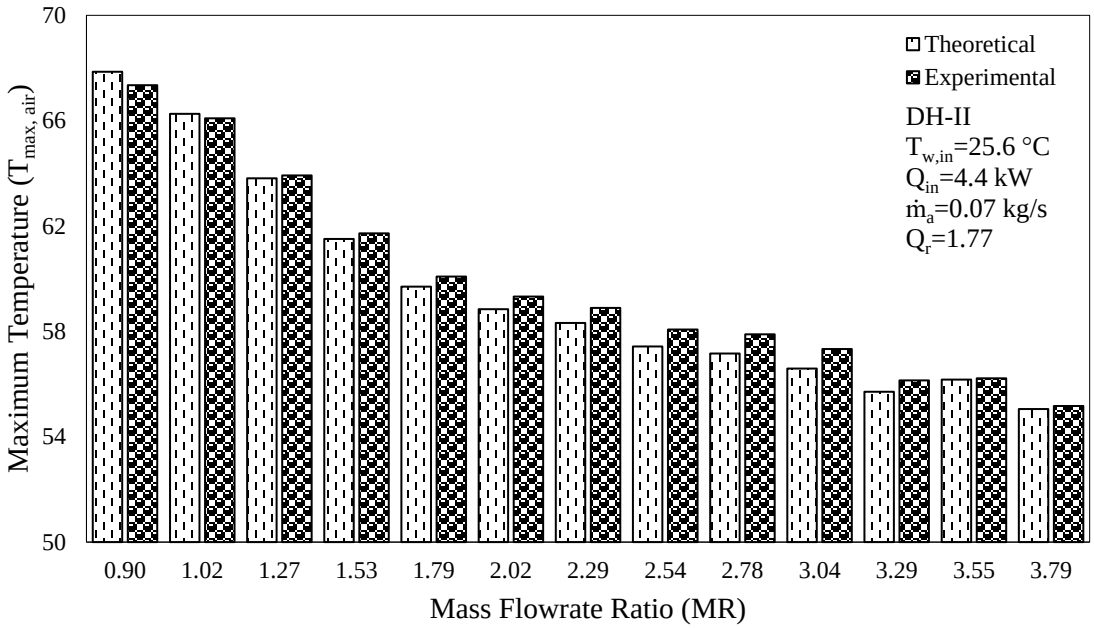

Figure 5.12 DH-II Cycle Theo & Exp: Mass flowrate ratio vs maximum cycle temperature

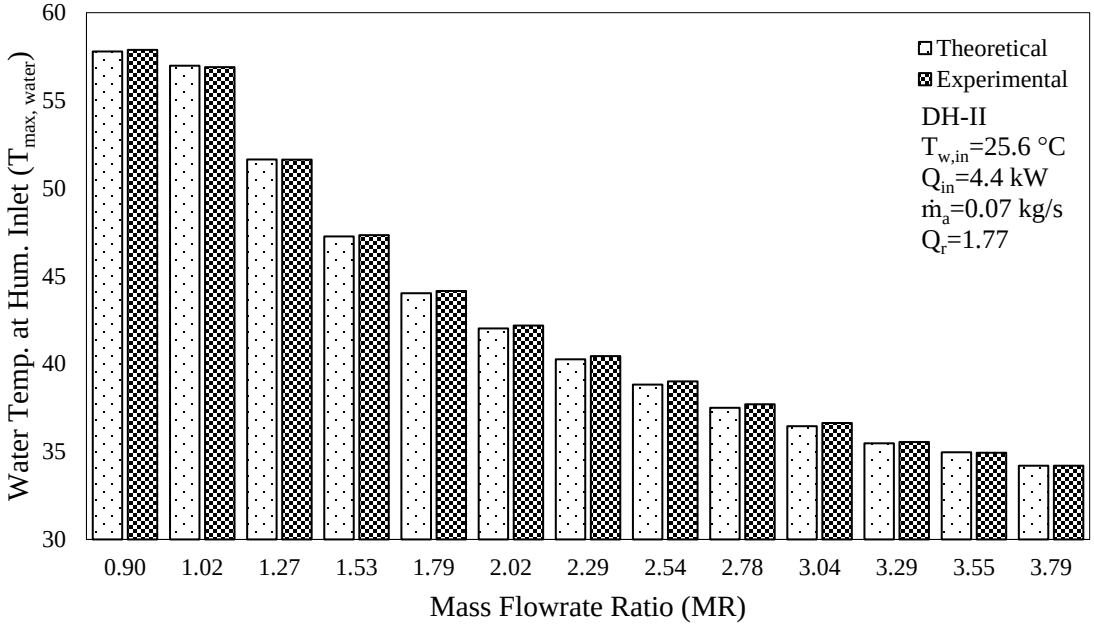

Figure 5.13 DH-II Cycle Theo & Exp: Mass flowrate ratio vs water temp. at hum. inlet

CHAPTER : 6

CONCLUSIONS AND FUTURE SCOPE

6.1 Conclusions

Humidification-dehumidification technique has aptitude to quench the freshwater needs of distant communities by decentralizing the process of brackish or seawater desalination. Over the past few years, numerous studies have suggested multiple ways to improve the thermal performance of HDH cycle, theoretically. Some articles have critically looked at the possibility of integrating an HDH setup with other systems (heat pump, reverse osmosis, co-generation, etc). The available literature has frequently discussed the water heated cycle in different layouts. In present study, modified air heated and dual heated HDH systems are investigated in a closed air-open water configuration. Despite their performance superiority in computational analysis, these cycles were never assessed in an experimental setting. Therefore, functional capabilities of MAH and DH humidification-dehumidification desalination systems are examined, and this analysis is subjected at exploring the performance of a fix sized HDH setup, along with comparative inspection of MAH and DH systems. Resultantly, the findings are summarized here;

- Performance of an experimental rig discussed in this study, imitates the on-field operation of humidification-dehumidification desalination system. In actual working conditions, there are a few parameters that are defined by the initial

conditions and cannot be fixed in a practical sense, like component effectiveness and temperatures of fluid streams across the cycle. These physical characteristics have often been overlooked by most theoretical studies. Therefore, this study has highlighted the effect of changing mass flowrate ratio and inlet seawater temperature on the performance indicators. The effect of changing MR on component effectiveness, component heat capacity ratio, maximum temperature of air and water streams, recovery ratio, gain output ratio and freshwater productivity, is observed for modified air heated and dual heated cycles. In addition, the impact of inlet seawater temperature on production rate is also indicated for MAH system.

- Comparative analysis has found that the performance of dual heated cycle in closed air-open water loop is superior than modified air heated cycle. Furthermore, increasing the heat input to water stream has shown performance improvement in dual heated HDH cycle.
- Results are compared with mathematical model to endorse the experimental outcomes. Maximum overall deviation in performance among all settings was found to be 6.05 %. In addition, maximum cycle temperature and water temperatures are found to be in good agreement with theoretical model.
- The concept of heat rate ratio Q_r is introduced, which signifies the effect of total energy distribution between water and air streams, in dual heated systems. It is deduced that the system performs better when heat rate ratio is greater than one or when more energy is supplied to the water stream, mainly because specific heat capacity of water is greater than air and its ability to retain thermal energy is better than the humid air. It can be concluded from the analysis that for same amount of

heat input, the CAOW air and water heated HDH cycles have better performance characteristics than the modified air heated cycle.

- Maximum productivity of CAOW modified air heated HDH cycle is found to be 72.7 kg/day with GOR of 0.53. Whereas the highest product water flowrate in the case of CAOW dual heated cycle with heat rate ratio less than one (0.89) came out to be 69.8 kg/day with the gain output ratio of 0.65. Meanwhile, the dual heated system indicated maximum overall freshwater productivity of 117.2 kg/day with GOR of 0.74 at heat rate ratio greater than one (1.77).

6.2 Recommendations and Future Scope

- In spite of the fact that air is easier to heat due to its low specific heat capacity, it also loses energy at a rapid pace as compared to water. Furthermore, heating unit and joints at multiple locations remained susceptible to leakage during the operation due to lack of moisture and temperature resistant seals. Accordingly, it is recommended here that system in case of air heating should be tightly insulated and diligently sealed.
- As evident from interpretation of component effectiveness values, size of dehumidifier needs to increase in order to attain higher performance. HDH cycles with post-humidification air heating perform better when dehumidifier is larger than the humidifying component.
- The extracted results from this study will serve as a link to the chain that seeks decentralization and sustainability of water desalination systems. It will also help

desalination experts and water technologists to gauge the abilities of MAH and DH humidification-dehumidification systems in the CAOW configuration.

- Present work can be extended in the future to analyze the impact of heat recovery on modified air heated and dual heated HDH systems. The system can be integrated with heat storage unit, solar air and water heaters to scale its performance with the renewable energy resource, for sustainable day and night operations. System configuration can be altered to evaluate its capacity under open-air or closed-water loops. Furthermore, with given system dimensions and operational characteristics, this study can serve as a reference for future designs to adapt and improve based on the presented results.

References

[1] A. Alkhudhiri, N. Darwish, N. Hilal, Membrane distillation: A comprehensive review, Desalination. (2012). doi:10.1016/j.desal.2011.08.027.

[2] C. Charcosset, A review of membrane processes and renewable energies for desalination, Desalination. (2009). doi:10.1016/j.desal.2008.06.020.

[3] E. Jones, M. Qadir, M.T.H. Van Vliet, V. Smakhtin, S. Kang, Science of the Total Environment The state of desalination and brine production : A global outlook, Sci. Total Environ. (2019). doi:10.1016/j.scitotenv.2018.12.076.

[4] H.M.N. AlMadani, Water desalination by solar powered electrodialysis process, Renew. Energy. (2003). doi:10.1016/S0960-1481(03)00014-4.

[5] International Atomic Energy Agency IAEA-TECDOC-1753, New Technologies for Seawater Desalination Using Nuclear Energy, Vienna, 2015.

[6] J.E. Miller, Review of Water Resources and Desalination Technologies, 2003.

[7] M. Al-Shammiri, M. Safar, Multi-effect distillation plants: State of the art, in: Desalination, 1999. doi:10.1016/S0011-9164(99)00154-X.

[8] O.K. Buros, The ABCs of Desalting, Int. Desalin. Assoc. Mass. (2000).

[9] A. Al-Othman, N.N. Darwish, M. Qasim, M. Tawalbeh, N.A. Darwish, N. Hilal, Nuclear desalination: A state-of-the-art review, Desalination. (2019). doi:10.1016/j.desal.2019.01.002.

[10] M. Kummu, H. de Moel, P.J. Ward, O. Varis, How close do we live to water? a global analysis of population distance to freshwater bodies, PLoS One. (2011). doi:10.1371/journal.pone.0020578.

[11] Y. Zhou, R.S.J. Tol, Evaluating the costs of desalination and water transport, Water Resour. Res. (2005). doi:10.1029/2004WR003749.

[12] United Nations, World Population Prospects 2019, 2019.

[13] T. Luo, R. Young, P. Reig., Aqueduct Projected Water Stress Country Rankings, World Resour. Inst. (2015).

[14] M. Luck, M. Landis, F. Gassert, Aqueduct Water Stress Projections: Decadal projections of water supply and demand using CMIP5 GCMs., 2015.

[15] WEF, The Global Risks Report 2019 - World Economic Forum, 2019.

[16] C. Strong, S. Kuzma, S. Vionnet, P. Reig, Achieving Abundance: Understanding the Cost of a Sustainable Water Future, 2020.

[17] World Bank Group, High and Dry: Climate Change, Water, and the Economy, 2016. doi:10.1596/k8517.

[18] J.S. Pal, E.A.B. Eltahir, Future temperature in southwest Asia projected to exceed a threshold for human adaptability, Nat. Clim. Chang. (2016). doi:10.1038/nclimate2833.

[19] SDG, Sustainable Development Goal 6: Synthesis Report on Water and Sanitation, 2018. doi:10.1126/science.278.5339.827.

[20] R. Bos, Manual on the Human Rights to Safe Drinking Water and Sanitation for

Practitioners, Water Intell. Online. (2016). doi:10.2166/9781780407449.

[21] FAO, Irrigation in the Middle East region in figures AQUASTAT survey 2008, 2009.

[22] S. Chowdhury, M. Al-Zahrani, Characterizing water resources and trends of sector wise water consumptions in Saudi Arabia, J. King Saud Univ. - Eng. Sci. (2015). doi:10.1016/j.jksues.2013.02.002.

[23] E. DeNicola, O.S. Aburizaiza, A. Siddique, H. Khwaja, D.O. Carpenter, Climate change and water scarcity: The case of Saudi Arabia, Ann. Glob. Heal. (2015). doi:10.1016/j.aogh.2015.08.005.

[24] K.H. Zaharani, M. Shayaa Al-Shayaa, M.B. Baig, Water conservation in the kingdom of Saudi Arabia for better environment: Implications for extension and education, Bulg. J. Agric. Sci. (2011).

[25] S. Lattemann, T. Höpner, Environmental impact and impact assessment of seawater desalination, Desalination. (2008). doi:10.1016/j.desal.2007.03.009.

[26] Saline Water Conversion Corporation, Annual Statistical Booklet for Operation and Maintenance Sector, 2019.

[27] A. Alkhudhiri, N. Bin Darwish, N. Hilal, Analytical and forecasting study for wastewater treatment and water resources in Saudi Arabia, J. Water Process Eng. (2019). doi:10.1016/j.jwpe.2019.100915.

[28] W.A. Abderrahman, Water management in ArRiyadh, Int. J. Water Resour. Dev. (2006). doi:10.1080/07900620600654785.

[29] O. Varis, A.K. Biswas, C. Tortajada, J. Lundqvist, Megacities and water management, Int. J. Water Resour. Dev. (2006). doi:10.1080/07900620600684550.

[30] G.P. Narayan, J.H. Lienhard V, Humidification Dehumidification Desalination, in: I.J. Kucera (Ed.), Desalin. Water from Water, Wiley-Scrivener, Salem, MA, 2014: pp. 425–472.

[31] K. Bourouni, R. Martin, L. Tadrist, M.T. Chaibi, Heat transfer and evaporation in geothermal desalination units, Appl. Energy. (2002). doi:10.1016/s0306-2619(99)00071-9.

[32] K. Bourouni, M.T. Chaibi, L. Tadrist, Water desalination by humidification and dehumidification of air: State of the art, Desalination. (2001). doi:10.1016/S0011-9164(01)00215-6.

[33] A.E. Kabeel, M.H. Hamed, Z.M. Omara, S.W. Sharshir, Water Desalination Using a Humidification-Dehumidification Technique—A Detailed Review, Nat. Resour. 04 (2013) 286–305. doi:10.4236/nr.2013.43036.

[34] A. Eslamimanesh, M.S. Hatamipour, Mathematical modeling of a direct contact humidification-dehumidification desalination process, Desalination. (2009). doi:10.1016/j.desal.2008.01.023.

[35] B.L. de O. Campos, A.O.S. da Costa, E.F. da Costa Junior, Mathematical modeling and sensibility analysis of a solar humidification-dehumidification desalination system considering saturated air, Sol. Energy. (2017). doi:10.1016/j.solener.2017.08.029.

[36] J.J. Hermosillo, C.A. Arancibia-Bulnes, C.A. Estrada, Water desalination by air humidification: Mathematical model and experimental study, Sol. Energy. (2012). doi:10.1016/j.solener.2011.09.016.

[37] J. hong Wang, N. yun Gao, Y. Deng, Y. li Li, Solar power-driven humidification-dehumidification (HDH) process for desalination of brackish water, Desalination. (2012). doi:10.1016/j.desal.2012.08.008.

[38] S. Al-Hallaj, S. Parekh, M.M. Farid, J.R. Selman, Solar desalination with humidification-dehumidification cycle: Review of economics, Desalination. (2006). doi:10.1016/j.desal.2005.09.033.

[39] E.H. Amer, H. Kotb, G.H. Mostafa, A.R. El-Ghalban, Theoretical and experimental investigation of humidification-dehumidification desalination unit, Desalination. (2009). doi:10.1016/j.desal.2009.06.063.

[40] H. Kang, Y. Yang, Z. Chang, H. Zheng, Z. Duan, Performance of a two-stage multi-effect desalination system based on humidification-dehumidification process, Desalination. (2014). doi:10.1016/j.desal.2014.04.004.

[41] M.I. Zubair, F.A. Al-Sulaiman, M.A. Antar, S.A. Al-Dini, N.I. Ibrahim, Performance and cost assessment of solar driven humidification dehumidification desalination system, Energy Convers. Manag. (2017). doi:10.1016/j.enconman.2016.10.005.

[42] D. Lawal, M. Antar, A. Khalifa, S. Zubair, F. Al-Sulaiman, Humidification-dehumidification desalination system operated by a heat pump, Energy Convers. Manag. (2018). doi:10.1016/j.enconman.2018.01.067.

[43] D.U. Lawal, M.A. Antar, A. Khalifa, S.M. Zubair, F. Al-Sulaiman, Experımental investigation of heat pump driven humidification-dehumidification desalination system for water desalination and space conditioning, Desalination. (2020). doi:10.1016/j.desal.2019.114199.

[44] H. Ghaebi, S. Ahmadi, Energy and exergy evaluation of an innovative hybrid system coupled with HRSG and HDH desalination units, J. Clean. Prod. (2020). doi:10.1016/j.jclepro.2019.119821.

[45] S.M. Zubair, M.A. Antar, S.M. Elmutasim, D.U. Lawal, Performance evaluation of humidification-dehumidification (HDH) desalination systems with and without heat recovery options: An experimental and theoretical investigation, Desalination. (2018). doi:10.1016/j.desal.2018.02.018.

[46] G.P. Narayan, R.K. McGovern, S.M. Zubair, J.H. Lienhard, High-temperature-steam-driven, varied-pressure, humidification-dehumidification system coupled with reverse osmosis for energy-efficient seawater desalination, Energy. (2012). doi:10.1016/j.energy.2011.11.007.

[47] E. Chafik, A new type of seawater desalination plants using solar energy, Desalination. (2003). doi:10.1016/S0011-9164(03)00364-3.

[48] E. Chafik, A new seawater desalination process using solar energy, Desalination. (2003). doi:10.1016/S0011-9164(02)01090-1.

[49] C. Yamali, I. Solmuş, Theoretical investigation of a humidification-dehumidification desalination system configured by a double-pass flat plate solar air heater, Desalination. (2007). doi:10.1016/j.desal.2006.02.053.

[50] A.M.I. Mohamed, N.A.S. Elminshawy, Theoretical investigation of solar humidification-dehumidification desalination system using parabolic trough concentrators, Energy Convers. Manag. (2011). doi:10.1016/j.enconman.2011.04.026.

[51] M.A. Antar, M.H. Sharqawy, Experimental investigations on the performance of an air heated humidification-dehumidification desalination system, Desalin. Water Treat. (2013). doi:10.1080/19443994.2012.714598.

[52] I. Houcine, M. BenAmara, A. Guizani, M. Maâlej, Pilot plant testing of a new solar desalination process by a multiple-effect-humidification technique, Desalination. (2006). doi:10.1016/j.desal.2005.11.022.

[53] M. Ben Amara, I. Houcine, A. Guizani, M. Măalej, Experimental study of a multiple-effect humidification solar desalination technique, Desalination. (2004). doi:10.1016/j.desal.2003.11.009.

[54] X. Li, G. Yuan, Z. Wang, H. Li, Z. Xu, Experimental study on a humidification and dehumidification desalination system of solar air heater with evacuated tubes, Desalination. (2014). doi:10.1016/j.desal.2014.07.008.

[55] G.P. Narayan, M.H. Sharqawy, J.H. Lienhard V, S.M. Zubair, Thermodynamic analysis of humidification dehumidification desalination cycles, Desalin. Water Treat. (2010). doi:10.5004/dwt.2010.1078.

[56] M.H. Sharqawy, M.A. Antar, S.M. Zubair, A.M. Elbashir, Optimum thermal design of humidification dehumidification desalination systems, Desalination. (2014). doi:10.1016/j.desal.2014.06.016.

[57] W.F. He, L.N. Xu, D. Han, Parametric analysis of an air-heated humidification-dehumidification (HDH) desalination system with waste heat recovery, Desalination. (2016). doi:10.1016/j.desal.2016.07.016.

[58] W.F. He, L.N. Xu, D. Han, L. Gao, Performance analysis of an air-heated humidification-dehumidification desalination plant powered by low grade waste heat, Energy Convers. Manag. (2016). doi:10.1016/j.enconman.2016.03.073.

[59] F.A. Al-Sulaiman, M.I. Zubair, M. Atif, P. Gandhidasan, S.A. Al-Dini, M.A. Antar, Humidification dehumidification desalination system using parabolic trough solar air collector, Appl. Therm. Eng. (2015). doi:10.1016/j.applthermaleng.2014.10.072.

[60] W.F. He, X.K. Zhang, D. Han, L. Gao, Performance analysis of a water-power combined system with air-heated humidification dehumidification process, Energy. (2017). doi:10.1016/j.energy.2017.04.136.

[61] N.A.A. Qasem, S.M. Zubair, Performance evaluation of a novel hybrid humidification-dehumidification (air-heated) system with an adsorption desalination system, Desalination. (2019). doi:10.1016/j.desal.2019.03.011.

[62] G.P. Narayan, J.H. Lienhard V, S.M. Zubair, Entropy generation minimization of combined heat and mass transfer devices, Int. J. Therm. Sci. (2010). doi:10.1016/j.ijthermalsci.2010.04.024.

[63] E.Z. Mahdizade, M. Ameri, Thermodynamic investigation of a semi-open air, humidification dehumidification desalination system using air and water heaters, Desalination. 428 (2018) 182–198. doi:10.1016/j.desal.2017.11.032.

[64] A.S. Nafey, H.E.S. Fath, S.O. El-Helaby, A.M. Soliman, Solar desalination using humidification dehumidification processes. Part I. A numerical investigation, Energy Convers. Manag. (2004). doi:10.1016/S0196-8904(03)00151-1.

[65] A.S. Nafey, H.E.S. Fath, S.O. El-Helaby, A. Soliman, Solar desalination using humidification-dehumidification processes. Part II. An experimental investigation, Energy Convers. Manag. (2004). doi:10.1016/S0196-8904(03)00152-3.

[66] C. Yildirim, I. Solmuş, A parametric study on a humidification-dehumidification (HDH) desalination unit powered by solar air and water heaters, Energy Convers. Manag. (2014). doi:10.1016/j.enconman.2014.06.016.

[67] T. Rajaseenivasan, K. Srithar, Potential of a dual purpose solar collector on humidification dehumidification desalination system, Desalination. (2017). doi:10.1016/j.desal.2016.10.015.

[68] A.E. Kabeel, E.M.S. El-Said, A hybrid solar desalination system of air humidification-dehumidification and water flashing evaporation. Part I. A numerical investigation., Desalination. (2013). doi:10.1016/j.desal.2013.04.016.

[69] A.E. Kabeel, E.M.S. El-Said, A hybrid solar desalination system of air humidification, dehumidification and water flashing evaporation: Part II. Experimental investigation, Desalination. (2014). doi:10.1016/j.desal.2014.02.035.

[70] G. Yuan, Z. Wang, H. Li, X. Li, Experimental study of a solar desalination system based on humidification-dehumidification process, Desalination. (2011). doi:10.1016/j.desal.2011.04.002.

[71] K. Zhani, H. Ben Bacha, Experimental investigation of a new solar desalination prototype using the humidification dehumidification principle, Renew. Energy. (2010). doi:10.1016/j.renene.2010.03.033.

[72] M.M. Farid, S. Parekh, J.R. Selman, S. Al-Hallaj, Solar desalination with a humidification-dehumidification cycle: Mathematical modeling of the unit, Desalination. (2003). doi:10.1016/S0011-9164(02)00994-3.

[73] H. Müller-Holst, M. Engelhardt, M. Herve, W. Schölkopf, Solarthermal seawater desalination systems for decentralised use, Renew. Energy. (1998). doi:10.1016/S0960-1481(98)00083-4.

[74] H. Müller-Holst, M. Engelhardt, W. Schölkopf, Small-scale thermal seawater desalination simulation and optimization of system design, Desalination. (1999). doi:10.1016/S0011-9164(99)00046-6.

[75] S. Al-Hallaj, M.M. Farid, A.R. Tamimi, Solar desalination with a humidification - dehumidification cycle: Performance of the unit, Desalination. (1998). doi:10.1016/S0011-9164(98)00224-0.

[76] Y.J. Dai, H.F. Zhang, Experimental investigation of a solar desalination unit with humidification and dehumidification, Desalination. (2000). doi:10.1016/S0011-9164(00)00084-9.

[77] H. Ben Bacha, T. Damak, M. Bouzguenda, A.Y. Maalej, Experimental validation of the distillation module of a desalination station using the SMCEC principle, Renew. Energy. (2003). doi:10.1016/S0960-1481(03)00167-8.

[78] J. Moumouh, M. Tahiri, M. Salouhi, L. Balli, Theoretical and experimental study of a solar desalination unit based on humidification–dehumidification of air, Int. J. Hydrogen Energy. (2016). doi:10.1016/j.ijhydene.2016.05.207.

[79] F. Nematollahi, A. Rahimi, T.T. Gheinani, Experimental and theoretical energy and exergy analysis for a solar desalination system, Desalination. (2013). doi:10.1016/j.desal.2013.02.021.

[80] R. Santosh, G. Kumaresan, S. Selvaraj, T. Arunkumar, R. Velraj, Investigation of humidification-dehumidification desalination system through waste heat recovery from household air conditioning unit, Desalination. (2019). doi:10.1016/j.desal.2019.05.016.

[81] A. Giwa, H. Fath, S.W. Hasan, Humidification-dehumidification desalination process driven by photovoltaic thermal energy recovery (PV-HDH) for small-scale sustainable water and power production, Desalination. (2016). doi:10.1016/j.desal.2015.09.018.

[82] H.E.S. Fath, A. Ghazy, Solar desalination using humidification-dehumidification technology, Desalination. (2002). doi:10.1016/S0011-9164(01)00431-3.

[83] J. Orfi, N. Galanis, M. Laplante, Air humidification-dehumidification for a water desalination system using solar energy, Desalination. (2007). doi:10.1016/j.desal.2006.04.022.

[84] C. Chiranjeevi, T. Srinivas, Experimental Analysis of Augmented Desalination by Cooling Integration, in: Energy Procedia, 2016. doi:10.1016/j.egypro.2016.11.196.

[85] S.A. Nada, H.F. Elattar, A. Fouda, Experimental study for hybrid humidification-dehumidification water desalination and air conditioning system, Desalination. (2015). doi:10.1016/j.desal.2015.01.032.

[86] F.R. Siddiqui, N.A.S. Elminshawy, M.F. Addas, Design and performance improvement of a solar desalination system by using solar air heater: Experimental and theoretical approach, Desalination. (2016). doi:10.1016/j.desal.2016.08.015.

[87] H. Ben Bacha, Dynamic modeling and experimental validation of a water desalination prototype by solar energy using humidification dehumidification process, Desalination. (2013). doi:10.1016/j.desal.2013.05.011.

[88] E. Deniz, S. Çınar, Energy, exergy, economic and environmental (4E) analysis of a solar desalination system with humidification-dehumidification, Energy Convers. Manag. (2016). doi:10.1016/j.enconman.2016.07.064.

[89] Y. Zhang, H. Zhang, W. Zheng, S. You, Y. Wang, Numerical investigation of a humidification-dehumidification desalination system driven by heat pump, Energy Convers. Manag. (2019). doi:10.1016/j.enconman.2018.11.018.

[90] S. Kline, F. McClintock, Describing uncertainties in single-sample experiments, Mech. Eng. (1953).

[91] G. Prakash Narayan, K.H. Mistry, M.H. Sharqawy, S.M. Zubair, J.H. Lienhard, Energy effectiveness of simultaneous heat and mass exchange devices, Front. Heat Mass Transf. (2010). doi:10.5098/hmt.v1.2.3001.

[92] H.M. El-Dessouky, H. T.; Ettouney, Fundamentals of Salt-Water Desalination, 1st

ed., Elsevier: Amsterdam, New York, Amsterdam, New York, 2002.

[93] N. Qasem, B. Imteyaz, M.A. Antar, Investigation of the effect of the top and the bottom temperatures on the performance of humidification dehumidification desalination systems, in: ASME Int. Mech. Eng. Congr. Expo. Proc., 2016. doi:10.1115/IMECE201667985.

[94] G.P. Narayan, Thermal Design of Humidification– Dehumidification Systems for Affordable Small-Scale Desalination, 2012. doi:10.1179/ida.2012.4.3.24.

[95] M.H. Hamed, A.E. Kabeel, Z.M. Omara, S.W. Sharshir, Mathematical and experimental investigation of a solar humidification-dehumidification desalination unit, Desalination. (2015). doi:10.1016/j.desal.2014.12.005.

[96] S.A. El-Agouz, A new process of desalination by air passing through seawater based on humidification-dehumidification process, Energy. (2010). doi:10.1016/j.energy.2010.08.005.

[97] C. Muthusamy, M. Gowtham, S. Manickam, M. Manjunathan, K. Srithar, Enhancement of productivity of humidification–dehumidification desalination using modified air heater, Desalin. Water Treat. (2015). doi:10.1080/19443994.2014.968876.

[98] S.A. Klein, Engineering Equation Solver-EES, F-Chart. (2019).

[99] W. Wagner, A. Pruß, The IAPWS formulation 1995 for the thermodynamic properties of ordinary water substance for general and scientific use, J. Phys. Chem. Ref. Data. (2002). doi:10.1063/1.1461829.

[100] R.W. Hyland, A. Wexler, Formulations for the Thermodynamic Properties of the Saturated Phases of H2O from 173. 15K to 473. 15K, in: ASHRAE Trans., 1983.

[101] K.G. Nayar, M.H. Sharqawy, L.D. Banchik, J.H. Lienhard, Thermophysical properties of seawater: A review and new correlations that include pressure dependence, Desalination. (2016). doi:10.1016/j.desal.2016.02.024.

Vitae

Name	:	Saad Abdul Jawad
Nationality	:	Pakistani
Date of birth	:	16/01/1995
Email	:	saadabduljawad@outlook.com
Address	:	Officer's Colony, Old D.C Office Rd, Narowal, 51600, Pakistan.
Academic Background	:	B.Sc. Mechanical Engineering University of Engineering & Technology, Lahore, Pakistan.
Research Interests	:	Energy Management, Desalination Systems, Multiphase Flows, Thermodynamics, Fluid Mechanics, Heat and Mass Transfer.

Publications:

1. DU Lawal, SA Jawad, MA Antar, Experimental and Theoretical Study on a Heat Pump Driven Open-Air Humidification Dehumidification Desalination System, Energy. (2020). doi:10.1016/j.energy.2020.118252.
2. Performance Analysis of Air Heated and Dual Heated Humidification-Dehumidification Desalination Cycles. (Drafting).